Department of Electrical and Computer Engineering

Human Gait Modelling with Step Estimation and Phase Classification Utilising a Single Thigh Mounted IMU for Vision Impaired Indoor Navigation

Kahala Nimsiri Abhayasinghe

This thesis is presented for the Degree of
Doctor of Philosophy
of
Curtin University

June 2016

Declaration

To the best of my knowledge and belief this thesis contains no material previously published by any other person except where due acknowledgment has been made.

This thesis contains no material which has been accepted for the award of any other degree or diploma in any university.

Human Ethics The research presented and reported in this thesis was conducted in accordance with the National Health and Medical Research Council National Statement on Ethical Conduct in Human Research (2007) – updated March 2014. The proposed research study received human research ethics approval from the Curtin University Human Research Ethics Committee (EC00262), Approval Number SMEC-105-11 and PT263/2013.

Signature: *Nimsiri Abhayasinghe*

Date: 14/06/2016

To my beloved parents for taking every effort to let me reach the targets that they could not reach and my beloved wife and two lovely sons for their unconditional love, understanding, commitment and moral support for making this work a success.

ABSTRACT

Wayfinding is one significant difficulty that a vision impaired person encounters, especially in unfamiliar environments. Although Global Positioning System (GPS) based navigation is possible in outdoors, the accuracy of GPS drops significantly in indoor environments due to screening of GPS signals. GPS may in some cases be sufficient for outdoor navigation but still lacks sub meter accuracy. Most of the existing indoor localization and path finding techniques depend on some infrastructure deployed in the environment, limiting access to these systems to a selected number of sites and requiring support of building managers and owners. This research focused on infrastructure free indoor pedestrian navigation and is a part of a project that develops a navigation aid for vision impaired.

The majority of existing gait analysis, pedestrian navigation and localization techniques use multiple sensors attached to the body and heavy wearable computing devices, which are not favoured by vision impaired. Based on the preliminary observations, this research focused on using a single thigh mounted IMU for step counting, gait analysis, gait modelling and travelled distance estimation.

Accurate step counting, angle estimation, gait modelling, step length estimation, gait phase detection and activity recognition play vital roles in improving the accuracy of pedestrian navigation systems. A pedometer algorithm based on zero crossing detection of single thigh mounted gyroscope signal was developed and implemented on an Apple iPhone 4S, which reported over 97.8% step detection accuracies even at slow walking speeds on level ground and over 94% accuracies on stairs well outperformed the existing accelerometer based hardware and software pedometers that demonstrate extreme poor accuracies at slow walking speeds.

The Gyro Integration based Orientation Filter (GIOF) was developed to estimate single axis orientation by integrating the gyro signal and compensating the integration error using acceleration data. The GIOF reported mean correlations greater than 99.5% and RMSE less than 2.5º against a Vicon Motion Capture System, compared to 3º RMSE reported in some Kalman Filter based techniques.

The computational demand of GIOF is about 50% of that of Complementary Filter (CF) on an 8-bit microcontroller.

Gait modelling was performed based on the gyro data of a thigh mounted IMU and the thigh angle estimated with GIOF. Regeneration accuracies above 99.9% and correlation below 0.5º was achieved in this work with harmonics models with 5 and 9 significant harmonics for thigh angle and gyro signal respectively. Harmonic models for 6 commonly observed gait patterns are presented and they were used to classify strides of a lengthy walk. Correlations above 99% and RMSE less than 2º were observed with the best matching models to the particular stride.

A model to estimate the step length based on the maximum flexion and extension angles is presented in this thesis, which reported a step length estimation accuracy of 54 mm RMSE and ±7% on a per step basis. A method to estimate peak flexion and extension using gyro peak is also presented and another model to estimate step length based on the gyro peaks and time between peak and zero-crossing of gyro signal is also presented. The accuracy reported was 56mm RMSE.

A gait phase identification technique using the gyro signal and its first time derivative of a single thigh mounted IMU is also presented. Six key points of the stride cycle that are required to identify five sub phases of the stride cycle (four sub phases of the Stance phase and the whole Swing phase), can be detected with the presented method. An indoor activity detection algorithm using the thing angle is also presented in this thesis. The algorithm can detect sitting, standing and walking with a mean accuracy of 83%. The feasibility of using a thigh mounted barometric pressure sensor to identify walking on travellator ramps and stairs, going in an escalator and on an elevator is also presented.

It can be concluded that gyroscopic data of a single thigh mounted IMU and the thigh angle derived from the gyro data can be used for human gait analysis, gait modelling and for navigation purposes achieving higher accuracies compared to accelerometer based techniques. The techniques presented in the thesis can also be used for rehabilitation applications such as foot drag, pre and post operation movement analysis of the lower limb etc. The accuracies achievable with these techniques are higher than the accuracies achieved in the techniques presented in literature that used acceleration as a main input.

ACKNOWLEDGMENTS

With a deep sense of gratitude, I acknowledge the invaluable guidance provided by my supervisor, Associate Professor Iain Murray, throughout this research. Without the consistent guidance, supervision, encouragement and support provided by him, this work would have been a nightmare.

I am grateful to Curtin University and the Department of Electrical and Computer Engineering of Curtin University for the financial support provided for pursuing the Ph.D. research, without which this research would not have been started. Special thanks goes to the heads of the department, Prof. Syed Islam, Prof. Sven Nordholm and Dr. Yee-Hong Leung, for their invaluable support throughout this work.

Very special thanks goes to all the participants, vision impaired and non-vision impaired, of the data collection of this work for their profuse contribution in making this work a real success without which this work would not have been meaningful.

I thank with warm regards, Megha, Sumedha, Lakini, Nimali, Chamila, Nuwan, Irwan and all other friends for making my stay in Perth memorable and comfortable. Without them, I would never get the happiness and the courage needed to conduct research.

Special thanks goes to Prof. Lalith Gamage and Dr. Malitha Wejesundara of the Sri Lanka Institute of Information Technology (SLIIT) for creating an opportunity for me to pursue Ph.D. research in Curtin University. I would also be grateful to all the staff of SLIIT, especially Dr. Lasantha Seneviratne, Lakmal Rupasinghe, Anuradha Jayakodi and Dhammika de Silva, for their support and courage given throughout this work.

I am much obliged to the staff members of the Department of Electrical and Computer Engineering, Curtin University, especially Zibby Cielma, Russel Wilkinson, Nicholas King and Mark Fowler for their support rendered in various ways during this work. I would also appreciate the collaboration of the colleges of

the research group, Shiva Sharif, Mais Zaher, Azadeh Nazemi, Rémy Dumont and Clémence Baijot which made my work easier and productive.

I express my deep sense of reverence and profound gratitude to my beloved parents for bringing me to this level and taking every effort to let me reach the world that they could not reach. Last, but not least, I would like to thank, with lots of love, my beloved wife and two lovely sons for all the scarification and stress they had to bare in supporting me to bring this work to a success.

TABLE OF CONTENTS

ABSTRACT ..... **IV**

ACKNOWLEDGMENTS ..... **VI**

TABLE OF CONTENTS ..... **VIII**

LIST OF FIGURES ..... **XII**

LIST OF TABLES ..... **XVI**

LIST OF ABBREVIATIONS ..... **XVII**

LIST OF PUBLICATIONS ..... **XIX**

1 INTRODUCTION **1**

1.1 INTRODUCTION 1

1.2 THE WAY-FINDING SYSTEM FOR VISION IMPAIRED 2

1.3 PROBLEM STATEMENT 4

1.4 OBJECTIVES OF THIS RESEARCH 6

1.5 NOVEL APPROACHES PRESENTED IN THIS THESIS 7

1.6 OUTLINE OF THE THESIS 7

2 HUMAN GAIT AND EXISTING TECHNOLOGY AND WORK ON GAIT ANALYSIS AND PEDESTRIAN NAVIGATION **9**

2.1 INTRODUCTION 9

2.2 HUMAN GAIT CYCLE 9

2.3 MOTION TRACKING AND CAPTURE TECHNOLOGY 11

2.3.1 Introduction *11*

2.3.2 Visual Measurements *11*

2.3.3 Mechanical and Electro–Mechanical Apparatus *12*

2.3.4 Optical Motion Capture Systems *13*

2.3.5 Inertial Sensors *14*

2.4 EXISTING WORK IN THE LITERATURE 16

2.4.1 Techniques Used for Pedestrian Localization *16*

2.4.2 Step Detection *17*

2.4.3 Estimation of Orientation *19*

2.4.3.1 Introduction 19

2.4.3.2 Orientation Estimation using Inertial Sensors 19

2.4.3.3 Existing Work on Orientation Estimation 22

2.4.4 Human Gait Modelling *24*

2.4.4.1 Gait Analysis using Optical Motion Capture Systems 24

2.4.4.2 Gait Analysis using Inertial Sensors 25

2.4.5 Step Length Estimation ... *27*
2.4.6 Activity Recognition ... *30*
2.5 SUMMARY AND CONCLUSIONS ... 31
3 METHODOLOGY ... 33
3.1 RESEARCH METHODOLOGIES ... 33
3.2 RESEARCH METHODOLOGY FOLLOWED ... 33
3.2.1 Construct a Model ... *34*
3.2.2 Algorithm Development ... *35*
3.3 WORK FLOW OF THIS RESEARCH ... 35
3.3.1 Data Collection and Analysis ... *35*
3.3.2 Modelling of Human Gait ... *35*
3.3.3 Gait Identification Algorithms ... *36*
3.3.4 Simulation of Algorithms ... *36*
3.3.5 Validation of Algorithms ... *36*
4 EXPERIMENTAL PLATFORM ... 37
4.1 INTRODUCTION ... 37
4.2 DATA CAPTURE APPLICATION FOR THE SMARTPHONE ... 37
4.3 OFF–THE–SHELF IMU ... 39
4.4 CUSTOM–MADE IMU ... 41
4.4.1 Construction and Specifications of the IMU ... *41*
4.4.2 Operation of Dongle–IMU System ... *43*
4.4.3 Calibration of IMU ... *44*
4.5 OPTICAL MOTION CAPTURE SYSTEM ... 45
4.6 SUMMARY ... 47
5 GAIT MODELLING AND ALGORITHMS ... 49
5.1 INTRODUCTION ... 49
5.2 FEASIBILITY STUDY FOR INERTIAL POCKET NAVIGATION ... 50
5.2.1 Introduction ... *50*
5.2.2 Empirical Observations ... *51*
5.2.3 Summary and Conclusions ... *53*
5.3 A GYROSCOPE BASED ACCURATE PEDOMETER ALGORITHM ... 54
5.3.1 Introduction ... *54*
5.3.2 Relationship between Gyroscopic Data and Movement of the Thigh ... *54*
5.3.3 Step Detection Algorithm ... *55*
5.3.3.1 Pre Processing of Data ... 55
5.3.3.2 Zero–Crossing Detector ... 56
5.3.3.3 Avoiding False Detections ... 56
5.3.3.4 Validating the Detected Zero Crossings ... 56
5.3.3.5 The Step Detection Algorithm ... 57

5.3.3.6 Implementation of the Algorithm 57
5.3.4 Empirical Results *58*
5.3.5 Discussion *60*
5.4 THIGH ANGLE ESTIMATION AND VALIDATION 61
5.4.1 Introduction *61*
5.4.2 Some Key Observations on Limb Synchronization *62*
5.4.3 Experimental Setup and Analysis Technique *63*
5.4.3.1 Experimental Setup 64
5.4.3.2 Data Analysis Technique 65
5.4.4 Gyro Integration based Orientation Filter (GIOF) *65*
5.4.5 Experimental Results *67*
5.4.5.1 Comparison of MAL vs. IMU 67
5.4.5.2 Real–time Implementation for Performance Comparison 69
5.4.6 Summary and Discussion *70*
5.5 HARMONIC MODELS FOR THIGH MOVEMENT DURING WALKING 72
5.5.1 Introduction *72*
5.5.2 Modelling of Thigh Angle *72*
5.5.3 Harmonic Models for Thigh Flexion and Extension Derived from IMU data *78*
5.5.4 Classification of Strides Using Harmonic Models *83*
5.5.4.1 Predicting Thigh Angle Using Harmonic Model 83
5.5.4.2 Classifying Strides 84
5.5.5 Summary and Discussion *88*
5.6 STEP LENGTH ESTIMATION 90
5.6.1 Introduction *90*
5.6.2 Step Length Model *90*
5.6.3 Estimating Maximum Thigh Flexion and Extension without Integration *92*
5.6.4 Step Length as a Function of Gyro Peaks *95*
5.6.5 Experiment and Results *96*
5.6.6 Summary and Discussion *101*
5.7 GAIT PHASE IDENTIFICATION 102
5.7.1 Introduction *102*
5.7.2 Identify Gait Phases from the Thigh Angle and Gyro Waveforms *102*
5.7.3 Summary *104*
5.8 ACTIVITY RECOGNITION 104
5.8.1 Introduction *104*
5.8.2 Indoor Activity Detection Algorithm *105*
5.8.2.1 Observations 105
5.8.2.2 Data Processing and the Algorithm 106
5.8.2.3 Experimental Setup 109
5.8.2.4 Empirical Results 109
5.8.3 Using Pressure Variation for Activity Detection *110*
5.8.4 Discussion *112*

5.8.5 Summary *112*

6 CONCLUSION AND FUTURE DIRECTIONS **113**

6.1 CONCLUSIONS 113

6.2 FUTURE DIRECTIONS 116

7 REFERENCES **119**

APPENDIX A **131**

COMPARISON OF KEY SPECIFICATIONS OF THE INERTIAL SENSORS 131

APPENDIX B **133**

CUSTOM WRITTEN MATLAB FUNCTIONS 133

Harmonic Extraction Function *133*

Function that Extracts Thigh Angle Peaks *134*

Zero-crossing Detector *135*

Matlab Code that was used to Extract Thigh Angle Peaks and Heal Contact Points *135*

LIST OF FIGURES

Figure 1.1 – Global distribution of vision impairment 1
Figure 1.2 – Proposed structure of the Way-finding system for vision impaired 3
Figure 1.3 – Functional block diagram of the Way-finding system for vision impaired 3
Figure 2.1 – Main Phases of the Gait Cycle 10
Figure 2.2 – Eight Sub Phases of the Gait Cycle 10
Figure 2.3 – Goniometer 12
Figure 2.4 – Error present in inertial sensor output 15
Figure 2.5 – Vector Direction of the Angular Velocity Following the Right Hand Rule 16
Figure 2.6 – The Inertial Frame 20
Figure 3.1 – Flow Chart of the Research Method Used 34
Figure 4.1 – User Interface of the Android Application 38
Figure 4.2 – Event-driven to time-driven conversion 39
Figure 4.3 – Devices used for the IMU 43
Figure 4.4 – Completed IMU and Dongle 43
Figure 4.5 – Format of a data frame of the IMU 44
Figure 4.6 – Alignment of the IMU for calibration 45
Figure 4.7 – Vicon active wand 46
Figure 5.1 – Reference Coordinates of the Phone Sensors 51
Figure 5.2 – Filtered Gyro-*x* with Thigh Angle 52
Figure 5.3 – Filtered Gyro-*x* and filtered vertical acceleration at the beginning of the walk 53
Figure 5.4 – Thigh angle with filtered gyro-*x* reading for level walking 55
Figure 5.5 – Flow Chart of the Step Detection Algorithm 58
Figure 5.6 – Thigh angle synchronized with the vertical and forward movements of the foot 63
Figure 5.7 – Thigh angle of left and right legs 63
Figure 5.8 – Marker and IMU placement on legs 64
Figure 5.9 – Reference axis of IMU data 66
Figure 5.10 – Gyro Integration based Orientation Filter (GIOF) algorithm 67

Figure 5.11 – Thigh angle computed from MAL data θ_{MAL} and IMU data θ_{IMU} for a sample trial 68
Figure 5.12 – Histograms of positive and negative peak angle errors 68
Figure 5.13 – Distributions of correlation and RMSE between θ_{IMU} and θ_{MAL} for vision impaired subjects 69
Figure 5.14 – Frequency spectrum of a sample trial and harmonic components picked from the function 74
Figure 5.15 – Amplitude distribution of first nine overtones of all trials normalised to the fundamental amplitude 74
Figure 5.16 – Original and reconstructed thigh angle waveform of a sample trial 75
Figure 5.17 – Histograms of correlation and RMSE between original and reconstructed thigh angle waveform using 5 harmonics 75
Figure 5.18 – Distribution of normalised harmonic amplitude of first four overtones of all female and male trials 76
Figure 5.19 – Distribution of initial phase of first five harmonics of all female and male trials 76
Figure 5.20 – Distribution of fundamental frequency (stride frequency) of female and male subjects 77
Figure 5.21 – Correlation and RMSE between original and reconstructed thigh angles for each stride 77
Figure 5.22 – Six common thigh angle patterns observed in all trials 79
Figure 5.23 – Harmonic models for six commonly observed thigh angle patterns 80
Figure 5.24 – Correlation and RMSE between original and reconstructed gyro signal for each stride 81
Figure 5.25 – Harmonic models of gyro signal for six commonly observed thigh angle patterns 82
Figure 5.26 – Thigh angle waveform reconstructed using harmonic model with 5 harmonics and the original thigh angle waveform for a long walk 84
Figure 5.27 – Correlation of each stride with model generated waveform for different cases 85
Figure 5.28 – RMSE of each stride with model generated waveform for different cases 87
Figure 5.29 – Correlation and RMSE of gyro signal of each stride to the model generated waveform for slow walking 88

Figure 5.30 – Thigh angle patterns for different activities 89
Figure 5.31 – Representation of leg positions during a step 91
Figure 5.32 – Simplified representation of leg positions during a step 92
Figure 5.33 – Synchronization of gyro and thigh angle waveforms 93
Figure 5.34 – Straight line approximations for the sections of the gyro curves that contribute to the thigh angle peaks 94
Figure 5.35 – Estimated peak thigh angle *vs*. integrated peak thigh angle with straight line approximation for positive and negative peak angles 95
Figure 5.36 – Error percentage of step length estimated as a function of thigh angle peaks 97
Figure 5.37 – Estimated step length *vs.* measured step length for step length as a function of thigh angle peaks 97
Figure 5.38 – Error percentage of step length estimated as a function of gyro peaks 98
Figure 5.39 – Estimated step length *vs.* measured step length for step length as a function of gyro peaks 98
Figure 5.40 – Error percentage of step length estimated as a function of thigh angle peaks of vision impaired subjects 99
Figure 5.41 – Estimated step length *vs.* measured step length for step length as a function of thigh angle peaks of vision impaired subjects 100
Figure 5.42 – Error percentage of step length estimated as a function of gyro peaks of vision impaired subjects 100
Figure 5.43 – Estimated step length *vs.* measured step length for step length as a function of gyro peaks of vision impaired subjects 100
Figure 5.44 – Normalised thigh angle, gyro signal and time derivative of gyro signal 103
Figure 5.45 – Thigh angle while standing, sitting and walking 106
Figure 5.46 – Indoor activity detection algorithm 107
Figure 5.47 – Envelope detected by the algorithm 108
Figure 5.48 – Walking detected by the algorithm 108
Figure 5.49 – Activities detected by the algorithm 108
Figure 5.50 – Pressure reading when walking on stairs 110
Figure 5.51 – Pressure reading on escalator going upwards and on travellator ramp going up and down 111

Figure 5.52 – Pressure reading when going down and up in an elevator 111

LIST OF TABLES

Table I – Duration of Sub Phases of Human Gait Cycle 11
Table II – Technical Details of YEI Technologies IMUs 41
Table III – Comparison of Key Specifications of the Inertial Sensors 42
Table IV – Stride-to-Stride Correlation Statistics of Vertical Acceleration and Roll of the Phone 51
Table V – Sample Results of One Subject 59
Table VI – Statistics of the Performance of the Algorithm for Different Activities 59
Table VII – Statistics of the Performance of the Algorithm for Walking on Flat Land with Different Stepping Rate 60
Table VIII – Correlation Statistics Between θ_{MAL} and θ_{IMU} 69
Table IX – Coefficients of Harmonic Models of the Six Common Thigh Angle Patterns 81
Table X – Coefficients of Harmonic Models of Gyro Signals of the Six Common Thigh Angle Patterns 83
Table XI – Phases of Gait Cycle as Identified in the Thigh Angle Waveform 103
Table XII – Signal Feature that can be Used to Detect Each Point of the Stride Cycle 104
Table XIII – Values Assigned for Activities 108
Table XIV – Overall Activity Detection Performance of the Algorithm 109

LIST OF ABBREVIATIONS

bpm	Beats per minute
CF	Complementary Filter
CSV	Comma Separated Value
DOF	Degree of Freedom
DSP	Digital Signal Processing
EKF	Extended Kalman Filter
FFT	Fast Fourier Transform
fps	Frames per second
FSR	Force Sensitive Resistors
GDOF	Gradient Descent based Orientation Filter
GIOF	Gyro Integration based Orientation Filter
GPS	Global Positioning System
I^2C	Inter IC
IC	Integrated Circuit
IMU	Inertial Measurement Unit
KF	Kalman Filter
Li-Po	Lithium Polymer
MAL	Motion Analysis Lab
MEMS	Micro Electromechanical Systems
RF	Radio Frequency
RFID	Radio Frequency Identification

RMSE	Root Mean Square Error
SPI	Serial Peripheral Interface
USB	Universal Serial Bus
UWB	Ultra–Wide Band
WiFi	Wireless Fidelity

LIST OF PUBLICATIONS

Publications Contributed to this Thesis

1. K. Abhayasinghe and I. Murray, "A novel approach for indoor localization using human gait analysis with gyroscopic data," Presented at Third International Conference on Indoor Positioning and Indoor Navigation (IPIN2012), 2012. [Online]. Available: http://www.surveying.unsw.edu.au/ipin2012/proceedings/submissions/22_Paper.pdf.
2. L. H. R. P. Chandrasiri and N. Abhayasinghe, "Portable Sensor Attachment," in *SAITM Research Symposium on Engineering Advancements – 2013*, Colombo, Sri Lanka, April, 2013, pp 37-40.
3. S. Jayalath, N. Abhayasinghe, "A Gyroscopic Data Based Pedometer Algorithm," in *The 8th International Conference on Computer Science & Education (IEEE ICCSE 2013)*, Colombo, Sri Lanka, April, 2013, pp 551-555.
4. R. Chandrasiri, N. Abhayasinghe and I. Murray. (2013, Oct.). "Bluetooth Embedded Inertial Measurement Unit for Real-Time Data Collection," in Forth International Conference on Indoor Positioning and Indoor Navigation (IPIN2013) [Online], Montbéliard, France, 2013, pp. 514–517. Available: http://ipin2013.sciencesconf.org/conference/ipin2013/eda_en.pdf [Nov. 19, 2013].
5. S. Jayalath, N. Abhayasinghe and I. Murray. (2013, Oct.). "A Gyroscope Based Accurate Pedometer Algorithm," in Forth International Conference on Indoor Positioning and Indoor Navigation (IPIN2013) [Online], Montbéliard, France, 2013, pp. 510–513. Available: http://ipin2013.sciencesconf.org/conference/ipin2013/eda_en.pdf [Nov. 19, 2013].
6. S. Jayalath, N. Abhayasinghe and I. Murray. (2013). "Accurate Pedometer for Smartphones," *International Journal of Systems and Control* [Online], 2013 vol. 1, Available: http://www.insightplanet.org/IJSC.html [Apr 3, 2014].
7. N. Abhayasinghe and I. Murray, "Human Gait Phase Recognition Based on Thigh Movement Computed using IMUs," in *2014 IEEE Ninth International Conference on Intelligent Sensors, Sensor Networks and Information*

Processing (ISSNIP) [Online], Singapore, April, 2014. Available: IEEE Xplore [Jun. 19, 2014]

8. N. Abhayasinghe and I. Murray, "The Application of "off-the-shelf" Components for Building IMUs for Navigation Research," Presented at Fifth International Conference on Indoor Positioning and Indoor Navigation (IPIN2014), Oct. 2014. [Online]. Available: http://www.ipin2014.org/wp/pdf/2A-3.pdf. [Accessed 1 Jul. 2015].
9. N. Abhayasinghe and I. Murray, "Human Activity Recognition Using Thigh Angle Derived from Single Thigh Mounted IMU Data," Presented at Fifth International Conference on Indoor Positioning and Indoor Navigation (IPIN2014), Oct. 2014. [Online]. Available: http://www.ipin2014.org/wp/pdf/2A-2.pdf.

Other Relevant Publications

1. K. Y. Chan, N. Rajakaruna, U. Engelke, I. Murray, N. Abhayasinghe, "Alignment parameter calibration for IMU using the Taguchi method for image deblurring," *Measurement*, vol. 65, pp. 207-219, 2015.
2. N. Rajakaruna, C. Rathnayake, N. Abhayasinghe and I. Murray, "Inertial Data Based Deblurring for Vision Impaired Navigation," Presented at Fifth International Conference on Indoor Positioning and Indoor Navigation (IPIN2014), 2014. [Online]. Available: http://www.ipin2014.org/wp/pdf/5C-2.pdf.

Chapter 1

INTRODUCTION

1.1 Introduction

285 million people of the world are estimated to be vision impaired: 39 million blind and 246 million with low vision [1]. According to the estimations of Vision Australia, 357,000 Australians are either blind or have low vision [2]. Moving through an unfamiliar environment is often difficult for people with limited or no vision. The situation is worse in indoors where landmarks have limited "uniqueness" (e.g. all halls appear similar). Although Global Positioning System (GPS) based navigation is possible outdoors for general navigation, the accuracy of GPS is not sufficient as a standalone system for vision impaired navigation [3] and the accuracy is not sufficient for indoor navigation and way finding even for non-vision impaired people because of its poor reception of satellite signals in indoors [4].

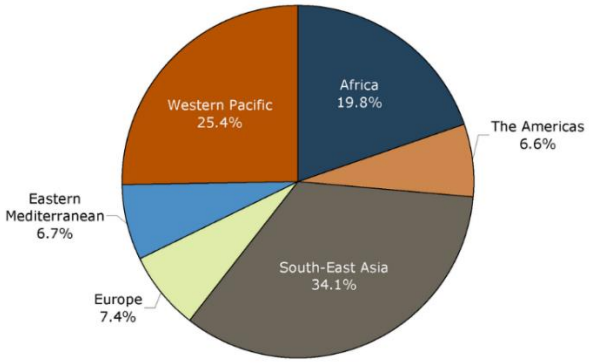

Figure 1.1 – Global distribution of vision impairment [5]

It is estimated that, about 90% of the vision impaired population of the world are known to have low income [1]. It can be seen in Figure 1.1 that majority of vision impaired population is from low income regions of world such as Africa and South East Asia, where funding is limited to support them [5]. Therefore, they are unable to afford high cost support devices for their day-to-day life activities. Given the low socio economic demographic of this group, any device developed for supporting them should be targeted to be low cost. The navigation system for vision impaired

people discussed in the next sub section examines these requirements. The research discussed in this thesis is a part of this project.

1.2 The Way-finding System for Vision Impaired

Most of traditional way-finding systems use heavy and bulky wearable computers that are inconvenient to be used by vision impaired people [6, 7, 8]. To the best of the author's knowledge, current research does not indicate to a practically usable indoor way-finding system for the vision impaired.

The work of this thesis is a part of the project described in this sub section that has aimed to develop a way-finding system for vision impaired that will guide them through an unfamiliar environment [8]. Key requirements of this project are low cost, portability and convenience of use, so that the vision impaired community can afford the system and get benefits from it. Figure 1.2 shows the overall system which consists of a centralised map generation system, two embedded devices: one for image and audio processing and the other for human gait analysis, and a smartphone for Human Computer Interface. The functional block diagram of the system is shown in Figure 1.3.

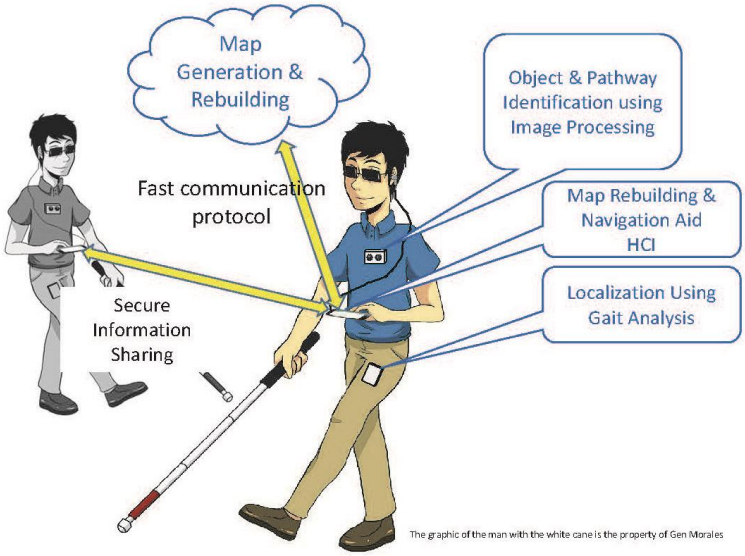

Figure 1.2 – Proposed structure of the Way-finding system for vision impaired [8]

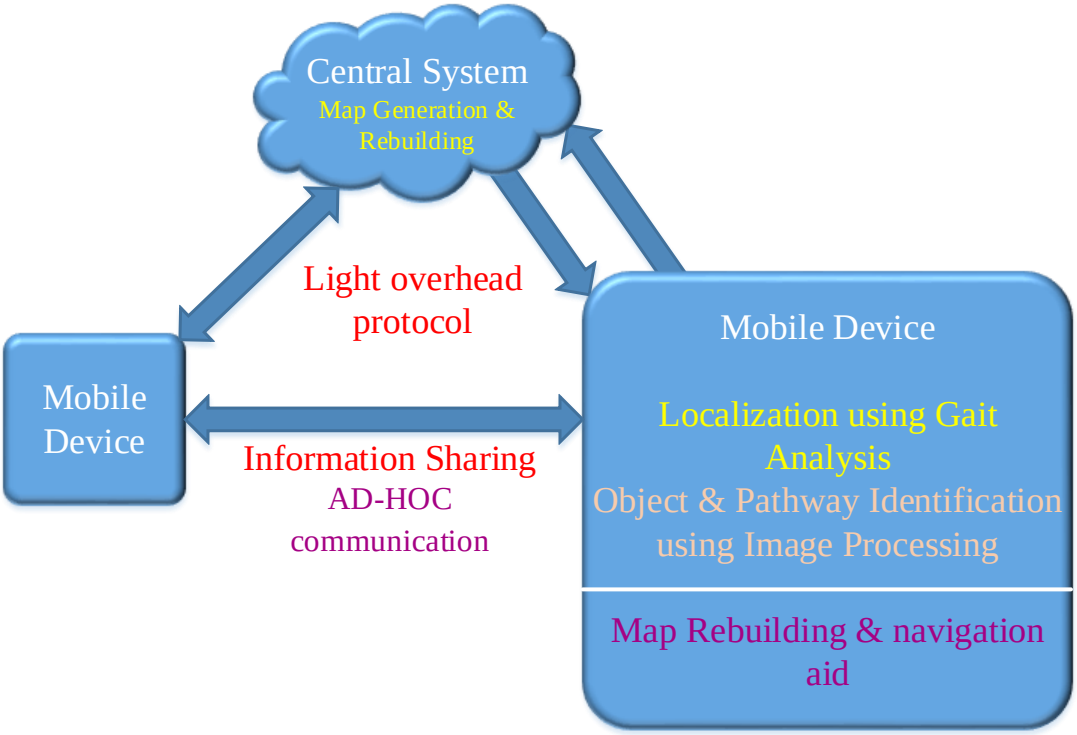

Figure 1.3 – Functional block diagram of the Way-finding system for vision impaired

The chest mounted device with stereoscopic camera and microphones is used to detect obstacles, pathways and landmarks using image processing techniques

while sound processing is used to identify sound generating landmarks of the environment the subject is navigating, such as elevators and public areas where many people are gathering, and to identify threats/risks such as vehicles [9]. The stereoscopic cameras are used to classify and estimate the distance to obstacles, alert the subject and update the centralised map.

The map system is self-building [10] and the map and other information related to navigation are collaboratively crowdsourced by all registered users. Any change in the system identified by the image processing unit will be passed to the centralized system so that the centralised map can be updated based on the trust of the particular sender and the number of repetitions of a given change by different users [11]. Information gathered and available with one user may be shared with other close by users of the system. The smartphone acts as the human computer interface, which is used to translate guidance information and alerts to the user as tactile, audio and voice messages. It is also used for running the map software navigation algorithms and as a communication device to transfer data to and from the centralised map server.

Displacement of the user is calculated by means of gait analysis and tracking with a single thigh mounted IMU (Inertial Measurement Unit) (placed in the trouser pocket or attached to the thigh). The step length and the direction are estimated from data collected from the thigh mounted IMU and the current position of the subject are estimated using a pedestrian dead-reckoning approach.

1.3 Problem Statement

The gait analysis component of the project discussed in Section 1.2 is addressed in the research discussed in this thesis and following are the problems addressed in this research.

- The accuracy of step detection (pedometer) algorithms is very poor at slow walking speeds. There is a high need of developing an accurate pedometer to improve the accuracy of way-finding in indoor pedestrian navigation systems and many other uses.

- Almost all indoor navigation systems are costly and therefore unaffordable to the vision impaired community. In reducing the cost, the algorithms used in wayfinding systems have to require lower computational resources. Almost all existing algorithms used for orientation estimation require high computational resources (when a mobile platform is considered) that increases the cost of the system as well as its weight. Therefore, a less computationally expensive orientation estimation algorithm, without compromising the estimation accuracy, is required to cater this constrain.
- Most human gait analysis approaches for navigation purposes using MEMS (Micro Electro-Mechanical Systems) sensors are based on acceleration measurements of a section of body. Acceleration measured by an accelerometer consists of both gravity and the linear acceleration of the section of the body onto which the sensor is attached. For accurate modelling of gait based on the acceleration, the gravity component has to be removed from the accelerometer reading. The gravity read by each axis of the accelerometer is neither a constant, nor a slow varying component due to the fast rotary movement of the sensor during human walking, which makes removal of gravity a difficult task. Therefore, complex algorithms are required for accurate removal of gravity component that results in costly hardware. Hence, there is a requirement of identifying gait modelling techniques that avoids accurate estimation of gravity.
- Continuous estimation of the step length improves the accuracy of approximation of the distance travelled by the user. Most of step length estimation techniques are either based on fixed step length or based on acceleration measurements. Hence, in this case too, higher amounts of computations required for accurate acceleration estimations limit the existing techniques being used in low cost devices. Therefore, a simple model for step length with minimal computation requirements is a requirement for accurate step length estimation in inertial navigation systems.

- Knowing the activity performed by the user helps avoiding false propagation estimates in navigation systems. Hence, accurate activity recognition helps improving the accuracy and performance of human tracking systems. Light weight activity recognition algorithms without compromising the accuracy of recognizing activities is another requirement for a low cost navigation aid.
- Existing step detection and gait analysis techniques use intense computations that restricts them being implemented in low cost processors. Therefore, existing techniques and algorithms are not favourable in navigation aids for vision impaired. Hence, there is a great requirement of developing algorithms that demand minimal computational resources so that they can be implemented in low end devices. However, the accuracy cannot be compromised.

1.4 Objectives of this research

The main objective of this research is to develop a model to estimate the step length of each step during walking by taking the thigh movement as the input such a way that this can be used for estimating the displacement of a vision impaired subject within the environment, who is navigating in an unknown environment. The specific outcomes of this study are as follows:

1. Design and develop a robust and accurate step detection (pedometer) algorithm to detect steps accurately even at low walking speeds.
2. Formulate efficient and accurate techniques for estimation of flexion and extension angles of the thigh during walking and validate them against standards.
3. Mathematically model human gait during walking.
4. Formulate algorithms to identify the activity the subject is performing.
5. Formulate a model to estimate the step length taking the thigh angle and/or gyroscopic data as the input.
6. All algorithms be computationally light weighted so that they can be implemented in low end hardware.

1.5 Novel Approaches Presented in this Thesis

This thesis presents several novel approaches and directives in human gait analysis. The step detection algorithm presented in this thesis uses single axis gyroscopic signal of a single thigh mounted IMU and achieved close to 100% accuracies in practical tests. To the author's best knowledge, the technique used in the pedometer algorithm is a novel directive and there are no other pedometer technique that could achieve this level of accuracy.

Human gait during level walking was modelled based on thigh angle and the gyro signal read by a thigh mounted IMU with above 99% regeneration accuracies. Modelling human gait based on the gyro signal measured from a thigh mounted IMU (angular velocity of the thigh) and the thigh angle is also a novel approach according to the author's best knowledge.

Further, the thigh angle estimation algorithm presented in this thesis is also a novel approach where the estimation of the angle is based on the integration of the gyro signal and only the integration drift correction is done with the angle calculated from the accelerometer signal.

The main concern in developing these techniques was that the algorithms to be demanding minimal computational resources, so that they can be implemented on low cost hardware. Although all these approaches are proven to be demanding less computational resources compared to techniques such as Kalman filters, and are novel techniques, they have demonstrated significantly higher accuracies compared to existing techniques.

1.6 Outline of the Thesis

This thesis is organised in six (6) chapters as listed.

- Chapter 2 (Human Gait and Existing Technology and Work on Gait Analysis and Pedestrian Navigation) presents the details of the human gait cycle, techniques used and technology currently available for human gait analysis.
- Chapter 3 (Methodology) explains the methodology used in this research.

- Chapter 4 (Experimental Platform) details the development of the hardware and software for data capture. It also discusses the details of the optical motion capture systems used to validate the orientation estimation technique used in this research.
- Chapter 5 (Gait Modelling and Algorithms) presents the main contributions of this research, namely, the step detection algorithm, the thigh angle estimation algorithm, the harmonic model for human gait, the activity detection algorithm and the step length estimation model.
- Chapter 6 summarises the thesis with main conclusion and some recommendations for future directives of research.

Chapter 2

HUMAN GAIT AND EXISTING TECHNOLOGY AND WORK ON GAIT ANALYSIS AND PEDESTRIAN NAVIGATION

2.1 Introduction

Human gait analysis for the purpose of pedestrian tracking and navigation is the main theme of this research. Thus an understanding of human gait cycle, motion tracking and capture techniques, and orientation estimation is important in developing novel techniques for gait analysis. Details about human gait and techniques used for gait capture, analysis and modelling are discussed in this chapter.

Human gait cycle is introduced in this chapter with details of its main phases and sub phases to provide an understanding of how a human walks and possible patterns that may be used to characterise human walking.

A variety of different methods are used in different subject areas for human motion tracking and capture. Each of these method has their own characteristics, purposes of usage, advantages and disadvantages. Details on these techniques with the situations and targeted application they are used for and their advantages and disadvantages are also discussed in this chapter.

The major areas investigated in this work are pedometer algorithms, orientation estimation algorithms, gait modelling, continuous step length estimation and human activity recognition. Details of some key examples available in literature on each of these topics are discussed in this chapter with the methods they have used, the features of these techniques and limitations of these techniques that restricts them being used in low cost systems.

2.2 Human Gait Cycle

Walking is the coordinated movement of limbs for the purpose of moving the body forward, while maintaining the stance balance. Gait is the pattern of moving a leg during walking and is repetitive [12].

The human gait cycle is defined as the period starting with an initial floor contact of one heel (Initial Contact) to the next similar posture. A gait cycle can be divided into two main phases: Stance and Swing. During Stance, the reference foot is in contact with the ground while the other foot is in swing, and Swing is where the reference foot is swinging over the ground while the other foot is in contact with the ground [12] as shown in Figure 2.1. The Stance phase is further divided into five sub phases: Initial Contact, Loading Response, Mid Stance, Terminal Stance and Pre-Swing whereas the Swing phase is further divided into three sub phases: Initial Swing, Mid Swing and Terminal Swing. Figure 2.2 shows the eight sub phases of the human gait cycle.

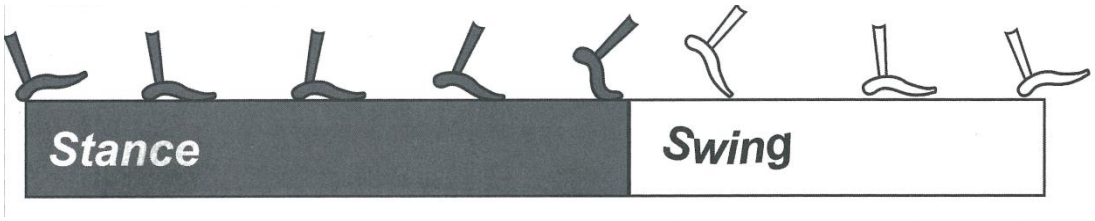

Figure 2.1 – Main Phases of the Gait Cycle [12]

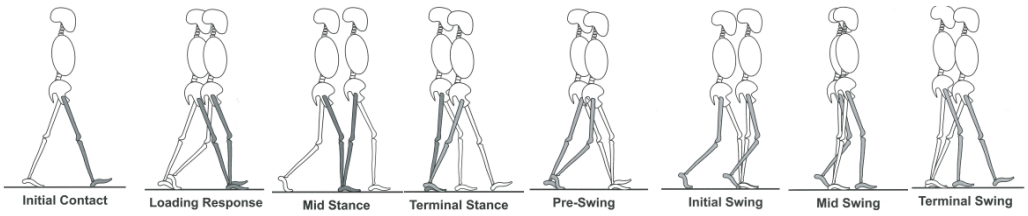

Figure 2.2 – Eight Sub Phases of the Gait Cycle [12]

Initial contact is the moment at which the heel of the reference leg contacts the ground and the other leg is by the end of Terminal Stance phase. The reference foot goes from heel contact to full foot contact during the Loading Response phase while the other leg has the Pre-Swing. By the end of the Loading Response, the body weight is fully transferred to the reference leg (known as single limb support) and during Mid Stance the body weight is tolerated by the reference leg while the other leg is in Initial Swing and Mid Swing phases. During the Terminal Stance, the heel of the reference leg starts moving away from the ground while the toe is still on the ground and the other leg is in Terminal Swing. By the end of the Terminal Stance of the reference leg, the other leg gets the Initial Contact. The last sub phase of Stance,

Pre-Swing, is where the reference foot moves further keeping the toe on the ground while the other leg is in Loading Response. During Initial Swing, Mid Swing and Terminal Swing phases, the reference leg is swinging above the ground while the other leg undergoes in Mid Stance and Terminal Stance phases. Table I shows the duration of each sub phase of the gait cycle as a percentage of the gait cycle.

TABLE I – DURATION OF SUB PHASES OF HUMAN GAIT CYCLE [12]

Sub Phase	Interval (of Gait Cycle)
Initial Contact	0% – 2%
Loading Response	2% – 12%
Mid Stance	12% – 31%
Terminal Stance	31% – 50%
Pre-Swing	50% – 62%
Initial Swing	62% – 75%
Mid Swing	75% – 87%
Terminal Swing	87% – 100%

2.3 Motion Tracking and Capture Technology

2.3.1 Introduction

Motion tracking and capture technologies vary from simple mechanical systems to high end optical motion capture systems. It can be seen in the literature that different motion capturing and tracking techniques are used depending on the nature of the application and accuracies required in the particular application. Different technology used for capturing and tracking motion for navigation and clinical/rehabilitation applications, with their features and characteristics, are discussed in this sub section.

2.3.2 Visual Measurements

The most fundamental measurement technique for taking joint movement measurements is by observation. Although it is not an appropriate technique for measurements in real–time applications, visual measurements are not uncommon in clinical and rehabilitation research. [13] and [14] are evidences for the usage of visual measurements in clinical research where the measurement is taken by a

specialist. Although both these report inter-measurement correlations above 79%, [14] reports more than 5% error between visual estimate and the actual value in 45% of the samples.

2.3.3 Mechanical and Electro–Mechanical Apparatus

A goniometer (Figure 2.3) is one of common angle measuring apparatus used to measure flexion and extension angles of joints in clinical and rehabilitation research. Watklns *et al.* reported above 98% intratester reliability and above 85% intertester reliability for knee angle measurements using goniometers [13]. However, Edwards *et al.* have reported that 22 % of the measurements taken for 27 knees in 16 patients were with 5º or more error [14]. Although 5º is an acceptable level of error, the mechanical goniometer cannot be used in real-time application such as pedestrian navigation, because there is not any means of taking the reading electronically. However, they are suitable for rehabilitation application where the measurement is taken when the subject is stationary.

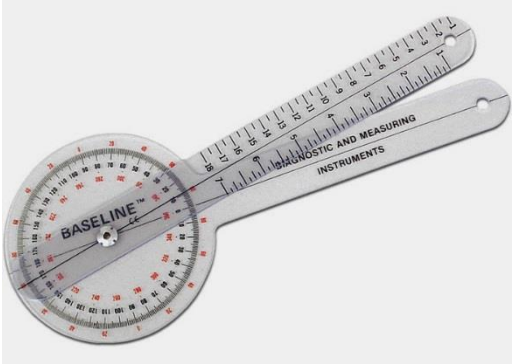

Figure 2.3 – Goniometer

However, electro–goniometers may be used in navigation applications. An electro-goniometer is a device similar to a mechanical goniometer with possibility of taking the measurement electrically by means of a potentiometer or a strain gauge. Electro–goniometers are often used in clinical tests to capture continuous motion of a joint. In [15], the authors have used an electro–goniometer as a reference for knee angle estimation using accelerometers and gyroscopes attached to the thigh and shank. To increase the accuracy of the goniometer reading, they have calibrated the goniometer before each sit–stand trial.

Force sensors, bend sensors and pressure sensors are some other methods used in research to identify foot contact with the ground. The work discussed in [16] used these sensors to detect which areas of the foot are contacted with ground and to detect the bending of the foot. The work discussed in [17] also used pressure sensors to detect the foot contact. This has been used to identify the acceleration pattern at the heel contact point. Although these devices make identification of key points of stride cycle easy, wearing these devices on the foot or shoes is not convenient. These devices may be effective in clinical tests, but become un-usable in real-time application due to inconvenience of wearing them.

2.3.4 Optical Motion Capture Systems

Optical motion capture systems are used extensively in gait analysis research both in navigation and clinical/rehabilitation applications. [18], [19] and [20] are examples that use optical motion capture systems for taking measurements as well as a baseline system. The development of an optical motion capture system and the algorithms used for real–time estimation of the marker coordinates in the space with reference to a calibrated origin are discussed in [21]. This system uses 6 cameras to record the position of reflective markers in the frame and use a server system to record data and estimate the positions of the markers.

Vicon [22], Tracklab OptiTrack [23] and Qualisys Oqus [24] are some examples for commercially available optical motion capture systems. These systems estimate the coordinates of retro–reflective markers with respect to a pre–calibrated origin of the environment. A number of Infra–red (IR) cameras equipped with IR emitters are used to illuminate markers and capture their positions. Triangulation techniques are used to estimate the coordinates of each marker and all other motions are estimated based on the marker coordinates. These systems are capable of capturing data at rates of several hundred frames per second (fps). Windolf *et al.* have reported an overall accuracy of 63±5 μm and overall noise level of 15 μm for Vicon-460 system with four cameras [25].

Optical capture systems provide higher accuracy in position and angular estimates compared to other techniques. However, these systems are suitable for laboratory experiments and are not usable outside the laboratory. Further, the activity

area is limited to few cubic meters. Hence, optical motion capture systems are not usable in real-time applications such as pedestrian navigation.

2.3.5 Inertial Sensors

Inertial sensors are the main signal source in most infrastructure–free navigation systems. In addition to navigation systems, inertial sensors are now increasingly be used in clinical and rehabilitation studies [26, 27, 28, 29]. The three main sensors used in inertial systems are accelerometer, gyroscope and magnetometer. This sub–section discusses the measurements that may be taken using each of these sensors, error components of those and techniques that may be used to minimize those errors.

Accelerometers

Accelerometers measure the linear acceleration asserted on the sensor [30]. As gravity is also a linear acceleration, the reading includes gravity. It should be noted that the gravitational acceleration is read as $-g$ towards earth due to the construction of an accelerometer [30]. Accelerometers may have one, two or three mutually orthogonal axis of measurement. The measurement of the i^{th} axis (where $i = x, y, z$) can be given by the simplified error model given in equation (2.1) [31].

$$\tilde{a}_i = a_i + S_i a_i + B_f + n_i \tag{2.1}$$

where $\tilde{a}_i$ is the acceleration output for the i^{th} axis, a_i is the acceleration applied along the i^{th} axis, S_i is the scale factor error (usually presented as a polynomial to include the non-linear effects), B_f is the zero–offset bias of the measurement and n_i is the random noise. The scale factor error, the zero–offset bias and the random noise are depicted in Figure 2.4. The scale factor error and the zero–offset bias can be compensated by laboratory calibration whereas a filter has to be used to filter out the random noise.

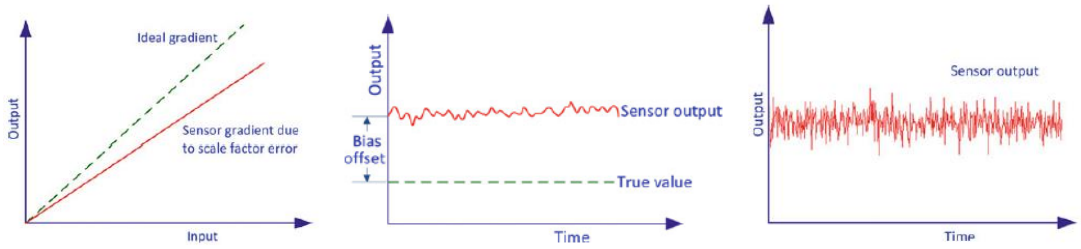

Figure 2.4 – Error present in inertial sensor output [30]

Scale factor error (left), Zero–offset bias (centre), Random noise (right)

Gyroscopes

Gyroscopes measure the angular rates with respect to an inertial frame of reference [30]. The direction of the angular velocity vector follows the right hand rule as shown in Figure 2.5 [32]. The word *gyro* is often used as a short form of the word *gyroscope*. In this thesis, these two words are interchangeably used. As there are no static rotations in the environment, a gyro does not read any environmental data as the accelerometer does with gravity. Therefore, the angular rate measured by the gyro is purely the angular rate of the device. However, there are error components contained in the gyro output, such as in the accelerometer. The angular rate measurement of the gyro along i^{th} axis (where $i = x, y, z$) can be given by the simplified error model:

$$\tilde{\omega}_i = \omega_i + S_i\omega_i + B_f + n_i \tag{2.2}$$

where $\tilde{\omega}_i$ is the angular velocity output for the i^{th} axis, ω_i is the angular velocity applied along the i^{th} axis, S_i is the scale factor error, B_f is the measurement zero–offset bias and n_i is the random noise [31]. Similar to the accelerometer, the scale factor error and the measurement zero–offset can be compensated by a laboratory calibration and the random noise by filters.

Although equations (2.1) and (2.2) illustrate the noise models for accelerometer and gyroscope respectively for most applications, there are many other noise types that may exist in these sensors. These errors are discussed in detail in [30].

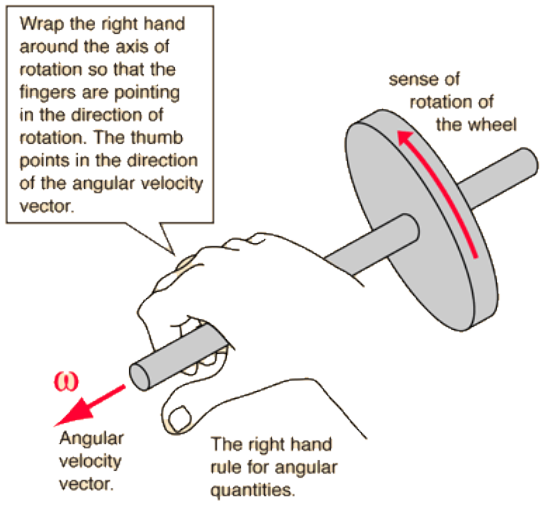

Figure 2.5 – Vector Direction of the Angular Velocity Following the Right Hand Rule [32]

Magnetometers and e-Compasses

Magnetometer measures the magnetic field along its three axes. Magnetometers are used in conjunction with accelerometer to estimate the north heading. An e-Compass is a device that directly gives the north heading reading [30]. Both these devices read the magnetic north and therefore, a correction is necessary to derive the geographic north heading. One main drawback in estimating north heading using these devices is that their reading is susceptible to ambient magnetic fields such as electromagnetic noise [30]. Further details on magnetometers and e-compasses are excluded as the focus of this research is on flexion/extension estimation of the thigh and hence pitch/roll estimation is sufficient.

2.4 Existing Work in the Literature

2.4.1 Techniques Used for Pedestrian Localization

For the purpose of this discussion, localization and tracking techniques used in indoor navigation systems may be divided into two main categories: infrastructure based and infrastructure free. Infrastructure based techniques use one or many pre-installed equipment, such as Radio Frequency Identification (RFID) tags [33], Ultra-Wideband (UWB) Radio Frequency (RF) signals [34], pre-installed markers in the environment [35], a pre-photographed environment [36], supplied maps (as in google indoor maps) and WiFi networks [37]. These systems give better localization

accuracies due to the fact that they have a reference system provided by the pre-installed units. Ultrasound has the highest localisation accuracy of 1 cm among these techniques, while UWB being the next with 15 cm accuracy [5]. However, the major issue with these systems is the need of pre-installed hardware in the building, which limits the availability of these systems. It should be noted that installing hardware to the building needs capital investment as well as the contribution and participation of building owners/ managers.

Alternatively, the infrastructure free techniques do not require any pre-installed components in the environment. Many of these techniques include Inertial Navigation systems that use inertial sensors to measure the movement of the human body during human locomotion and predict the distance and direction travelled. Some of these systems use standalone sensors or IMUs [6, 7, 38] while the others use inertial sensors available in mobile phones [39, 40, 41, 42, 43]. The advantage of these systems is the lower implementation cost compared to infrastructure based systems and they don't require any additional components be installed in the building, which makes them more flexible. However, the benefit of not having to implement any infrastructure for inertial navigation systems comes at the cost of their lower accuracies compared to some infrastructure based systems due to the fact that they do not have a well-defined origins and reference points.

2.4.2 Step Detection

Accurate step detection is a critical component of an inertial pedestrian navigation system. A Pedometer is a device that is used for detecting steps, usually in exercise activities like running and jogging. With increasing usage of smartphones consisting built-in inertial sensors, usage of pedometer software have also become popular. However, although these software and hardware pedometers perform sufficiently accurate when performing exercise activities, they perform very poor at slow walking speeds that are usually observed in indoor navigation, particularly for the vision impaired [44, 45, 46, 47, 48].

Jerome and Albright [44] have compared the performance of five commercially available talking pedometers with the involvement of 13 vision impaired adults and 10 senior adults, and observed that the step detection accuracy for all of them were poor (41 – 67%) while walking on flat land and the situation was

deteriorated when ascending stairs (9 – 28%) or descending stairs (11 – 41%). Crouter *et al*. [45] have compared 10 commercially available electronic pedometers and confirmed that they underestimate steps in slow walking. Garcia *et al*. [46] have compared the performance of software pedometers and hardware pedometers and observed that both these types are comparable in all walking speeds and both types have demonstrated poor accurately in slow (58 to 98 steps·min^{-1}) walking speeds: 20.5% ± 30% for hardware pedometer and 10% ± 30% for software pedometer.

Waqar *et al*. [47] have used an accelerometer based pedometer algorithm with fixed threshold in their indoor positioning system. They have reported a mean accuracy of 86.67% in their 6 straight walk trials of 40 steps each, with a minimum accuracy of 82.5% and a maximum of 95%. The median accuracy was 85%. Having a 15% error in the step count is not appropriate for vision impaired navigation.

A Smartphone pedometer algorithm based on an accelerometer is discussed by Oner *et al*. [48] and their algorithm demonstrated better accuracies at walking speeds higher than 90 beats per minute (bpm) (or steps per minute), but its performance degrades as speeds fall below 90 bpm. Their algorithm has over counted steps and the error was approximately 20% at 80 bpm, 60% at 70 bpm and 90% at 60 bpm.

Lim *et al*. [49] have proposed a foot mounted gyroscope based pedometer, but the authors have not mentioned the accuracy of their system. Further, they use force sensitive resisters (FSR) to detect the toe and heel contacts, and hence the accuracy of step detection should be higher as they can easily detect the Initial Contact using the FSR. Using many devices to measure parameters at the foot is not very convenient and having these additional sensors at the foot increases the number of wires required from them to the controller of the system.

Ayabe *et al*. [50] have examined the performance of some commercially available pedometers in stair climbing and bench stepping exercises and reported that the pedometers could count steps with an error of ± 5% at speeds of 80 to 120 steps·min^{-1}. However, the accuracy was poor for short step sizes and lower stepping rates (> ± 40% at 40 steps·min^{-1}).

Most of the examples discussed here used accelerometer data to detect steps and they perform poorly at slow walking speeds. The main reasons for this poor performance at low speeds are the static value (gravitational acceleration) present in the accelerometer, slow response of accelerometer and that most of these algorithms cannot adopt their threshold levels to suit with the pace of walking. This indicates the requirement of developing a step detection technique that can perform accurately at all walking speeds including slow walking.

2.4.3 Estimation of Orientation

2.4.3.1 Introduction

This research focused in gait analysis and modelling using signals of a single thigh mounted IMU. In addition to the raw sensor signals, the thigh angle was also considered as a possible parameter for modelling. Orientation estimation algorithms are used to estimate the thigh angle from the raw sensor signals. The following discussion summarises the basics on orientation estimation and different techniques used in orientation estimation using inertial sensors.

2.4.3.2 Orientation Estimation using Inertial Sensors

There are several methods of representing the orientation of a system. Some of them are using Euler angles, Quaternions and axis angles [51]. Out of these methods, this thesis uses Euler angles because of its simplicity. Although Euler angles suffer from a phenomenon called *Gimbal Lock* when the pitch angle is at ±90º [51, 52], this is not a problem for the work discussed in this thesis as the flexion and extension of the thigh does not reach 90º. The three orientation angles, Pitch, Roll and Yaw are defined as shown in Figure 2.6. Out of these three angles, pitch and roll estimations are considered in this thesis. The estimation of these two angles may be done using three methods: using accelerometer measurement only, using gyroscopic measurement only and using both accelerometer and gyro measurements [53]. These three techniques with their advantages and drawbacks are discussed in the following sub sections.

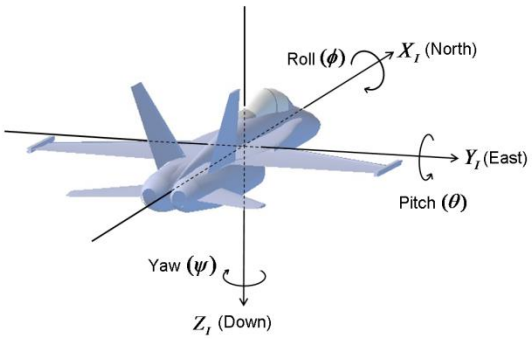

Figure 2.6 – The Inertial Frame [52]

Estimating Angles with Accelerometer

The pitch ($\hat{\theta}_{accel}$) and the roll ($\hat{\phi}_{accel}$) can be estimated using the *x*, *y* and *z* measurements of the accelerometer as given by equation (2.3).

$$\hat{\theta}_{accel} = \arcsin\left(\frac{a_x}{g}\right)$$
$$\hat{\phi}_{accel} = \arctan\left(\frac{a_y}{a_z}\right) \tag{2.3}$$

where a_x, a_y and a_z are the acceleration measured along *x*, *y* and *z* axis by the accelerometer and *g* is the gravitational acceleration [53]. These angles are accurate if the accelerometer is only reading gravity. However, when there is an additional acceleration on the body, by means of vibration or external force, then the results will be affected, making them unusable in most cases.

Estimating Angles with Gyroscope

The gyroscope can also be used to estimate the pitch and the roll. Rate gyros are normally unaffected by acceleration, which makes gyro-based angle estimates immune to external forces. Therefore, gyro-based angle estimated are usable in situations where accelerometers cannot be used for angle estimations. If the pitch and roll are as defined before and the rate gyros are sampled at a fixed interval *T*, the new estimates of pitch and roll, $\hat{\theta}^+$ and $\hat{\phi}^+$, can be estimated using Euler Integration as [53]:

$$\begin{aligned}\hat{\theta}^{+} &= \hat{\theta} + T\dot{\theta}, \quad \text{and} \\ \hat{\phi}^{+} &= \hat{\phi} + T\dot{\phi}\end{aligned} \tag{2.4}$$

where $\hat{\theta}$ and $\hat{\phi}$ are the previous estimates of pitch and roll angles, and $\dot{\theta}$ and $\dot{\phi}$ are the angular velocities along pitch and roll axes.

Although the angle estimated by this method is immune to external forces, if even a small error exists in the gyro measurement can cause the angle to drift due to integration of the error [51, 53]. It is also clear that the initial angle should be known to estimate the pitch and roll using equation (2.4). As each method described earlier has its own advantages, disadvantages and limitations, fusing (mixing) the accelerometer and gyroscope measurements can increase the accuracy and reliability of the angle estimates [51, 53]. In fact, the drift caused by the gyro integration is corrected by the angle estimated by the acceleration. Following is a discussion of some techniques used to fuse accelerometer and gyroscope measurements.

Sensor Fusion for Improved Angle Estimation Accuracy

It was seen in the previous discussion that estimating pitch and roll using either acceleration or angular rate only has their own limitations, which can be compensated by fusing gyro and acceleration data. The method used for this is that the angle derived using gyro measurement is corrected using the angle derived using acceleration. The fused pitch and roll angles ($\hat{\theta}$ and $\hat{\phi}$) can be estimates as shown in equation (2.5) [53].

$$\begin{aligned}\hat{\theta} &= \hat{\theta}^{+} + L\left(\hat{\theta}_{accel} - \hat{\theta}^{+}\right) \\ \hat{\phi} &= \hat{\phi}^{+} + L\left(\hat{\phi}_{accel} - \hat{\phi}^{+}\right)\end{aligned} \tag{2.5}$$

All terms in equation (2.5) are as defined for (2.3) and (2.4), except *L*, which is the fusing factor. *L* is a constant that takes a value between 0 and 1 (inclusive) for the Complementary Filter (CF) [54]. When $L = 0$, the angle estimation is purely on Euler Integration and when $L = 1$, it is purely on acceleration and takes more contribution from Euler Integration when *L* is close to 0 and from angle estimated from acceleration when close to 1. CF is known to be fast and simple method for fusing gyro measurement and acceleration to estimate tilt angles.

The Kalman Filter (KF), on the other hand, has a dynamically selected *L* [53, 54]. The advantage of KF is that the parameters can be selected to constrain the outputs within certain range, rate of change, directions, etc. so that the estimated angles have better accuracy [30, 54]. However, it can be seen that the KF implementations have a greater number of computations compared to the CF [26, 54].

Gradient Descent based Orientation Filter (GDOF) [55] (also known as Madgwick Filter) is another comparatively efficient orientation estimation algorithm. It may be seen that the accuracy of GDOF falls below Extended KL (EKF) [56].

2.4.3.3 Existing Work on Orientation Estimation

Much of previous work available in literature on orientation estimation of IMUs and techniques used in commercially available IMUs are based on Kalman filters. Although Kalman filters give a much better accuracy of output, they require a number of matrix computations to be performed [26]. Performing many matrix calculations require longer processing times, especially in low end (8-bit) microcontrollers.

Won *et al*. have used a Kalman Filter in combination with a Particle Filter in their orientation and position estimation technique [26]. Their experiments have shown that they can estimate pitch and roll with errors less than 1º with the proposed method when the initial orientation is known. They have reported errors greater than 2º for EKF. However, this has been achieved with the expense of high computational cost. They have executed their computations in an Intel Core2 Duo Processor E8400 with 3 GB memory and the execution times were greater than 40 s. As 40 s is a significantly longer time as far as walking rates (approximately 60 steps per minute) are considered, this system is not practically usable in real time navigation systems at this time. It is obvious that the time taken for the processing will be much longer when implemented in a low end embedded system.

Luinge and Veltink have discussed a human body segment orientation measurement technique using an IMU, where they have used Kalman filtering to fuse gyroscope and accelerometer to derive roll and pitch of the device [57]. They have compared the error of orientation estimated by sensor fusion against the orientation error when only accelerometer or the gyroscope is used to estimate the orientation.

The authors have observed about 3º Root Mean Square Error (RMSE) for the forearm where the movement is the highest, compared to about 2º and 1º RMSE for trunk and pelvis respectively, with their Kalman filter implementation. The root mean square value of the inclination error is about 10º for the forearm when only accelerometer was used to estimate the inclination.

YEI Technologies use Kalman filters to compute the orientation of YEI 3-space sensors [58]. These sensors contain high end microcontrollers, which contribute to the relatively high price of US$ 150 for the basic version without wireless connectivity.

Complementary Filter [54] and Gradient Descent based Orientation Filter (GDOF) [55] are two less computationally expensive alternatives for orientation estimations of low cost IMUs. Alam *et al*. have compared the accuracy of explicit complementary filter (ECF) and GDOF with both simulated data and data collected with a MPU-6050 IMU [56]. They have reported errors in the scale of 10º for GDOF and 5º for ECF for the roll angle and 5º and 2º for GDOF and ECF respectively for pitch angle with simulated data. However, they have not reported error characteristics for these filters for data measured with MPU-6050. Further, the movements they have considered were simple roll and pitch movements where the orientation remains constant for some period after a change. Estimating orientation accurately is easier in this scenario as the accelerometer gives a stable value when stationary.

GDOF is used in x-IMU [59] for its orientation estimations and it uses a microcontroller with a DSP as the processor. The cost of x-IMU is £249.

Orientation estimation techniques discussed earlier are suitable where higher accuracy is needed and the computational expense is not of concern. However, the main concern of the vision impaired navigation system was the cost which drove the focus of the project to find less computationally expensive techniques for pedestrian tracking. Further, the positioning of the sensors has to be convenient for vision impaired people as they may have difficulty with accurate placement of said devices.

2.4.4 Human Gait Modelling

A number of different approaches are available in literature for detecting and modelling of human gait. They are generally based on the hip, chest, foot or thigh movements. Some work exist in literature use optical tracking systems to track the motion for the purpose of gait modelling/analysis while others use inertial sensors to track motion. Majority of existing research that use inertial sensors recognise or model gait based on the acceleration of a particular section of the body. With the increasing availability of low cost gyroscopes, the usage of them in addition to accelerometers has increased. Although, availability of literature for gait analysis and modelling using gyroscopes or gyroscope-accelerometer combination was limited by the time of the commencement of this research, literature is becoming increasingly available.

Although many other mathematical [60] and mechanical [61] models are available in literature, the discussion of those is excluded in this thesis as they are purely theoretical approaches. The examples discussed next are modelling techniques based on experimental data.

2.4.4.1 Gait Analysis using Optical Motion Capture Systems

Literature suggests that optical systems have been used for gait analysis for a significant time in the history. M. P. Murray (in 1967) has presented the ranges of normal values for 20 simultaneous gait components including the displacement patterns of head, neck, trunk and upper and lower limbs [18]. In this study he has used interrupted-light photography to capture the motion of different sections of the body of subjects walking in front of a camera. Reflective markers have been attached to specific anatomical landmarks and a strobe light flashing 20 times per second allowing 20 samples per second capture rate. Images captured have been used to measure the angles of motion of all considered sections of the body. The movement curves presented in this paper may be considered as a norm for that age group because the measurements have been taken from 60 normal men from 20 to 65 years of age.

Geisheimer *et al.* have presented a high resolution Doppler model for human gait [19]. The authors have used an infrared motion capture system to derive the Doppler model. In order to identify the patterns in the Doppler spectrum, they have

compared the outputs generated using this model with the data recorded from the Doppler radar system. In this work, they have tried to identify the motion of different sections of the body during walking by means of the Doppler spectrum. However, it is observed in the paper that these patterns are not very clearly visible in the Doppler spectrum.

According to literature, many researches have used optical tracking systems to study joint angles during gait, which is generally used in clinical applications. These usually do not discuss any other modelling other than gait pattern recognition. Due to immobility of optical motion capture systems, they cannot be used in navigation applications. However, optical systems are used as reference for validation purposes of the navigation techniques being developed by researchers.

2.4.4.2 Gait Analysis using Inertial Sensors

Techniques using inertial sensors, accelerometers in particular (due to their high availability in the past compared to gyroscopes and low cost), are often used in navigation research due to their higher portability. With recent increased availability of low cost MEMS (Micro Electro-Mechanical Systems) gyroscopes, the usage of gyroscope in gait analysis and modelling has increased in the recent past. Some commonly used gait analysis and modelling techniques available in literature using accelerometers, gyroscopes and combinations of those are discussed in this sub section.

Tong and Granat have utilised two single–axis gyroscopes to analyse movement of the thigh and the shank during walking [62]. They have estimated the thigh and the shank inclination and the knee angle and validated the results against an optical tracking system. The paper also presents the angular velocity of the thigh and the shank as a time series during a stride cycle. The scope of this work was identifying normalized waveform patterns for inclinations and angular velocities of the thigh and shank. They have used two techniques to compensate the integration drift: automatically resetting the angle at each gait cycle and low pass filtering. The authors have achieved correlation coefficients above 0.90 between the angles and angular velocities derived using their techniques and these values derived from the optical tracking system.

A personal positioning system based on walking locomotion analysis is presented in [36]. In this work, authors have used a hip mounted accelerometer and a gyroscope for estimating acceleration of the body accurately. They have estimated the gravitational vector using both accelerometer reading and gyroscope reading using a Kalman filter so that the linear acceleration components of the hip can be estimated with better accuracy. In this work too, the gait modelling is based on acceleration and the distance travelled is formulated as a function of the hip acceleration. They have recognized the activities (flat walking, climbing stairs and using an elevator) with above 85% accuracy.

Bamberg *et al.* presented a gait analysis technique using shoe–integrated inertial sensors [16]. They have detected heel–strike and toe–off as well as estimated foot orientation and position. They have utilised force sensors, bend sensors, pressure sensors and electric field height sensors in addition to accelerometers and gyroscopes to identify the key calibration points of the stride cycle such as heel contact and toe off. Although this may permit detecting many gait phases, it increases the complexity of the system as well as the system becomes uncomfortable to the use. The results have been validated against an optical motion analysis system and the RMSE reported for the pitch is 5.2 ± 2.0^{o} (for 195 samples) and the RMSE for the displacement is 8.5 ± 5.5 cm.

Zijlstra and Hof have modelled spatio-temporal gait parameters based on a single 3–axis accelerometer [63]. In this paper, they have studied the acceleration pattern of the pelvis (hip) along all three axes during the gait cycle. They have modelled step length and walking speed as functions of hip displacement derived from the hip acceleration. The hip displacement is derived by double integrating acceleration. The error between the estimated and measured step length and walking speed were lower than 16%. This level of error in a navigation system is not desirable especially when used by vision impaired due to the fact that as they cannot see the environment, they may end up in a disaster such as falling off an edge or a step.

Ibrahim has used a hip mounted accelerometer for gait modelling and has derived harmonic models for body acceleration for different activities [64]. He has used a 3–axis accelerometer attached to the hip of the subjects as the input in his

studies. A liner predictive model has been used to estimate the fundamental frequency of the signal. It has been discovered that there are 12 significant harmonic components in the spectrum of the acceleration signal. Harmonic models for the acceleration of the trunk while flat walking, slope up, slope down, stairs up and stairs down are presented and the difference in the harmonic models for these activities in all three axes are discussed. The author has claimed that the harmonic model derived is a good fit for the original signal, but the figures indicate that there are large deviations of the reconstructed signal to the original.

Qiuyang and Zaiyue have used spectral model to predict the thigh angle during level walking. They have also used linear predictive techniques to estimate the frequencies [65]. However, in this work they have not mentioned how many harmonics are required to reconstruct the original waveform accurately. The thigh angle is reconstructed using the harmonic components extracted and compared with the original. They have reported mean square errors of 0.2 rad (11.5º) for some subjects. It can be seen from the figures that the deviation in the predicted waveform to the original is very high.

2.4.5 Step Length Estimation

Step length estimation is an important part of a pedestrian navigation system based on dead reckoning. Several different models available in literature for estimating step length during level walking. Most of these models are based on the step frequency, the height of the subject and the acceleration of the body or leg and some are presented in the following discussion. Activities such as running and jogging were not considered in this study because these activities are not performed by vision impaired people during navigation.

Shin *et al.* have presented a model for step length as a function of the stride frequency and the variance of acceleration of a hip mounted IMU [66]. The step length, l_s, in their model is given by:

$$l_s = \alpha \cdot f_s + \beta \cdot \nu_a + \gamma \tag{2.6}$$

where f_s is the step frequency, ν_a is the variance of the acceleration and α, β and γ are pre-learnt parameters. The authors claim above 95% accuracy of the model,

however, it is not clear in the paper if the trials were performed using a single subject or many.

Gusenbauer *et al.* have presented a model to estimate step length as a function of stride frequency only [67]. The model, however, incorporates a parameter to represent the random walk, which is modelled as Gaussian noise with a varying standard deviation that depends on the step frequency. Their model is given by

$$l_s = a + b \cdot f_s + \omega \tag{2.7}$$

where f_s is the step frequency, *a* and *b* are pre-estimated parameters and ω is the random walk parameter. The errors reported in their experiments for three different scenarios are 4%, 2.76% and 12.35%. These experiments have been conducted using a smartphone carried on the subject's hand, in front of the subject.

The step length as a function of step frequency and the height of the subject is presented in [68]. In their work, the IMU is hand held. Their model is given as

$$l_s = h \cdot (a \cdot f_s + b) + c \tag{2.8}$$

where *h* is the height of the subject and f_s is the step frequency. *a*, *b* and *c* are pre-learnt parameters. They have reported error between 2.5% and 5% for the total distance travelled. The experiment had been conducted with the involvement of 10 test subjects.

Lee *et al*. have incorporated gyroscope integration of a hand held device in the step length estimation model in addition to the step frequency and acceleration variance [69]. In this model, a correction is added to the normalised step length to estimate the actual step length and the correction factor is estimated as a function of the difference of the measured and norm of afore said parameters. The model is given by

$$l_s = \alpha \cdot (v_a - v_0) + \beta \cdot (f_s - f_0) + \gamma \cdot (GI_s - GI_0) + l_0 \tag{2.9}$$

where v_a, f_s and GI_s are acceleration variance, step frequency and the gyro integral for the particular step and these parameters with subscript '0' are the norms of each parameter. l_s is the estimated step length and l_0 is the normalised step length. α, β

and γ are the scaling factors for each parameter of their linear combination model. In an experiment conducted with the involvement of a single subject walking 3 circles around a rectangular path of 400 m long, has reported RMSE of 14.18, 4.23 and 11.68 cm.

Zhao *et al.* have modelled the step length as a function of the amplitude of the waist-swing in vertical direction [70]. They have presented 2 models, a simple model assuming no bending of the knee at toe off, and an advanced model assuming the knee bending. The two models are given by

$$l_s = 2\sqrt{l^2 - (l-h)^2} \tag{2.10}$$

and

$$l_s = \sqrt{(l^2 + l_f^2) - (l-h)^2} + \sqrt{l^2 - (l-h)^2} + l_f \tag{2.11}$$

where l_s is the step length, h is the amplitude of the waist-swing, l and l_f are the length of leg when the knee is not bent and bent respectively. The authors claim that they achieved 96.9% accuracy in walking distance estimation with this model.

All the models discussed are based on the acceleration measured, height of the subject, step frequency, length of leg or a combination of these parameters. A different approach for modelling step length is used by Diaz and Gonzalez [71], where they have modelled the step length as a function of opening angle, which is measured as the angle of the thigh between the heel off and the initial contact: *i.e.*, the difference between the maximum and the minimum of the thigh angle for a given step. To the author's best knowledge, this is the only approach found in literature that uses the thigh angle extrema to estimate the step length. Their model is given by

$$\begin{aligned} l_s &= a \cdot \Delta\theta + b \\ \Delta\theta &= (\theta_{\max} - \theta_{\min}) \end{aligned} \tag{2.12}$$

where l_s is the step length and θ is the thigh angle. The constants a and b are personalised parameters fitting each regression line. They have reported 0.15% mean error for distance estimation in an experiment conducted with the involvement of 1 test subject who has walked 10 trail on the same path. The parameters a and b were

derived from the same subject while walking on a treadmill in an optical motion analysis lab. Although very low error is reported, this work cannot be considered as accurate because only one subject was participated in the experiment. The reliability of the algorithm against different subjects is questionable.

2.4.6 Activity Recognition

The majority of the existing work on human activity detection use 3-axis accelerometers to measure the trunk or the leg movement while few uses a gyroscope in conjunction with the accelerometer. Bocksch *et al*. have discussed an activity classification method that uses a 9-degree of freedom IMU [72]. They detect standing, running, walking, being in the car, lying, cycling and falling in their system. The magnetometer is used to detect the car entry and exit by analysing the magnetic distortion, whereas the other inertial sensors are used to detect other activities. The device is placed on the belt (hip mounted) and they could detect walking, running, throwing and lying with 100 % accuracy and standing, entering a car and cycling with 92 %, 76 % and 72 % accuracies respectively. However, their algorithms are computationally intensive and may require high processing and memory capabilities in the device.

Kwapisz *et al*. have discussed an activity recognition system using the accelerometer data of a mobile phone placed in the pocket [73]. In this system, they have processed the average, standard deviation, average absolute difference, average resultant acceleration, time between peaks and binned distribution of acceleration data. They have considered the activities walking, jogging, ascending stairs, descending stairs, sitting, and standing. They could achieve detection accuracies above 90 % for walking, jogging, sitting and standing, but 61.5 % accuracy for walking upstairs and 55.5 % accuracy for walking downstairs. Their technique too, requires higher computational capabilities than what is available in current low end microcontrollers.

Most of these existing techniques use threshold detection of the accelerometer to detect the activities, which performs less accurately in slow walking speeds and stair climbing. Further, they require significant computations to be performed, which is not favourable for low cost devices.

2.5 Summary and Conclusions

Walking is a synchronised movement of a human's lower limb for the purpose of navigation. The main contributors to the walking are the person's legs. It is clear that the major movement of a leg during normal walking is the flexion (backward) and extension (forward) and that movement can be considered as a rotary motion around the hip joint. Hence, measuring rotary movement (angular velocity) of the thigh is more meaningful than measuring the linear movement (linear acceleration). A literature review was conducted to confirm this argument and the findings are presented in this chapter discussing some theories and work available in literature on the areas relevant to this thesis. The discussion started with explaining details of the gait cycle and its sub phases followed by a discussion on the technology available for gait measurement and capturing. Details on work available in literature on pedestrian navigation, step detection, orientation estimation of IMUs, human gait recognition and modelling, step length estimation and activity recognition were also presented in this chapter.

Great deal of research into gait recognition and characterisation techniques focus on the use of inertial sensors to measure the acceleration of trunk, foot or thigh movement [41], [63], [74]. In addition, gyroscopes were used in conjunction with accelerometers to measure the trunk movement in some other systems [38], [75].

The argument that the rotary movement of the thigh gives more meaningful data for gait analysis compared to linear measurements, was confirmed in the preliminary studies and experiments conducted (presented in Section 5.2), by the observation that the gyroscopic data of a thigh mounted device (a smartphone placed in the subject's trouser pocket) gives better details and information on the thigh movement than an accelerometer does [76]. The correlation of the signal between strides was higher for the gyroscopic data than accelerometer data. It was also observed that thigh is the best position for the inertial sensor against hip and hand. Therefore, it was concluded that a thigh mounted inertial sensor and gyroscopic data to be selected as key inputs of this study.

This page is intentionally left blank.

Chapter 3

METHODOLOGY

3.1 Research Methodologies

Research methodologies are generally divided into two main categories. They are:

1. Social sciences methodology; and
2. Science and engineering methodology.

Social science methodology is used in researching social issues, concepts and ideas, whereas science and engineering methodology is used technical research. As the goal of this research falls under science and engineering, Science and Engineering Methodologies are appropriate. There are many different methods under Science and Engineering Methodology that are suitable for different research areas as discussed in [77].

3.2 Research Methodology Followed

The main objectives of the research discussed in this thesis are development of models for human gait and algorithms to identify gait features. Therefore a combination of “Construct a Model” and “Algorithm Development” methods for scientific research discussed in [77] was used as the main research method. The flow chart in Figure 3.1 depicts the main steps of the research method used, which is further described in details later.

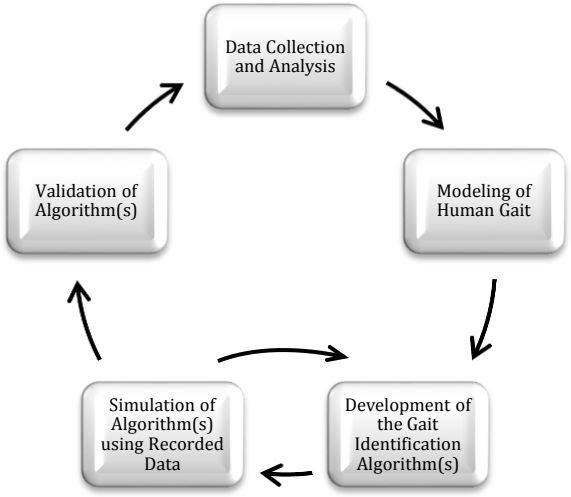

Figure 3.1 – Flow Chart of the Research Method Used

3.2.1 Construct a Model

This research method is more appropriate for mathematics, theoretical physics, theoretical chemistry, theoretical geology, theoretical astronomy, or theoretical biology [77]. This may be started with a hypothesis and developed until a satisfactory model is derived, based on experimental results. Another variant of this mode of research is the modelling without any experimental results. However, the modelling was done based on the experimental results in the research discussed in this thesis. The steps that may be followed for this model are as follows:

1. Identify a regularity or relation discovered through experimental investigation.
2. Build mental pictures to explain regularity, and develop hypothesis about origin of phenomenon.
3. Identify basic mathematical relations from which regularity might result.
4. Using analytical or numerical techniques, determine whether experimental regularities result from the starting mathematical equations.
5. If incorrect, find new mathematical starting point.
6. If correct, predict new regularities to be found in future experiments.

3.2.2 Algorithm Development

This method is appropriate for developing an algorithm for achieving a certain goal. The techniques involved in this method may include proofs that a programme is correct or can terminate or ideas that underlie new classes of computer languages. The steps that may be followed in this method are as follows:

1. Learn the vocabulary and concepts of an existing area of computer science.
2. Develop a new conceptual method for solving a problem in this area.

3.3 Work Flow of this Research

3.3.1 Data Collection and Analysis

Initial collection of data was conducted to identify better carrying positions for the data collection device. The carrying positions tested were based on techniques presented in the literature. Once the best carrying position was identified form the analysis of these data, further collection of data was conducted to collect data required for step detection and gait modelling and analysis were conducted to test collected data and to identify the requirement of further data collection.

3.3.2 Modelling of Human Gait

Human gait was modelled targeting two applications: gait modelling for level walking and step length estimation, using the thigh movement data collected with multiple male and female subjects. The accuracy of the model was evaluated by analysing the correlation and the error between the model generated data and the collected data. Part of the data set was used to derive the models and the balance was used to evaluate the models.

To identify gait patterns and establish models, data were collected with the participation of multiple non-vision impaired male and female subjects known to have no disability or other impairments. Once the patterns are identified and initial models are established for non-vision impaired subjects, data were collected from vision impaired subjects to study the differences.

3.3.3 Gait Identification Algorithms

Gait identification algorithms were developed for different purposes using parameters derived from the data collected. The algorithms derived are discussed in Chapter 5. Lower computation requirements were targeted when developing the algorithms so that they can be implemented on low end microcontroller platforms.

3.3.4 Simulation of Algorithms

The algorithms were simulated on Matlab with pre collected data to confirm the performance of them. Modifications to the algorithms were done until they perform satisfactorily.

3.3.5 Validation of Algorithms

Once the algorithms are tuned up in simulation, they were implemented and verified. Reference systems such as Vicon optical motion capture system were used in some cases were as others were verified in real application with the involvement of test subjects.

Chapter 4

EXPERIMENTAL PLATFORM

4.1 Introduction

The work presented in this thesis used three different experimental platforms. A fourth platform was tested for possibility of using in this work and was discontinued. At the beginning of this work, a smartphone with in-built inertial sensors was used to capture data. An Android application was developed, which is discussed in Section 4.2. Due to limitations of using a phone in capturing movement of multiple sections of the body, an off-the-shelf IMU system was tested for feasibility of use in this research. Details of these IMUs and test results are discussed in Section 4.3. Due to data losses occurred when more than one units of the off–the–shelf IMU was used, a custom made IMU was developed and used to capture inertial data in the latter stages of this work and the design and the construction of the custom–made IMU is discussed in Section 4.4. Details of the optical motion capture system installed in the MAL are discussed in Section 4.5. MAL was used to capture data for verifying the thigh angle estimation algorithm and data needed for developing step length estimation algorithm.

4.2 Data Capture Application for the Smartphone

At the early stages of the work presented in this thesis, sensor data were collected using Android based smartphones with gyroscope. An application was developed to record accelerometer, gyroscope, magnetometer and orientation data from the in–built sensors at a rate of 100 samples per second. 100 samples per second was selected so that the sub-gait level details can be extracted even for fast gait which is about 3 steps per second.

Accessibility was also a concern when developing this application. The details of the activity performed can be recorded as a voice message, so that the application may be used by vision impaired people and no paper records are needed to track the activity performed. Further, to make the application accessible, the full screen was assigned as a button and screen press sequences such as press–and–hold,

release and tap (short press) were used to trigger the voice recording and sensor data recording. When each event is triggered, it is informed to the user as the voice message to improve the accessibility. The user interface of the application is shown in Figure 4.1.

Figure 4.1 – User Interface of the Android Application

The main challenge faced in developing the application is that the Android Sensor Manager (the interface available to access sensor data) uses an event driven architecture [78]. Sensor data are updated only when a change in value occurs. However, for digital signal processing purposes, the sensors prefered to be sampled at a consistent sampling rate. Therefore, it was required to convert the event driven architecture of Android Sensor Manager into a time driven architecture as follows. A set of temporary variables keep the latest updates of the sensor values provided by the Sensor Event Listener of the Sensor Manager. A timer is run at 10 ms timing to provide 100 Hz sampling rate. Each time the timer ticks, the aforementioned last sensor values are taken as the new sample of sensor values. This way, the sensor samples are produced at 10 ms intervals, so that the sampling rate is kept constant at 100 samples per second. The event–driven to time–driven conversion is shown in the flow chart in Figure 4.2.

All values with the sample time are stored into a comma separated value (CSV) file in the phone storage with the date and time that the trial started as the name of the file. A unique file name for each trial is created this way. The voice label (that explains the activity performed) recorded prior to the sample is also saved as an audio file with the same file name (with appropriate file extension), so that one can easily identify the audio label and sensor data pair.

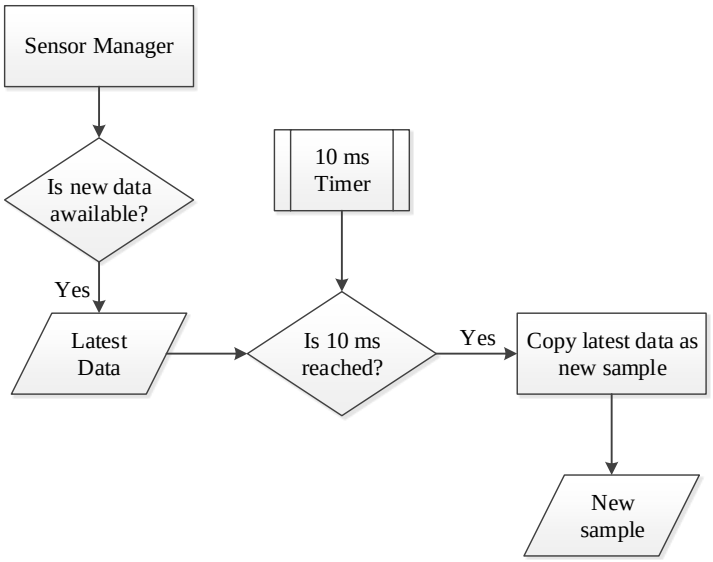

Figure 4.2 – Event-driven to time-driven conversion

Although a smartphone could be successfully used to capture the motion of a single body section of many blind and non–blind subjects, capturing motion of multiple sections is difficult with smartphones due to synchronization issues and difficulty to communicate between phones. Further, attaching smartphone on to multiple sections of the body is not convenient. Another limitation in using smartphones for data recording is that, the user has to rely on the data made available from the Android operating system, and these data are not properly time synchronized as a result of the event driven architecture. It was decided to explore the possibility of using multiple IMUs for data capture due to these limitations.

4.3 Off–the–Shelf IMU

The application in the smartphone can be used for collecting inertial data of a single section of the body. Although attaching a smartphone to a section like hip or thigh is not very convenient, for sections like foot and shank, the smartphone

becomes practically unusable because of the size. Further, smartphone becomes unusable when inertial data of more than one section of the body has to be recorded synchronously because multiple smartphones cannot be easily synchronized. Due to these reasons, it was decided to use multiple IMUs when data of multiple sections were to be collected.

YEI 3–Space Bluetooth IMUs were selected for this purpose [58]. These IMUs communicate with the host computer via Bluetooth. The IMU includes a 3–axis accelerometer, a 3–axis gyroscope and a 3–axis magnetometer. The specifications of these sensors are given in Table II. These IMUs have two modes of data collection. One of them is the poling mode where the host computer request a sample from the IMU and the second is the streaming mode where the host computer sends a sampling frequency to the IMU at the initialization and the IMU samples and streams data to the host for a pre–set period. Software was written for the host computer by modifying the sample code provided by the vendor to test the poling mode. It was observed that 100 samples per second sampling rate is unachievable when the IMU is sending data via Bluetooth in this mode. Therefore, the software was modified to use the streaming mode of the IMU. The IMU was configured to sample data at 10 ms intervals. With this method, it was possible to receive data at 100 samples per second with 3 sensors simultaneously when the sensors are not in motion. However, during the testing done with the involvement of multiple blind and non–blind subjects, it was observed that there were packet losses when the sensor is in motion which causes the total set of data after the packet loss becomes unreadable. Further, the data presented by these sensors are not the raw sensor data, but biased and scaled data. Due to these reasons, these IMUs were not used for any data recording.

TABLE II – TECHNICAL DETAILS OF YEI TECHNOLOGIES IMUS [58]

Sensor	Parameter	Value
Accelerometer	Bit size	14 bits
	Max. Range	±8 g
Gyroscope	Bit size	16 bits
	Max. Range	±2000º/s
Magnetometer	Bit size	12 bits
	Max. Range	±8.1 G

4.4 Custom–made IMU

As YEI sensors didn't work as expected at 100 samples per second data rate, it was decided to develop a custom–made IMU for collecting inertial data particularly when data of multiple sections are to be recorded. These custom–made Inertial Measurement Unit (IMU) were used for data collections in the latter parts of the research due to the convenience they offered. This sub section discusses the development and features of the custom made IMU. Some parts of this discussion are published in [79].

Although there are several commercially available options for 9 degree of freedom (DOF) IMUs [58], [59], they were not opted for mainly because they do some pre–processing before presenting sensor data to the user. Raw data is required for this project because developing an efficient orientation estimation algorithm was also a scope. Further, they have limited sampling rates, especially when using wireless connectivity. Another reason was their high price: £309.00 for x–IMU and US$309.00 for YEI 3–space Bluetooth version. There was also a need of a customizable low cost IMU platform for the work of the rest of the project. The construction, specifications and the operation of the IMU are discussed in next sub sections.

4.4.1 Construction and Specifications of the IMU

The IMU was implemented using "*Off–the–shelf*" boards to make the building process easier. The inertial sensor used for the IMU is MPU–9150 by Invensense that consist of a 3–axis accelerometer, a 3–axis gyroscope and a 3–axis

magnetometer in a single IC (Integrated Circuit) [80]. A 9–axis sensor was selected to minimise the error caused by the spatial diversity of having three sensors. Key specifications of MPU–9150 are shown in Table III and they are compared with two other 9–axis sensors, LSM9DS0 from STMicroelectronics [81] and BMX055 from Bosch Sensortec [82] in Appendix A. All these sensors have comparable specifications and are used in mobile applications. The MPU–9150 communicates with an application processor through I^2C (Inter IC) bus.

The application processor used for the IMU is an Arduino Pro Mini board that contains an Atmel Atmega 328 8–bit microcontroller and operated with a 3.3 V supply [83]. 3.3 V operation was selected so that a 3.7 V Li–Po (Lithium–Polymer) battery can power the system. The microcontroller is operated at 8 MHz and has I^2C and SPI (Serial Peripheral Interface) interfaces.

TABLE III – COMPARISON OF KEY SPECIFICATIONS OF THE INERTIAL SENSORS [80]

Specification	Accelerometer	Gyroscope	Magnetometer
Measurement Ranges	±2 g, ±4 g, ±8 g, ±16 g	±250 °/s, ±500 °/s, ±1000 °/s, ±2000 °/s	±1200 μT
Sensitivity	16384 LSB/g , 8192 LSB/g, 4096 LSB/g, 2048 LSB/g	131 LSB/°/s, 65.5 LSB/°/s, 32.8 LSB/°/s, 16.4 LSB/°/s	0.3 μT/LSB
Zero-point Offset	± 80 mg (x, y), ± 150 mg (z)	± 20 °/s	±1000 LSB
Noise Density	400 μg/$\sqrt{Hz}$	0.005 °/s /$\sqrt{Hz}$	N/A

The IMU communicates with the data logging computer through a wireless link using an nRF24l01+ 2.4 GHz transceiver. nRF24l01+ transceivers can give an air baud rate of 2 Mbps and one master can communicate with up to six slave devices simultaneously [84]. The radio board communicates with the application processor through SPI interface.

The IMU is powered by a 3.7 V 900 mAh Li–Po battery which can keep the IMU running in data transmission mode for more than 2 days continuously before the battery is fully drained. The three boards used for the IMU are shown in Figure 4.3.

The data streamed from the IMU is received by a “dongle” built using an Arduino Nano and an nRF24l01+ with a low noise amplifier and an external antenna. The external antenna option was selected to have a higher gain at the receiving end to avoid data loss as much as possible and to increase the range of operation. Both IMU and dongle were enclosed in 3D printed enclosures to allow the IMU to be used in different mounting positions and these to be secure for human use (no electrical contact with the body). The assembled IMU, enclosed IMU and the dongle are shown in Figure 4.4. The dimensions of the IMU are 55 mm × 41 mm × 23 mm without the strapping loops and the total cost was about AUD 35.

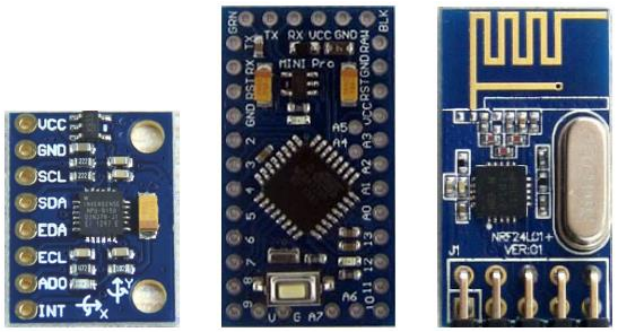

Figure 4.3 – Devices used for the IMU

MPU-9150 (left), Pro-mini (centre), nRF2401+ (right)

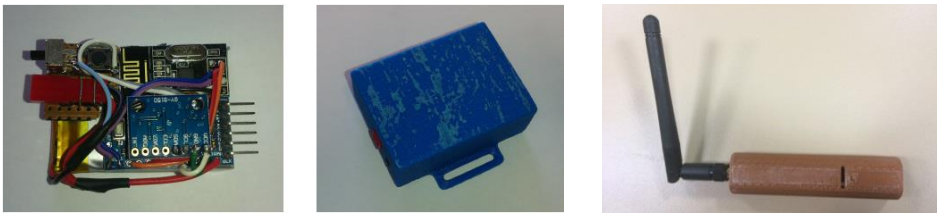

Figure 4.4 – Completed IMU and Dongle

Assembled IMU (left), IMU with enclosure (centre), Dongle (right)

4.4.2 Operation of Dongle–IMU System

As the dongle collects data from more than one IMU, they have to operate in synchronization. To achieve this, at the initialization, all IMUs wait to receive a synchronization signal. The dongle poles each IMU and send the time stamp of the dongle which is recorded by the IMUs together with the IMU time stamp (the time at which the synchronization signal is received). Thereafter, each IMU is switched into

data collection mode in which they sample the inertial sensors at 10 ms intervals (100 samples per second) and each data sample is returned to the dongle with the sample time computed with respect to the time of the dongle. Testing of the system indicated that the synchronisation of the IMUs is accurate to ±1 ms, which is acceptable as the time between samples is 10 ms. The data frame transmitted by the IMU has eleven 16–bit values that are organised as shown in Figure 4.5. The frame carries the sensor ID, time stamp of the sample, and *x*, *y* and *z* –axis data of accelerometer, gyroscope and magnetometer in that order.

Data received by the dongle are routed to the computer through USB interface with commas and line breaks inserted, which can be recorded using terminal software and saved into a CSV file easily. Time stamp of each sample is the time stamp generated by the IMU that reflects the time of the sample. Therefore, any delays that may occur in the terminal software does not affect the operation of this system. No processing of raw sensor data is done either in IMU and dongle so that the performance of the low cost processors is sufficient to achieve the targeted sampling rates (100 samples per second of all sensors). Raw data collected by this system are converted to human readable measurements by mapping binary data into acceleration, angular velocity and magnetic field strength with units of *g* (gravity), º/s (degrees per second) and μT (micro Tesla) after data being recorded. This conversion was done because the binary data are unusable if the scale setting of the sensor is unknown. Once the data are converted to human readable measurements, they can be used by other researchers for any further processing.

Sensor ID	Time Stamp	A_x	A_y	A_z	G_x	G_y	G_z	M_x	M_y	M_z

Figure 4.5 – Format of a data frame of the IMU

A, *G* and *M* indicate accelerometer, gyroscope and magnetometer in that order and the subscript indicate the relevant axis

4.4.3 Calibration of IMU

As no pre–processing of sensor data is performed inside the IMU, calibration data is pre–recorded as follows. To estimate the gyro offsets, gyro data were recorded while the IMU is stationary and average the values and used as an estimate

for the gyro offset. Further filtering was used to estimate the gyro offset continuously, as discussed further in Chapter 5.

Data required for accelerometer offset and scale error corrections were recorded by holding positive and negative directions of each orthogonal axis of the accelerometer to be vertical (in the direction of gravity as shown in Figure 4.6). These measurements were taken while the readings on the other axes approaching zero. The offset and the scale error were computed using these readings. After performing the offset and scale error correction, the measurements needed to estimate the axis misalignments were taken by keeping each edge of the IMU body vertical. The misalignments were computed by the accelerations read by each axis when a particular edge is vertical. The calibration procedure used is explained further in [30].

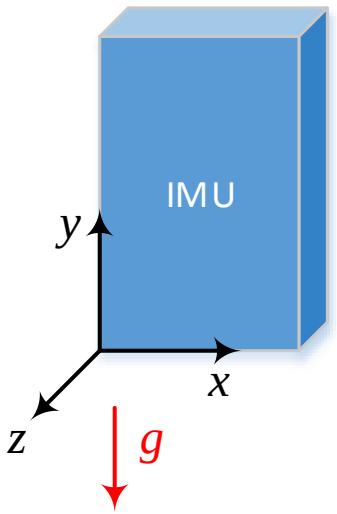

Figure 4.6 – Alignment of the IMU for calibration

4.5 Optical Motion Capture System

The Vicon Motion Capture System [22] installed in the Motion Analysis Lab (MAL) of the School of Physiotherapy and Exercise Science of Curtin University was used to capture data required for validating the orientation estimations done using the developed IMU and to capture data needed for the development of step length estimation model. The MAL is equipped with 14 advanced semi–infra–red Vicon F40 cameras and Vicon controller with a workstation computer for real–time

3D motion capture. The system can estimate the coordinates of spherical retro reflective markers attached to the body or the object in motion, with respect to a pre–calibrated system origin with sub–millimetre accuracies [25].

The Vicon system was calibrated at the beginning of each experiment by waving its calibration tool (Vicon active wand shown in Figure 4.7) over the capture area, so that the cameras can adjust their settings. Further calibrations were performed to check if all cameras are properly calibrated, by placing markers on the walk–way and observing the measurements of each camera and manually adjusting the camera settings. This procedure was followed only once by the beginning of the total capture and these settings were saved in the profile of the experiments.

Vicon Nexus 1.8.5 motion processing software is used in the MAL to capture data and it was also used to regenerate the captured records. Each trial recorded was rerun through the motion capture pipelines of the software to regenerate the motion and then all markers were labelled appropriately. Gap filling was done when necessary to retrieve missing and broken marker tracks. Data were cropped at the beginning and the end of the trial if all markers were not available. Once the trial is regenerated to cover the full walking length, the coordinates of the markers were exported to a CSV file. The rest of the analysis was done in Matlab, so that performing batch processing is easier.

Figure 4.7 – Vicon active wand [22]

4.6 Summary

Three systems used for data capture during the work of this thesis, mobile phone software, custom made IMU and the Vicon system, were discussed in this section. In addition, the off–the–shelf IMUs that were tested, by the involvement of several blind and non–blind subjects, for feasibility to be used in this work was also discussed. The development of the mobile phone software, how the custom made IMUs were built and their features were discussed in detail. Specifications of the Vison Optical Motion Capture system used for capturing data for validation purposes and to capture data required for step length model was also discussed in this chapter. How these techniques were used in particular experiments are discussed in relevant sections of Chapter 5.

This page is intentionally left blank.

Chapter 5

GAIT MODELLING AND ALGORITHMS

5.1 Introduction

This chapter presents the main contributions of the research discussed in this thesis by presenting the observation made during the preliminary experiments conducted to check the feasibility of inertial pocket navigation, followed by discussions on the following:

- Pedometer algorithm designed and developed based on the preliminary observations
- Thigh angle estimation algorithm with the validation of the results of the algorithm
- Harmonic modelling of the thigh angle and the gyroscopic waveform of the thigh mounted IMU
- Models for estimating step length as a function of thigh angle peaks as well as gyro signal peaks
- The possibility of detecting gait phases using gyro signal and its first time derivative and an algorithm for detecting indoor human activities based on thigh angle.

The existing algorithms for step detection and gait analysis comprise of heavy computations that restricts them being implemented in low end hardware. Hence, all the algorithms discussed in the thesis were targeted to be implemented on low cost devices and hence high end computations were eliminated as much as possible. Although this is the case, the accuracies of the algorithms were targeted to be comparable or better than existing gait analysis algorithms and techniques that use complex computations.

5.2 Feasibility Study for Inertial Pocket Navigation

5.2.1 Introduction

In this study, the feasibility of using single–point inertial sensors embedded to mobile devices was investigated. The main objective was to check the possibility of gait identification using a device placed in the subject's trouser pocket. Some of the content discussed in this subsection is published in [76].

Sensor data were collected while multiple male and female subjects were performing different activities. The activities considered were walking on flat land, walking up/down stairs and walking on an inclined plane upwards and downwards. To identify the best carrying position, two positions were considered when walking on the flat land. They are the hip–pocket (pocket of the trouser) and the hip (clipped to the belt). The activity performed by the subject was recorded as a voice label with the feature included in the data logging software discussed in Section 4.2.

Data collection was performed with a specific orientation of the data collecting device (an Android Smartphone) with respect to the body. When the device is carried in the hip–pocket, it was placed in the right hand side hip–pocket with an upright portrait orientation, screen facing forward. The phone was attached to the belt on the right hand side hip with an upright portrait orientation, screen facing outward.

The reference axis of the accelerometer, *x*, *y* and *z*, are as indicated in Figure 5.1 and the *x*, *y* and *z* coordinates of the gyroscopic sensor are measured around *x*, *y* and *z* axes marked on Figure 5.1 and the direction of gyro data follows the right hand rule for rotary vectors (is as in Figure 2.5). In the analysis, the vertical orientation angle was taken as 0^{o} when the phone is kept in a vertical position.

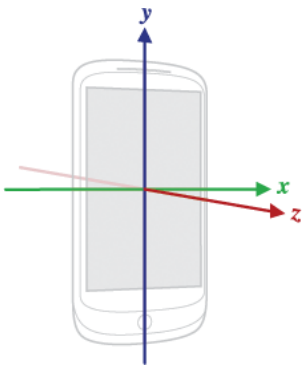

Figure 5.1 – Reference Coordinates of the Phone Sensors [98]

5.2.2 Empirical Observations

Data were collected with the participation of 5 male and 5 female participants, all having no vision impairment and known to have no other walking impairment or disability. By comparing the waveforms and the timing, it was observed that there is a closer correlation of acceleration and gyroscopic data to the gait cycle when the device is carried in the hip–pocket than when attached to the hip. This is because the sensors read the inertial parameters of the thigh. Stride–to–stride correlation of vertical acceleration and the rolling angular rate of the device (gyroscopic *x*–axis) of ten consecutive steps extracted from the middle of the walk were computed. Table IV shows the statistics of the computed correlations of gyro–*x* and vertical acceleration readings. The results indicated that there is a higher correlation of gyro–*x* between steps than the vertical acceleration.

TABLE IV – STRIDE-TO-STRIDE CORRELATION STATISTICS OF VERTICAL ACCELERATION AND ROLL OF THE PHONE

	Vertical Acceleration	**Roll of the Phone**
Number of steps (total/per person)	100/10	60/10
Mean correlation	0.887305	0.907205
Standard deviation	0.074488	0.055523
Minimum correlation	0.635118	0.701938
Maximum correlation	0.988070	0.976055

It was further observed that when the gyro data is filtered with a simple sixth order Butterworth low–pass filter having a cut–off frequency of 5 Hz, the resultant waveform can be used to easily identify the steps. The Butterworth filter was

selected as it gives a maximally flat pass-band and hence the output of the filter is accurate over the interested frequency band. As the fall-off of Butterworth filter is not very sharp, 6th order was selected to improve the selectivity of the filter. Further, when the filtered version of gyro–*x* is plotted with the vertical orientation of the device (i.e. the thigh angle), it was observed that, the gyro–*x* reading is closely related to the movement of the thigh as seen in Figure 5.2. It can be seen that the stride cycles can easily be identified by the zero crossings of the filtered version of gyro–*x* data. The gyro–*x* reading gives the rolling angular velocity of the device, and hence of the thigh. Filtering was done to suppress any noise introduced to gyro data due to the lose attachment of the device to the body, and any other noise. The filtering frequency was selected to avoid vibrations occurred at different foot touching events. A closer look at the gyro waveform with thigh angle is available in sections 5.3 to 5.8.

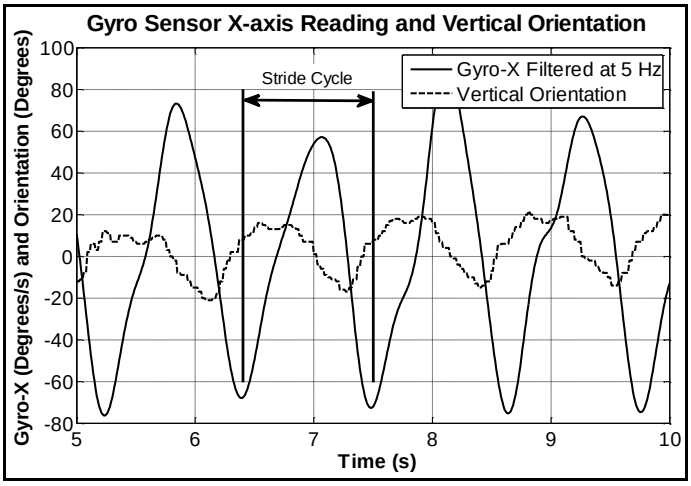

Figure 5.2 – Filtered Gyro-*x* with Thigh Angle

One major issue in existing step identification techniques, both hardware based and mobile phone based, is their very poor performance in detecting steps at slow walking speeds [44], [45], [46]. These techniques are based on threshold detection of the accelerometer reading and very low movements cause insufficient reading to be detected as a step, which is the reason for poor step identification accuracies at slow walking speeds. The main issue in acceleration based step detection is that the accelerometer reads gravity and the errors caused in filtering out gravity to derive the linear acceleration. As can be seen in Figure 5.3, the accelerometer reading is contaminated with gravity and identifying a feature in that

waveform for detecting steps is more difficult than detecting zero crossings in the gyro signal which has a zero average. It can be clearly seen in the figure that zero crossings are clearly visible in gyro signals even at the beginning of the walk where deflection of the signal is typically lower. However, the slower steps cannot be clearly recognized in the vertical acceleration signal.

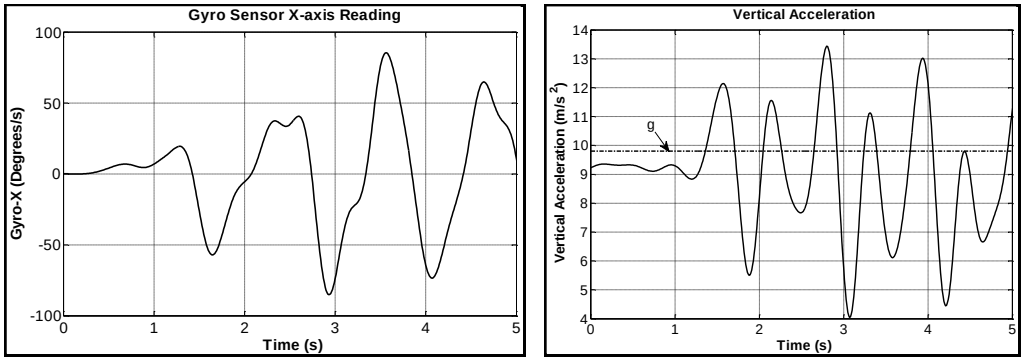

Figure 5.3 – Filtered Gyro-*x* (left) and filtered vertical acceleration (right) at the beginning of the walk

The periodic nature of the gyro signal was also observed in the data recorded while walking up/down stairs and walking on an inclined plane upwards and downwards which supports the thesis that the gyro signal may be used for step detection during these activities too.

5.2.3 Summary and Conclusions

During experiments conducted with the involvement of 10 volunteers, it was observed that a single thigh mounted IMU embedded in a smartphone (placed in trouser pocket) gives sufficient information needed for step detection and gait analysis. Inter–step correlation of gyro signal was better than that of the acceleration signal. Therefore, it was concluded from this study that the gyro data of a single thigh mounted IMU provides sufficient information for gait analysis for pedestrian navigation.

5.3 A Gyroscope Based Accurate Pedometer Algorithm

5.3.1 Introduction

Accurate step counting is a critical parameter in pedometer based indoor localization systems in improving their accuracy and reliability. Existing step detection techniques, both hardware and software, does not satisfactorily cater the accuracies demanded by localization systems especially at low walking speeds observed in natural walking [44], [45], [46]. Situation may be worse with vision impaired indoor navigation is considered, especially in an unfamiliar environment. Most of existing pedometers use accelerometer data in detecting steps and are based on threshold detecting [47], [48].

The pedometer algorithm discussed in this section is based on the proposal made by the author of this thesis in [79], which states that a single thigh mounted gyroscope may be used in human gait identification for indoor localization. The implementation of this algorithm in an Apple iPhone was done in collaboration with Sampath Jayalath, as his final year project under the supervision and guidance of the author. The work presented in this section is published in [85], [86] and [87].

One of the main concerns in developing the algorithm was to make it light weight which is favourable when implementing the algorithm on low cost devices and smart devices without loading the device heavily. Heavy computations such as Kalman filters were eliminated in the algorithm due to this reason.

5.3.2 Relationship between Gyroscopic Data and Movement of the Thigh

A stride cycle is measured from the Initial Contact of one heel to the next Initial Contact of the same heal [12]. At the Initial Contact, the extension of the thigh is a maximum. Figure 5.4 shows the thigh angle computed using gyroscopic data and low–pass filtered (with a 6^{th} order Butterworth low pass filter with cut–off frequency of 5 Hz) gyroscopic *x*–axis reading (according to the reference coordinates shown in Figure 5.1). Initial Contact points and the stride cycle identified based on the orientation are marked on the graph. The initial thigh angle when the leg is at rest was calculated using accelerometer data and the gyro data is integrated to derive the thigh angle thereafter. For this computation, the static value of the gyroscopic data was removed by deducting the average gyro value from gyro signal per each sample.

It can be clearly seen that the filtered gyroscopic data is close to zero at the Initial Contact point of the particular leg and has a negative gradient. Hence, the period from one negative gradient zero crossing point to the next of the filtered gyroscope reading is a stride cycle as shown in the figure.

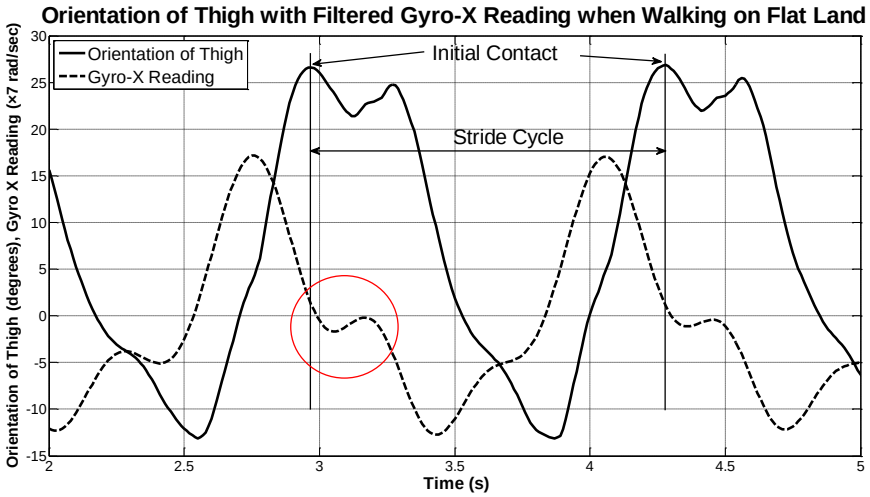

Figure 5.4 – Thigh angle with filtered gyro-*x* reading for level walking

It was also observed that the negative gradient zero–crossing corresponds to the Initial Contact of that leg when walking on stairs and on an inclined plane. Therefore it is clear that zero crossing detection of filtered gyroscopic data may be used in detecting the stride cycle, hence the steps, even if the person is walking on stairs or on a ramp. Later findings about the synchronization of the thigh angle waveform, gyro signal and the gait cycle are presented in Section 5.4.

In line with these observations, the device is assumed to be in vertical placement where forward and backward rotation of the thigh is read as gyro–*x* reading. Hence the real time processing is limited to gyro–*x* only.

5.3.3 Step Detection Algorithm

5.3.3.1 Pre Processing of Data

Before attempting to identify zero crossings, the gyro–*x* data is filtered with a 6^{th} order discrete Butterworth low–pass filter with cut–off frequency of 3 Hz. 3 Hz was selected as the cut–off frequency because the mean speed of fast gait is in the range of 2.5 steps per second [88]. The Butterworth filter was selected as it gives a maximally flat pass-band and hence the output of the filter is accurate over the

interested frequency band. As the fall-off of Butterworth filter is not very sharp, 6th order was selected to improve the selectivity of the filter. The cut–off frequency was lowered as much as possible for better smoothness of the waveform so that the unwanted oscillations around zero are minimal, but still the stride cycle is visible in the waveform.

5.3.3.2 Zero–Crossing Detector

A 2–point zero–crossing detection was used to simplify the algorithm. Both positive and negative zero–crossings were detected by alternating the polarity of the zero–crossing detector because the positive zero–crossing corresponds to the starting point of Pre Swing of the particular leg, or the Initial Contact of the other leg. Hence, the total count of zero–crossings is the number of steps the person has walked.

5.3.3.3 Avoiding False Detections

As indicated by the circle in Figure 5.4, the filtered gyroscopic signal may cross zero with a negative gradient more than one time during the period from Initial Contact to Loading Response. However, because this period is between 0–10% of the gait cycle [12] a timeout mechanism was used to avoid this unwanted zero–crossing being detected. Once a zero–crossing is detected, the zero–crossing detector remains disabled for 100 ms to avoid detecting these multiple zero crossings. 100 ms was selected as 15% of the stride cycle assuming a step frequency of 1.5 steps per second for slow gait [88]. This time delay is 30% of the stride cycle of average fast gait of 3 steps per second and hence it will not disturb the detection of the next zero–crossing of fast gait.

5.3.3.4 Validating the Detected Zero Crossings

A threshold detection mechanism was used in the algorithm to validate each zero–crossing detected. As shown in Figure 5.4, the gyroscopic reading reaches the corresponding peak after the zero–crossing point. However, in the area marked by the circle, the relative maximum is well below the peak of the signal and that relative maximum does not correspond to the middle of the swing of a leg, hence should not be counted as a step. The application includes a calibration mode where the user has to walk with the slowest possible speed so that the smallest deflection of the gyroscope signal is learnt by the algorithm. After detecting a zero–crossing, the algorithm checks for the peak that follows the zero–crossing, and checks if it is larger

than the threshold. The counter is incremented only if the peak is larger than the threshold.

5.3.3.5 The Step Detection Algorithm

A flow chart illustrating the step detection algorithm is depicted in Figure 5.5. It should be noted that both positive and negative zero–crossings are detected by the algorithm and the polarity to be checked is toggled after each detection. However, the polarity toggling is not indicated in the figure to reduce graphical complexity.

5.3.3.6 Implementation of the Algorithm

The algorithm was implemented in Matlab for simulation purposes and after confirming the outcomes of the algorithm using pre–recorded data, it was implemented in an Apple iPhone 4S. During the implementation it was noticed that the algorithm may count the movements of the phone while in the hand, when placing the phone in the pocket before the trial and taking out of the pocket after the trial. As Apple license does not allow use of some phone features [89], such as ambient light sensor to detect placement in the pocket, a time out mechanism and a manual correction was used at the beginning and at the end of the trial respectively. After pressing the start button, the application allows a timeout to allow user to place the phone in the pocket. The algorithm starts detecting steps only after the timer has timed out. Manual decrement of the total count by one was done to compensate the false count at the end when the phone is taken out of the pocket.

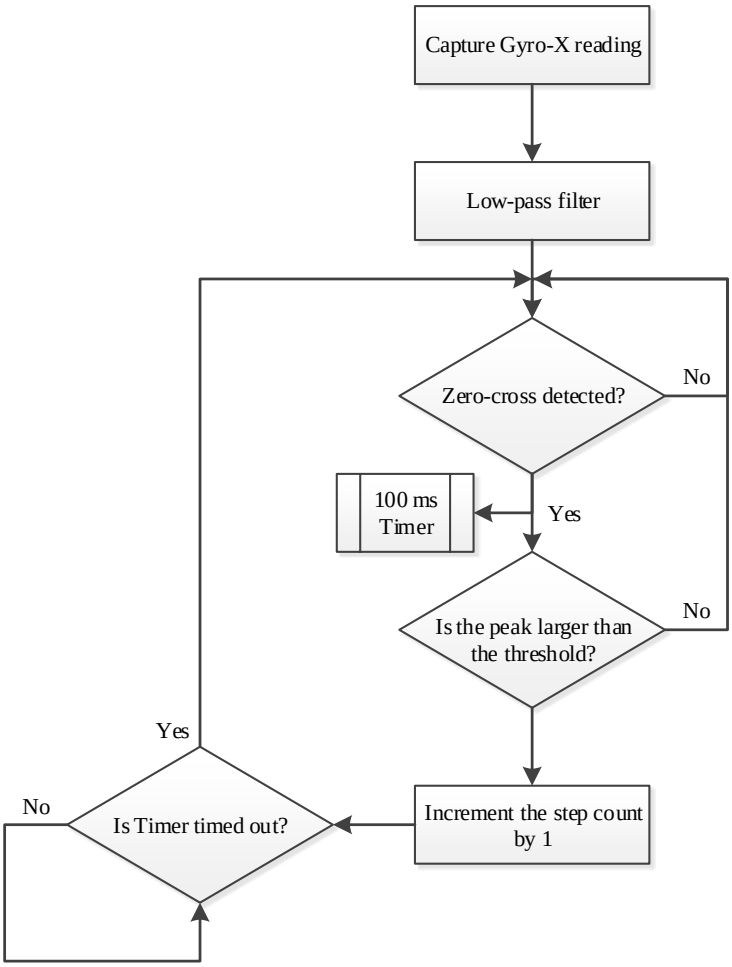

Figure 5.5 – Flow Chart of the Step Detection Algorithm

5.3.4 Empirical Results

The simulations indicated that the accuracy of step counting of the algorithm on pre–recorded data was 100% for all the trials. The algorithm was tested in the real world for five different activities: walking on flat land, upstairs, downstairs, ramp upwards and ramp downwards, with the involvement of 5 male and 5 female volunteers. They were asked to place the phone vertically in the pants pocket and perform the relevant activity. The tests were conducted in two stages: first with normal walking speed and then with five different stepping rates (50, 75, 100, 125 and 150 steps·min^{-1}). The actual number of steps that the subject travelled was counted for each trail by a manual recorder.

Table V shows sample results of a single subject performing different activities with normal stepping rate. In that set of trials, the algorithm showed above 95% accuracy in every activity.

TABLE V – SAMPLE RESULTS OF ONE SUBJECT

Activity	Actual No. of Steps	Steps Counted by Algorithm	Accuracy (%)
Slow level walking (< 60 steps·min^{-1})	27	26	96.30
Fast level walking (> 100 steps·min^{-1})	49	49	100.00
Going up stairs	11	11	100.00
Going down stairs	11	11	100.00
Ramp up	40	40	100.00
Ramp down	43	41	95.35

Table VI shows statistics of actual number of steps, number of steps counted by the algorithm and the accuracy in all trials. It can be seen that the algorithm has shown a minimum mean accuracy of 94.55% for going downstairs and the minimum reported accuracy for all the trials of 90.91% on stairs (both up and down). However, the minimum accuracy reported by the algorithm for walking on flat land is 96.00% with a maximum of 100%. The algorithm has reported accuracies greater than 95% for walking on an inclined surface with a mean accuracy of 97.17% for going down and 98.18% for going up.

TABLE VI – STATISTICS OF THE PERFORMANCE OF THE ALGORITHM FOR DIFFERENT ACTIVITIES

Activity	Actual No. of Steps		Steps Counted by Algorithm		Accuracy (%)			
	Mean	*Var*	*Mean*	*Var*	*Mean*	*Var*	*Min*	*Max*
Slow level walking (< 60 steps·min^{-1})	28.50	2.45	27.60	2.64	96.82	1.16	96.00	100.00
Fast level walking (> 100 steps·min^{-1})	49.10	1.29	48.50	0.65	98.80	1.73	96.08	100.00
Going up stairs	11.00	0.00	10.70	0.21	97.27	17.36	90.91	100.00
Going down stairs	11.00	0.00	10.40	0.24	94.55	19.83	90.91	100.00
Ramp up	43.30	2.01	42.50	1.45	98.18	1.87	95.45	100.00
Ramp down	42.20	1.36	41.00	1.20	97.17	2.02	95.24	100.00

The second set of experiments were conducted for walking on flat land and on stairs only, where the subjects were asked to walk with five stepping rates: 50, 75, 100, 125 and 150 steps·min^{-1}. For walking on flat land, the minimum accuracy of

94.59% was reported at 75 steps·min^{-1} whereas the mean accuracy for that speed was 97.89%. However, the minimum accuracy reported at 50 steps·min^{-1} was 96% and the accuracy was greater than 96% at all other stepping speeds. The statistics are shown in Table VII.

The minimum accuracy reported in going up stairs and down stairs was 90.91% where the total number of steps considered in each case was 11. Although this is the absolute minimum, the lowest mean accuracy reported when walking up stairs was 96.36% and that is at 75 and 125 steps·min^{-1}. For walking down stairs, the lowest mean accuracy reported was 95.45% for the stepping speeds of 50 and 125 steps·min^{-1}.

TABLE VII – STATISTICS OF THE PERFORMANCE OF THE ALGORITHM FOR WALKING ON FLAT LAND WITH DIFFERENT STEPPING RATE

Level Walking Speed	**Actual No. of Steps**		**Steps Counted by Algorithm**		**Accuracy (%)**			
	Mean	***Var***	***Mean***	***Var***	***Mean***	***Var***	***Min***	***Max***
50 steps·min^{-1}	25.90	1.09	25.50	0.85	98.49	3.43	96.00	100.00
75 steps·min^{-1}	37.80	0.96	37.00	1.20	97.89	2.58	94.59	100.00
100 steps·min^{-1}	51.00	1.00	49.90	1.29	97.85	1.89	96.00	100.00
125 steps·min^{-1}	62.50	0.65	62.00	0.40	99.21	0.63	98.39	100.00
150 steps·min^{-1}	74.50	0.65	73.90	1.69	98.92	0.66	97.26	100.00

5.3.5 Summary and Discussion

An efficient and accurate pedometer algorithm was presented with the experiment results in this section. One of the targets in this work was to make the step detection algorithm require minimum computational resources so that it can be implemented on a low cost processor without loading the system. Achieving the target, the pedometer algorithm was implemented with minimal computational complexity avoiding high end techniques such as Kalman filtering, but still experimentally proven to be providing accuracies close to 100% even at slow walking speeds, compared to accuracies below 50% in existing algorithms at slow walking speeds. Further, according to the best of the knowledge of the author, a thing mounted gyroscope had not been used in pedometers in the past.

Trials of walking on stairs had to be limited to 11 steps per trial due to limited access to long stairways. Due to this reason, the false count at the end of the trail is large as a percentage to the total number of steps. This may be the reason for low accuracies shown on stairs. Although the number of steps will be less in practical circumstances, the phone will not be taken out of the pocket at the end of the stair case and hence the aforementioned error count will not occur. In addition, the vendor have restricted using some facilities of the phone to detect whether the phone is in the pocket.

Kwon *et al*. have used the step detection algorithm discussed in this section in their cross–platform and cross–device pedometer system and reported higher step detection accuracies [90]. They have tested the algorithm on an iPhone 4S, iPhone 5S, Galaxy Nexus and Nexus 5 over about 6000 steps and reported 0.81%, 2.27%, 0.88% and 0.91% error percentages. Except for iPhone 5S, the error percentage reported by all other devices is under 1%, which indicates the performance of the algorithm is much better than other pedometer algorithms, despite the fact that the phone has a restricted placement in the trouser pocket.

Although heavy computations are not included in the algorithm in order to make it possible to be implemented in low cost devices and smart devices without loading them heavily, the algorithm was experimentally proven to have better performance compared to existing high end techniques. Hence, the pedometer algorithm can be considered to have better step detection accuracy despite its simplicity.

5.4 Thigh Angle Estimation and Validation

5.4.1 Introduction

Orientation estimation is an important task in thigh angle based gait analysis. As only flexion and extension of the thigh was considered in this study, single axis orientation was the main focus. Most of orientation estimation algorithms available are based on Kalman Filters [26], [58], [57]. Although Kalman filters are fast enough in personal computers or workstations, implementing them in low end real time embedded systems is not an easy task. One main drawback in using these techniques is that the embedded devices have to be capable of executing these in real time,

usually achievable with a 32–bit microcontroller with a digital signal processor (DSP), which increases the cost and power consumption. As the application processor used in the low cost custom made IMU discussed in Section 4.4 is an 8–bit microcontroller running at 8 MHz, implementation of computationally less expensive orientation estimation algorithms was an important task.

This section discusses a computationally economical algorithm (Gyro Integration based Orientation Filter – GIOF), that may be implemented in a low cost 8–bit microcontroller, to estimate single dimensional orientation by fusing accelerometer and gyroscopic data of an IMU. One of the main targets was to develop the algorithm to demand minimal computational resources while serving accuracies comparable to existing high-end algorithms. GIOF was used to estimate the flexion and extension angles of the thigh (herein after also referred to as the "thigh angle") and validate the results of GIOF against Vicon Optical Motion Analysis system, which is well documented to be accurate enough for measuring motion of human body for clinical and rehabilitation purposes [25]. The work presented in this chapter is submitted to IEEE Transactions of Biomedical Engineering on Dec 11, 2015 as second revision and is under review.

5.4.2 Some Key Observations on Limb Synchronization

To enable identifying key points of stride cycle in the thigh angle waveform, the foot movement with the thigh movement was captured in MAL. Details of the experiment are discussed later in this section. Figure 5.6 shows a time synchronized plot of the thigh angle with the vertical and forward movements of the foot. The maximum thigh angle was misinterpreted as the Initial Contact point previously, but by observing the foot movement waveforms, it was identified that the local minima of the thigh angle waveform next to the maximum (point 'a' of Figure 5.6) refers to the Initial Contact point. Further, it can be seen that the minimum (point 'b' of Figure 5.6) of the thigh angle waveform is the toe–off point of the stride cycle. The stride cycle and its two main phases, Stance and Swing, are shown in the figure.

The synchronization of the movement of the two thighs was also measured and depicted in Figure 5.7. It can be seen that the toe–off of one leg is closely related to the Initial Contact of the other leg.

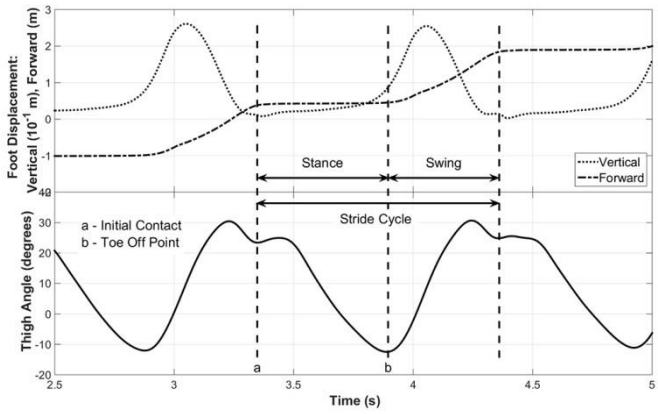

Figure 5.6 – Thigh angle synchronized with the vertical and forward movements of the foot

Vertical and forward movements of the foot are used to identify the key points of the thigh angle waveform.

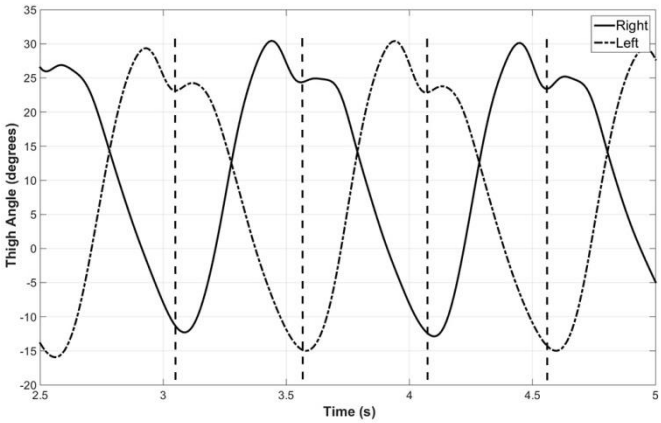

Figure 5.7 – Thigh angle of left and right legs

This indicates that the toe off of one leg is synchronized with the initial contact of the other leg as shown by vertical dashed lines.

These observations indicate that proper estimation of the thigh angle of one leg is sufficient to identify key points of the stride cycle of both legs on subjects without gait impairment, in this scenario. However, these observations were made with the Vicon optical motion capture system and it is necessary to compare the thigh angle computed with IMU data for the purpose of validation.

5.4.3 Experimental Setup and Analysis Technique

The experiment was conducted with the participation of 9 female and 10 male volunteer participants. All participants are non–vision impaired and known to have no other impairment or disability. The experimental setup, the procedures followed

in the experiment and the analysis techniques are discussed in this section. MAL and IMU data were recorded in two independent systems. How they were synchronized in the analysis is also discussed in this section.

5.4.3.1 Experimental Setup

This experiment was conducted in MAL (discussed in Section 4.5). Figure 5.8 shows the marker positioning on the subject's legs. A custom made IMU discussed in Section 4.4 (with a shape more suitable for mounting on thigh) was attached to the right thigh of the subject and two markers were placed on that as shown in Figure 5.8 to capture the tilt of the IMU. A marker cluster was attached to the subject's left thigh to capture the thigh angle of the left leg. A marker was attached to the heel of each shoe to capture the movement of the heel (or the foot), so that the Initial Contact and the toe–off points can be identified.

The Vicon system was calibrated before collecting data of each batch of test subjects as discussed in Section 4.5. The IMU data were recorded in a laptop that operated independent to the Vicon system. Both data were sampled at 100 samples per second. IMU and Vicon data logging were manually triggered separately before the subject started their trial. The subjects were asked to walk in a straight line with their natural walking style with normal gait of about 2 steps per second. Both MAL and IMU data were recorded for 20 walking trials (10 trails in each direction of the MAL capture area) per each subject.

Figure 5.8 – Marker and IMU placement on legs

The left picture shows the full placement. The top two pictures on the right shows the marker cluster attached to the left thigh of subject and the markers on it (left) and the custom made IMU attached on the right thigh and the markers placed on it (right) and the right lower picture shows the markers attached to the heels.

5.4.3.2 Data Analysis Technique

As MAL and IMU data were recorded in independent systems, they were pre–processed separately. Vicon Nexus software was used to pre–process MAL data and export coordinates of each marker into comma separated value (CSV) format. These coordinates were then used to compute the thigh angles using Matlab.

The algorithm discussed in Section 5.4.4 was used to compute the thigh angle using IMU data. Both angle data were then resampled (interpolated) at 1000 samples per second and sent through an extrema detection algorithm to pick all maxima and minima of the two waveforms. Both waveforms were then trimmed at identical points of the two waveforms, starting from a minimum and ending at a minimum. The identical points were identified manually by visually comparing the two waveforms. Although by definition, the beginning of a stride cycle is the Initial Contact where the thigh angle is a maximum, cropping was dome from a minimum to a minimum to extract maximum possible number of stride cycles. These trimmed waveforms were then used to compute the correlation coefficients and the error characteristics between the two methods.

5.4.4 Gyro Integration based Orientation Filter (GIOF)

The thigh angle is estimated by fusing accelerometer and gyroscope data. The gyroscopic signal is low–pass filtered using a moving average filter with 10–sample window size to remove the high frequency noise. Further, another moving average low–pass filter was used to compute the static error of the gyroscope and remove it from the gyroscopic signal. When compared with the thigh angle computed from MAL data, it was observed that the gyro integration does not drift when the window size is 150 samples. 150–samples is approximately two strides long.

The reference axis of the IMU is shown in Figure 5.9 and it is clear that only gyroscopic *z*–axis data is needed to measure the angular velocity of forward and backward movements of the thigh.

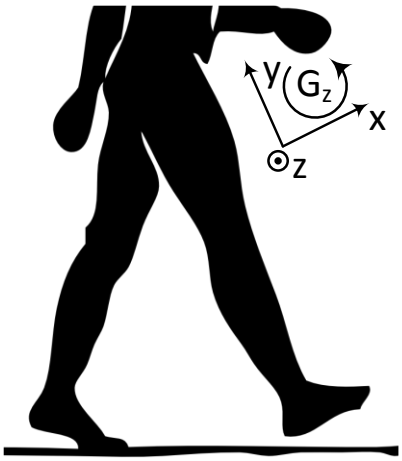

Figure 5.9 – Reference axis of IMU data

The thigh angle estimation is based on integration of gyro–z signal and the integration drift is compensated by zero–acceleration update when the total acceleration read by the accelerometer is within a certain thresholds (typically gravitational acceleration + noise margin). Hence, one condition for zero acceleration update was taken as:

$$\gamma_1 < \sqrt{a_{x_k}^2 + a_{y_k}^2 + a_{z_k}^2} < \gamma_2 \tag{5.1}$$

where a_{i_k} $(i = x, y, z)$ is the acceleration of $i-$ axis measured at time stamp *k*. The parameters γ_1 and γ_2 are selected to accommodate the noise embedded in the accelerometer reading and $(\gamma_1 + \gamma_2)/2$ to be equal to gravitational acceleration, g.

The second condition for taking zero acceleration updates is the angular velocity to be close to zero, which implies that the thigh is not in motion. It was observed that this condition improves the smoothness and the accuracy of the thigh angle. The condition is given as

$$g_{k_z} < \gamma_3 \tag{5.2}$$

where g_{k_z} is the angular velocity of $z-$ axis measured at time stamp k and γ_3 is selected to accommodate error in gyro data.

When the conditions in (5.1) and (5.2) are satisfied, thigh angle update is taken from the accelerometer reading and otherwise gyro is integrated to get the thigh angle update. Trapezoidal rule was used in the integration of the gyro reading

instead of using rectangle method which is commonly used in literature. The GIOF is shown as pseudo code in Figure 5.10 and line 6 of it illustrates the use of trapezoidal rule for integration. Note that the square root calculation of (5.1) is not performed in the algorithm and γ_1 and γ_2 are squared instead, to reduce the computational demand.

Inputs : a_{k_x}, a_{k_y}, a_{k_z}, g_{k_z}, $g_{(k-1)_z}$, θ_{k-1}, t_k, t_{k-1}
Outputs: θ_k

1. Read inputs
2. $\Delta t = t_k - t_{k-1}$
3. **if** $\gamma_1^2 < \left(a_{k_x}^2 + a_{k_y}^2 + a_{k_z}^2\right) < \gamma_2^2$ **and** $g_{k_z} < \gamma_3$ **then**
4. $\quad\quad \theta_k = atan2\left(a_{k_x}, a_{k_y}\right)$
5. **else**
6. $\quad\quad \theta_k = \theta_{k-1} + 0.5 \cdot \Delta t\left(g_{k_z} + g_{(k-1)_z}\right)$
7. **end if**
8. **return** θ_k

Figure 5.10 – Gyro Integration based Orientation Filter (GIOF) algorithm

$\boldsymbol{a_{i_k}}$ $(\boldsymbol{i} = \boldsymbol{x}, \boldsymbol{y}, \boldsymbol{z})$ is the acceleration of $\boldsymbol{i}-$ axis measured at time stamp *k*; $\boldsymbol{g_{k_z}}$ and $\boldsymbol{g_{(k-1)_z}}$ are gyroscope $\boldsymbol{z}-$ axis reading measured at time stamps *k* and (*k-1*); $\boldsymbol{t_k}$ and $\boldsymbol{t_{k-1}}$ are the time values of time stamps *k* and (*k-1*); $\boldsymbol{\theta_{k-1}}$ is the previous estimation of thigh angle and $\boldsymbol{\theta_k}$ is the current estimation of thigh angle.

5.4.5 Experimental Results

5.4.5.1 Comparison of MAL vs. IMU

Trimmed versions of the angle computed using MAL data (θ_{MAL}) and IMU data (θ_{IMU}) were used to compute the correlation of the two waveforms. θ_{MAL} and θ_{IMU} of one of the trials are shown in Figure 5.11 with the correlation coefficient. It was observed that the correlation of the two waveforms was higher when the correlation was calculated for a single stride cycle. However, the intention was to find the correlation for the entire trial. The analysis of 361 trials of 19 subjects (10 male and 9 female) reported a mean correlation of 99.58% between θ_{IMU} and θ_{MAL} with a standard deviation of 0.34%. The maximum and minimum correlations reported were 99.96% and 97.33% respectively. The correlation statistics of the trials are shown in Table VIII.

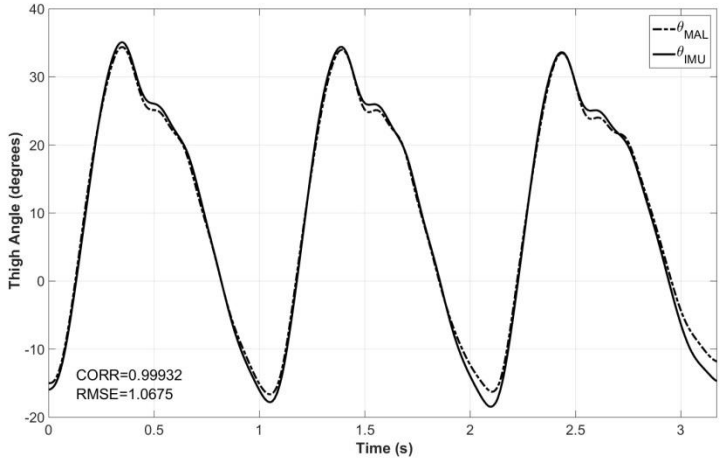

Figure 5.11 – Thigh angle computed from MAL data ($\boldsymbol{\theta_{MAL}}$) and IMU data ($\boldsymbol{\theta_{IMU}}$) for a sample trial

Correlation coefficient of the two waveforms is 0.99932 and RMSE is 1.0675 for this trial.

In addition to estimating correlation of the two waveforms, the error of the peak values was also calculated to check the goodness of the thigh angle estimation. The error of the estimated peak value was considered because the maximum and the minimum of the thigh angle are used to estimate the open angle and the swing angle of the stride. The histograms of the positive peak error and negative peak error are shown in Figure 5.12. The distributions show that the majority of error lies between ±3º. The RMSE for the positive and negative peaks are 2.0954º and 2.4967º respectively. The RMSE of each trial was also calculated and the mean of RMSE for all 374 trials was 1.8477º with a standard deviation of 0.56766º.

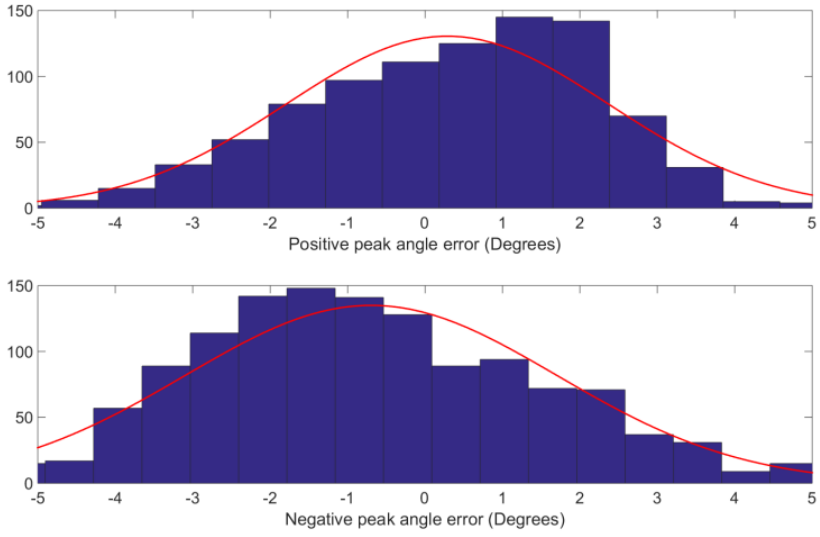

Figure 5.12 – Histograms of positive and negative peak angle errors

TABLE VIII – CORRELATION STATISTICS BETWEEN θ_{MAL} AND θ_{IMU}

	No. of Subjects	No. of Trials	Correlation Coefficient			
			Mean	***Max***	***Min***	***Std***
Males	10	196	0.9960	0.9995	0.9822	0.003114
Females	9	178	0.9955	0.9996	0.9733	0.003559
All	19	374	0.9958	0.9996	0.9733	0.003337

The same experiment was conducted with the involvement of 6 male and 4 female vision impaired subjects. With a total of 138 trials, the mean correlation between the thigh angle θ_{IMU} and θ_{MAL} was 99.16% with a standard deviation of 0.67%. The minimum and maximum correlations were 96.38% and 99.92%. The mean RMSE for all 138 trials was 1.9317º with a standard deviation of 0.4949º. The distributions of correlation and RMSE between θ_{IMU} and θ_{MAL} for vision impaired subjects are shown in Figure 5.13. These results imply that the algorithm gives comparable results in the case of vision impaired subjects too.

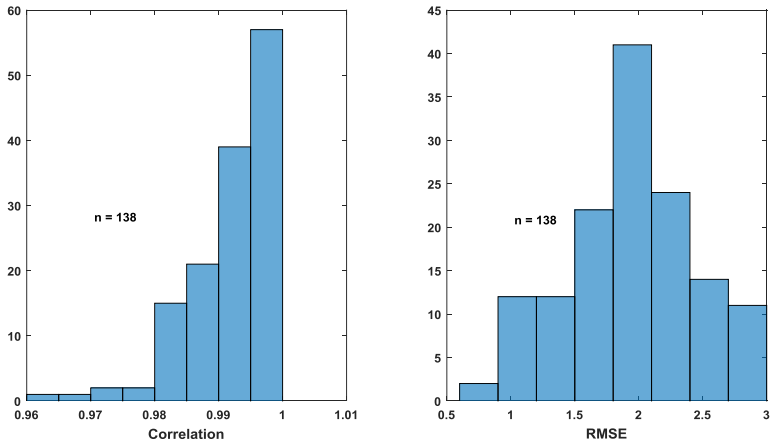

Figure 5.13 – Distributions of correlation and RMSE between $\boldsymbol{\theta_{IMU}}$ and $\boldsymbol{\theta_{MAL}}$ for vision impaired subjects

5.4.5.2 Real–time Implementation for Performance Comparison

The GIOF was implemented in the IMU discussed in Section 4.4 to compare its performance with complementary filter implementation. The execution time for GIOF and complementary filter implementation were measured separately by implementing complementary filter on the same platform. Complementary filter is selected to compare the performance as it is known to be a faster filter that consumes

lower amount of resources. It was observed, in Matlab analysis, that the complementary filter gives correlation close to afore mentioned correlations, when $\alpha = 0.9999$. Therefore, this value was used in the implementation. The first order complementary filter discussed in [54] was implemented in the microcontroller and is given by:

$$\theta_k = \alpha(\theta_{k-1} + \omega_k \cdot \Delta t) + (1-\alpha)a_k \tag{5.3}$$

where $\theta_k$and θ_{k-1} are the new and previous estimates of the thigh angle, ω_k is the current gyro reading, Δt is the sample time, a_k is the angle estimated by taking $atan2$ of the accelerometer readings.

The average execution time reported for the complementary filter implementation was approximately 570 µs on Arduino pro mini that has an 8–bit microcontroller running at 8 MHz. The execution time for GIOF was about 225 µs on the same platform when not performing $arctan$ and about 500 µs when performing $arctan$. The average execution time is about 250 µs for walking trials. This implies that the GIOF is computationally economical (by a factor of ½). Further, although the complementary filter had similar correlations when $\alpha = 0.9999$ in Matlab simulations, in real time implementation, the output of complementary filter drifted for that α value. Higher the α, the higher the output depends on the integration, which causes more drift in the output, but smoother the output is. Therefore, to minimize the drift α had to be reduced to 0.999 in the real time implementation.

All six (accelerometer and gyro) raw sensor data were low–pass filtered with a second order Butterworth low–pass filter with cut–off frequency of 10 Hz. A gyro calibration was performed to estimate the offset of each gyro axis and the offset was subtracted from the raw sensor data during computation. The thigh angle estimated by both GIOF and complementary filter in real–time in the IMU in several test trials were comparable.

5.4.6 Summary and Discussion

A novel single axis orientation estimation algorithm, Gyro Integration based Orientation Filter (GIOF) was presented in this section with a comparison of the

angle estimated by GIOF with a reference optical motion capture system. It was shown that the correlation of the angle estimated by GIOF to the angle measured by the reference system is above 97% with mean correlations above 99.5%. It was also shown that GIOF gives comparable results with vision impaired subjects. Two main features of GIOF are that it does a correction to the estimated orientation using acceleration, only when the acceleration is restricted to read gravity and that it uses trapezoidal rule instead of rectangle method for gyro integration.

Achieving one of the targets, the GIOF was proven to consume one half of the computation time consumed by the complementary filter on a low end 8-bit processor. The complementary filter is known to have lower computational demands and hence the comparison was done against it. The main reason for this is that the GIOF does not perform $arctan$ in each computation. Instead, it performs $arctan$ only when the accelerometer reading is stable which saves a number of floating point calculations. On the other hand, the complementary filter performs $arctan$ in its each iteration, hence consume more processor time. Further, the complementary filter produces low drift when α is lower, but the output becomes less smooth. However, the drift in the output is avoided to a great extent because the GIOF corrects the angle using the accelerometer.

Although memory expensive, a moving average filter has shown better performance in removing the bias of the gyro reading. With properly selected window size, the drift in the estimated angle may be significantly reduced with the moving average filter. However, the delay occurred in the filter becomes larger when the window size increases. For the window size selected in the analysis (150 samples), for a sampling rate of 100 samples per second, the moving average filter produces its output using 75 samples from either side of the current sample, which maps into a delay of 750 ms. This delay is not preferable for real time implementations, hence a high pass filter may be desirable in real–time implementation. Further, a buffer of 150 samples has to be maintained for the moving average filter, which is also not desirable for low end embedded systems.

Compared with RMSE of 3º reported in [57] for the forearm with Kalman filters, the RMSE of less than 2.5º and mean RMSE of 1.85º reported by GIOF is accurate enough for thigh angle estimation for gait analysis. This indicates that the

GIOF has achieved better processing speed on low end processors without compromising the accuracy.

Although the GIOF was implemented to estimate pitch of the IMU, it can easily be extended to 2–D and estimate both pitch and roll. Further, it may be extended to fuse magnetometer and gyroscope to estimate the yaw as well.

5.5 Harmonic Models for Thigh Movement during Walking

5.5.1 Introduction

Different gait modelling and identification approaches exist in literature using trunk movement [64], [72], foot movement [91], [92] or thigh movement [93]. Some of these techniques use acceleration whereas the others use the rotation or the orientation of the particular body section.

This section presents harmonic models for thigh flexion and extension of commonly observed stride patterns, derived from empirical data collected from a single thigh mounted IMU. It also presents harmonic models for the gyroscopic data of a thigh mounted IMU for the same stride patterns. Further, the possibility of classifying stride patterns using the derived harmonic models is discussed in this section. Data used for this analysis are same as collected in the experiment discussed in Section 5.4. The work presented in this chapter is submitted to Elsevier Measurement on Dec 11, 2015 and is under review.

5.5.2 Modelling of Thigh Angle

The flexion and extension (thigh angle) of both thighs shown in Figure 5.7 indicates that the two legs are in synchronization and hence, modelling one leg will help predicting the movement of the other leg in case of no other disability exists. Further, modelling of one leg may be sufficient to analyse the motion of both legs.

Raw data collected was used to estimate the thigh angle using GIOF discussed in Section 5.4.4. Then the thigh angle was cropped from a minimum (toe off) to a minimum excluding the first and the last strides of the walk. The rest of the analysis was performed on these cropped thigh angle waveforms.

As seen in Figure 5.7 and also verified in previous research [94], [95] that the thigh angle for level walking is periodic. The most common way of modelling a periodic signal is a harmonic model

$$y(t) = b + \sum_{n=1}^{N} a_n \cos(2\pi n f_0 t + \phi_n),\ n = 1, 2, \ldots \tag{5.4}$$

where f_0 is the fundamental frequency and n being the harmonic number with N^{th} harmonic be maximum significant harmonic. a_n and ϕ_n are the amplitude and the initial phase of the n^{th} harmonic [96]. The dc component present in the waveform is denoted by b.

To estimate values for these unknown parameters in the harmonic model in (5.4) empirically, the spectrum of each trial was derived using FFT (Fast Fourier Transform) function in Matlab. The number of frequency components in the FFT output was selected as the length of the time series sample instead of a power of 2, due to limited sample length. In addition to functions available in Matlab for deriving FFT and extracting peaks, a custom made function was used to extract the harmonics from the frequency spectrum. Figure 5.14 shows the frequency spectrum of a single trial and the harmonics extracted from the spectrum (shown by circles) by the function. The function also picks up the DC component of the spectrum. It can be seen that the fundamental has the highest amplitude, which was the feature used in the custom made function (listed in Appendix B) that identifies the fundamental frequency and extracts the amplitudes and initial phases of a specified number of harmonics (given as an input argument to the function) when the frequencies, amplitudes and phases of FFT are given as input to the function.

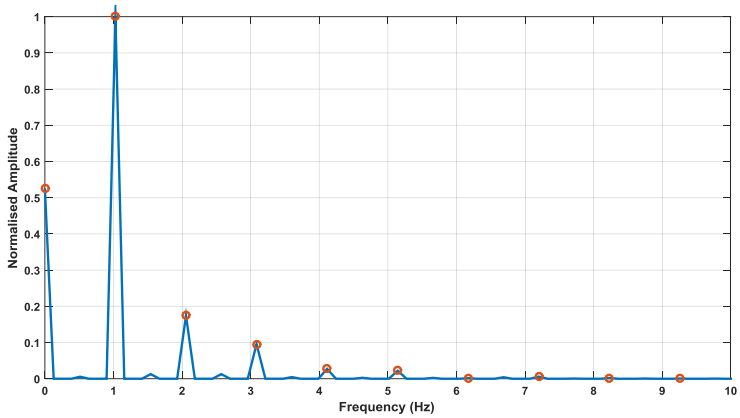

Figure 5.14 – Frequency spectrum of a sample trial and harmonic components picked from the function (shown by circles)

Figure 5.15 shows the amplitude distribution of first nine overtones of the frequency spectrum of all 372 trials, normalized to fundamental amplitude. It is seen by the figure that the median amplitude becomes lower than 1 % of the fundamental amplitude beyond fifth overtone. (The dash–dot line close to the bottom of the plot shows the 1 % of the fundamental amplitude.) Therefore, it can be concluded that, only first five harmonics are the significant frequency components of the thigh angle waveform for level walking.

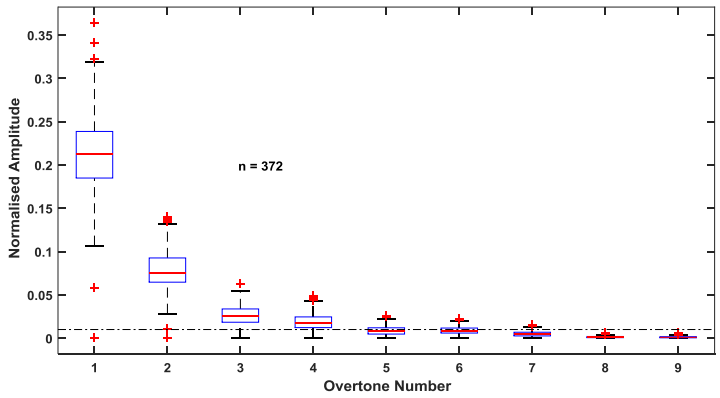

Figure 5.15 – Amplitude distribution of first nine overtones of all trials normalised to the fundamental amplitude

Based on this observation, the thigh angle waveform for each trial was reconstructed using (5.4) with coefficients of first five harmonics extracted from the same trial. The original and reconstructed thigh angle waveform of a sample trial is shown in Figure 5.16 and histograms of the correlation and RMSE between the original and the reconstructed waveforms of all 372 trials are shown in Figure 5.17.

It can be seen that the majority of the correlation between the original and the reconstructed signals is greater than 0.995 while the majority of RMSE is less than 2º, which indicates that the thigh angle waveforms can be accurately represented using harmonic model in (5.4) with five harmonics. This result is much better than the correlations achieved by Ibrahim with 12 harmonics for accelerometer [64].

The distributions of normalised amplitudes and initial phase of first five harmonics of all female and male trials are shown in Figure 5.18 and Figure 5.19. The amplitudes are normalized to fundamental amplitude. The figures indicate that the normalized amplitudes of the overtones are smaller for males than for females in the selected sample base, but phase of the harmonics are comparable.

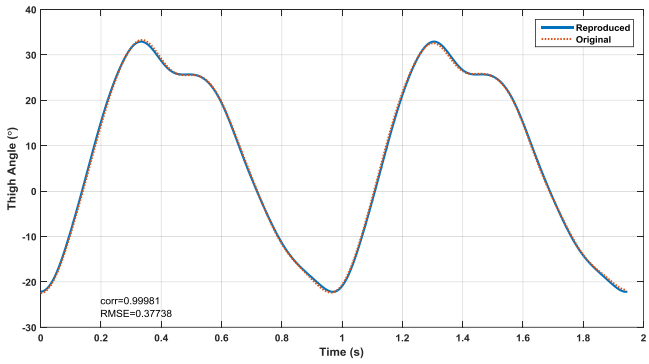

Figure 5.16 – Original and reconstructed thigh angle waveform of a sample trial

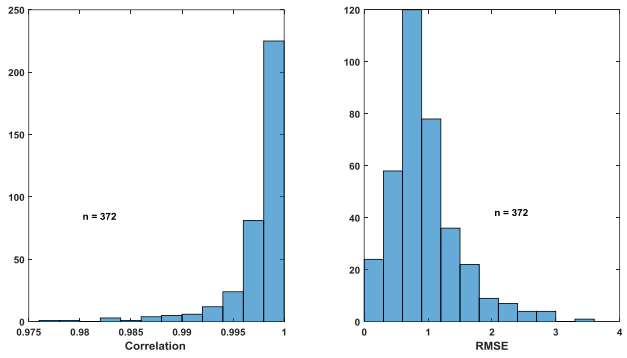

Figure 5.17 – Histograms of correlation and RMSE between original and reconstructed thigh angle waveform using 5 harmonics

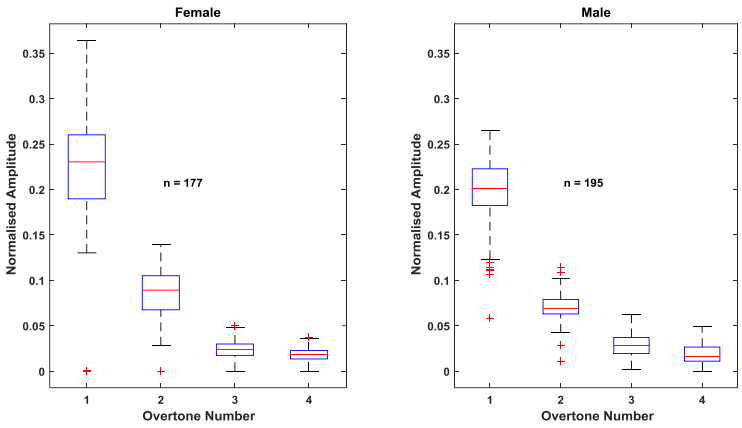

Figure 5.18 – Distribution of normalised harmonic amplitude of first four overtones of all female and male trials

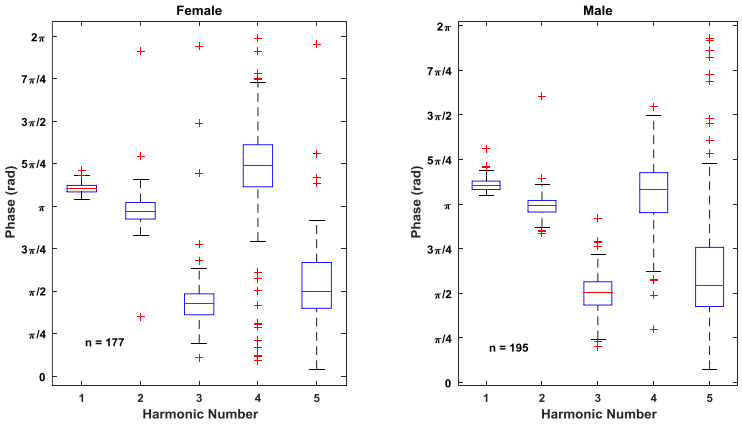

Figure 5.19 – Distribution of initial phase of first five harmonics of all female and male trials

The fundamental frequencies of the FFT, i.e. the stride frequencies of females were lower than to males in the subject sample volunteered for the trials. The peak stride frequency for females is about 0.925 Hz while for males that is close to 1 Hz. The distributions of the fundamental stride frequencies of female and male subjects are shown in Figure 5.20. The stride frequency was also computed using the stride time and compared with the fundamental frequency extracted from the spectrum. The error between stride frequencies estimated using stride time and the fundamental frequency was (0.0479±0.0029)% for a total of 750 strides for all subjects, which indicates that estimating the stride frequency using stride time is accurate.

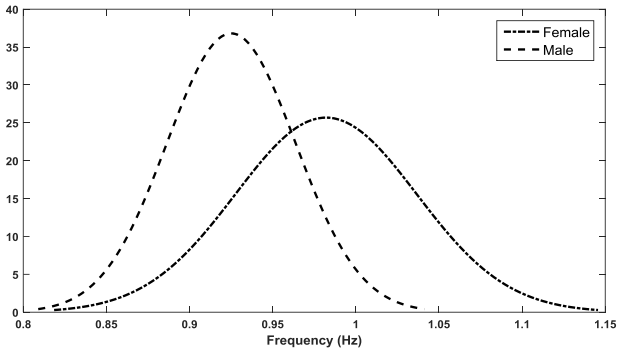

Figure 5.20 – Distribution of fundamental frequency (stride frequency) of female and male subjects

The next stage of processing was to perform spectral analysis for each stride. Each stride was extracted from a minimum to the next minimum of the thigh angle waveform and the spectral data were extracted for each stride using the same procedure followed to extract the harmonic model for the full trial. The extracted stride was cascaded four times before using FFT function to derive the spectrum in order to increase the data length as well as the resolution of the FFT output. In this case too, the number of frequency components of FFT output was selected as the input data length. Each stride was then reconstructed using (5.4) and the correlation and RMSE between the original and the reconstructed waveforms were computed. As seen in Figure 5.21, the majority of correlation is greater than 0.999 and the majority of RMSE is below 0.5º, which indicates that the model in (5.4) with five harmonics can be used to represent the thigh angle with high accuracy when each stride is considered.

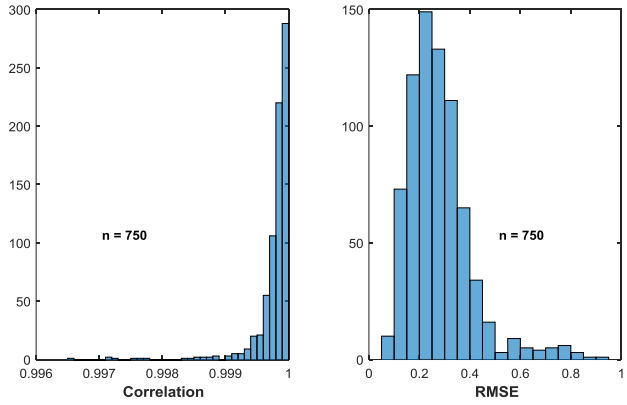

Figure 5.21 – Correlation and RMSE between original and reconstructed thigh angles for each stride

5.5.3 Harmonic Models for Thigh Flexion and Extension Derived from IMU data

To establish harmonic models for thigh angle derived from IMU data for level walking, thigh angle for each stride was plotted. It was observed that some stride patterns are frequently found in the set of 750 strides collected from all subjects, both male and female. Therefore, it was decided to formulate harmonic models for those frequently observed stride patters. Figure 5.22 depicts six such thigh angle patterns starting with almost no oscillation after the main maximum (end of swing and heal contact) and ending with a pattern where the secondary peak is approximately as strong as the primary peak. The reasons for these stride patterns as observed in the experiments are as follows.

- **Pattern 1**: The heal contact is exactly at the end of the swing of the reference leg and the foot is almost flat by the time of the heal contact so that no oscillation of thigh is visible during Loading Response.
- **Pattern 2**: The heal contact is slightly after the end of the swing of the reference leg and the foot is having a small angle to ground so that an angle change in the thigh is slightly visible during Loading Response.
- **Pattern 3**: The heal contact is slightly after the end of the swing of the reference leg and the foot is having a larger angle to ground than to previous case so that a larger angle change in the thigh is visible during Loading Response.
- **Pattern 4**: The heal contact occurs after the end of the swing of the reference leg, so that the leg moves downwards before heal contact and the foot is in an angle to ground by the time of the heal contact. Hence, an oscillation of the thigh is visible during Loading Response.
- **Pattern 5**: The heal contact occurs after the end of the swing of the reference leg, so that the leg moves downwards before heal contact and the foot is in an angle to ground by the time of the heal contact. More oscillation of the thigh is visible during Loading Response in this case compared to the previous.
- **Pattern 6**: The heal contact occurs after the end of the swing of the reference leg, so that the leg moves downwards before heal contact

and the foot is in an angle to ground by the time of the heal contact. A strong oscillation is visible during Loading Response so that the secondary peak is comparable to the primary peak.

For deriving harmonic models for these six patterns, sample trails that have thigh angle patterns similar to each of these patterns were collected using the following procedure:

Each stride was resampled to 2000 sample points and normalised in time and amplitude. The stride time was normalised to 1s while the amplitude was normalized in such a way that the minimum of the waveform be 0 and the maximum be 1. Then all strides having RMSE less than 2.5 % to each of the selected stride pattern (each of Figure 5.22) were extracted from all 750 strides. The stride waveforms extracted such a way was used to estimate a mean waveform to represent each of the wave patters shown in Figure 5.22. Harmonic models as given in (5.4) were derived for each of these mean curves with five significant harmonics and are depicted in Figure 5.23. *n* in the right hand side figure for each pattern indicates how many samples of similar shape were used to derive the mean thigh angle pattern for each different pattern. Table IX shows the normalised amplitudes and initial phases extracted for the six models.

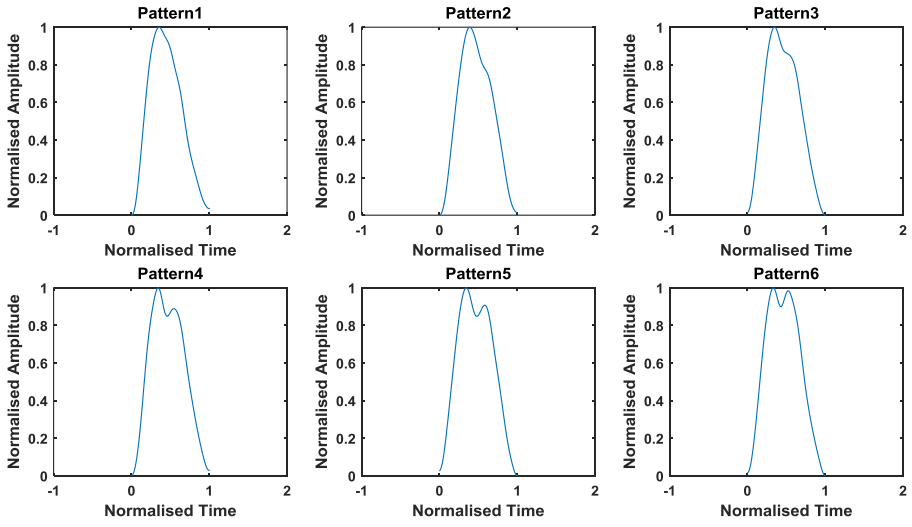

Figure 5.22 – Six common thigh angle patterns observed in all trials

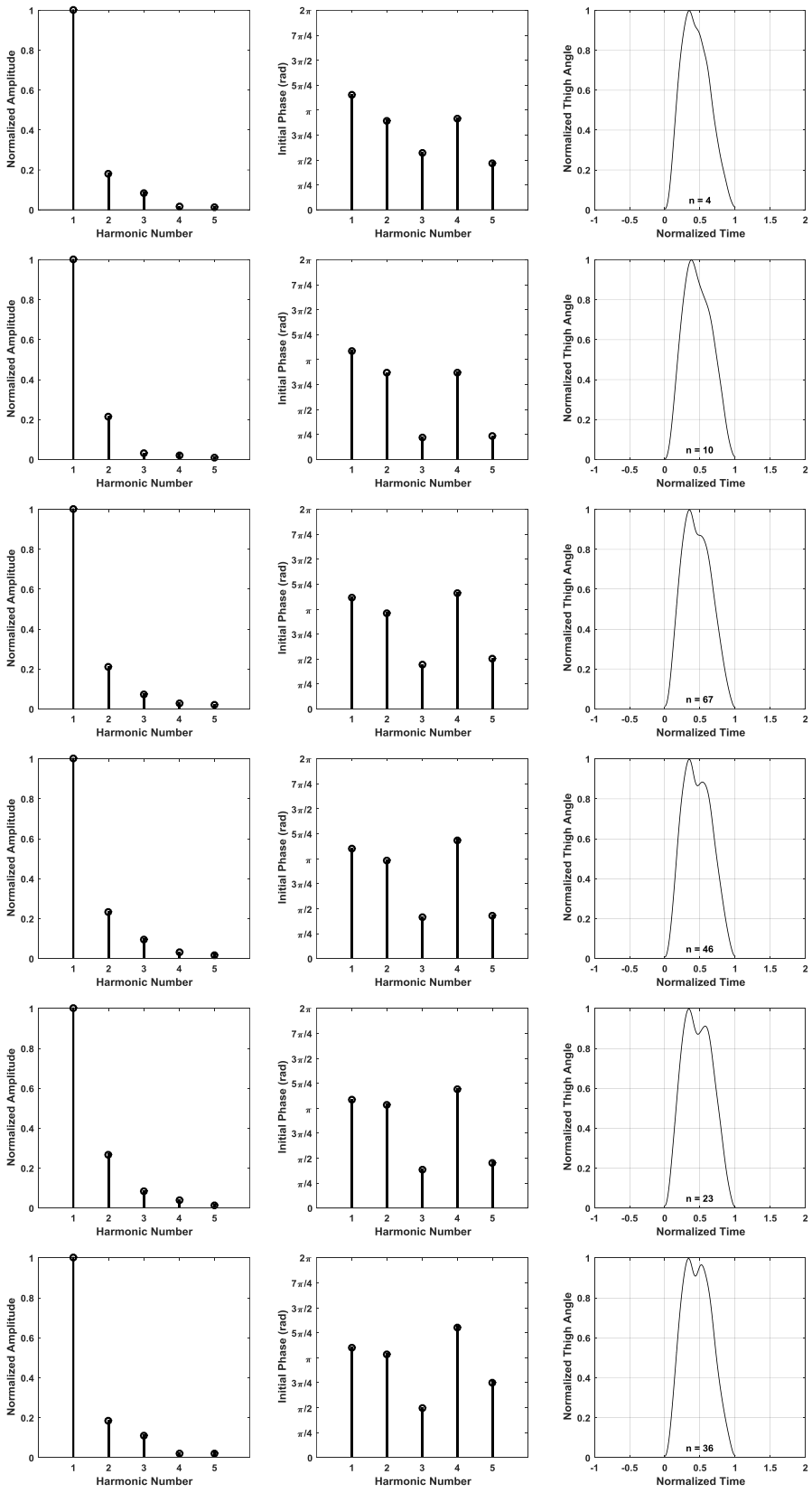

Figure 5.23 – Harmonic models for six commonly observed thigh angle patterns

TABLE IX – COEFFICIENTS OF HARMONIC MODELS OF THE SIX COMMON THIGH ANGLE PATTERNS

Model	1st Harmonic		2nd Harmonic		3rd Harmonic		4th Harmonic		5th Harmonic	
	a_n	ϕ_n (rad)	a_n	ϕ_n (rad)	a_n	ϕ_n (rad)	a_n	ϕ_n (rad)	a_n	ϕ_n (rad)
1	1	3.6133	0.18150	2.8125	0.08525	1.7860	0.015085	2.8816	0.013952	1.4683
2	1	3.4174	0.21348	2.7200	0.03001	0.6868	0.022038	2.7407	0.010615	0.7321
3	1	3.5088	0.20959	3.0176	0.07352	1.3860	0.028212	3.6534	0.019884	1.5846
4	1	3.4504	0.23148	3.0875	0.09581	1.2984	0.030199	3.727	0.018138	1.3387
5	1	3.4057	0.26781	3.2431	0.08322	1.1994	0.038494	3.7332	0.014827	1.4261
6	1	3.4515	0.18452	3.2409	0.10950	1.5581	0.021041	4.0952	0.022180	2.3650

The spectrums of the gyro signals for each stride were also derived using FFT. It was seen that there are nine significant harmonic components in the case of gyro signals. In a similar way to thigh angle, the gyro signal was also reconstructed using the amplitudes and initial phases of the first nine harmonics using (5.4). The histograms of correlation and RMSE between original and reconstructed gyro signals are shown in Figure 5.24. It can be seen from the figure that the gyro signal can be reconstructed using the harmonic model with nine significant harmonic components with better regeneration accuracies than that of the thigh angle waveform.

The spectrums of the gyro signals of afore mentioned stride patterns were also derived. The normalized amplitudes and initial phases of first nine harmonics of the spectrum of the gyroscopic signals of the six commonly observed stride patterns are shown in Figure 5.25 and the coefficients are tabulated in Table X.

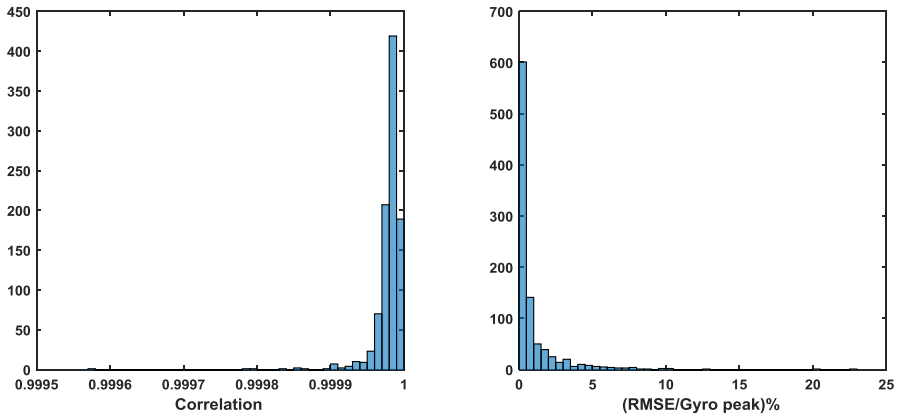

Figure 5.24 – Correlation and RMSE between original and reconstructed gyro signal for each stride

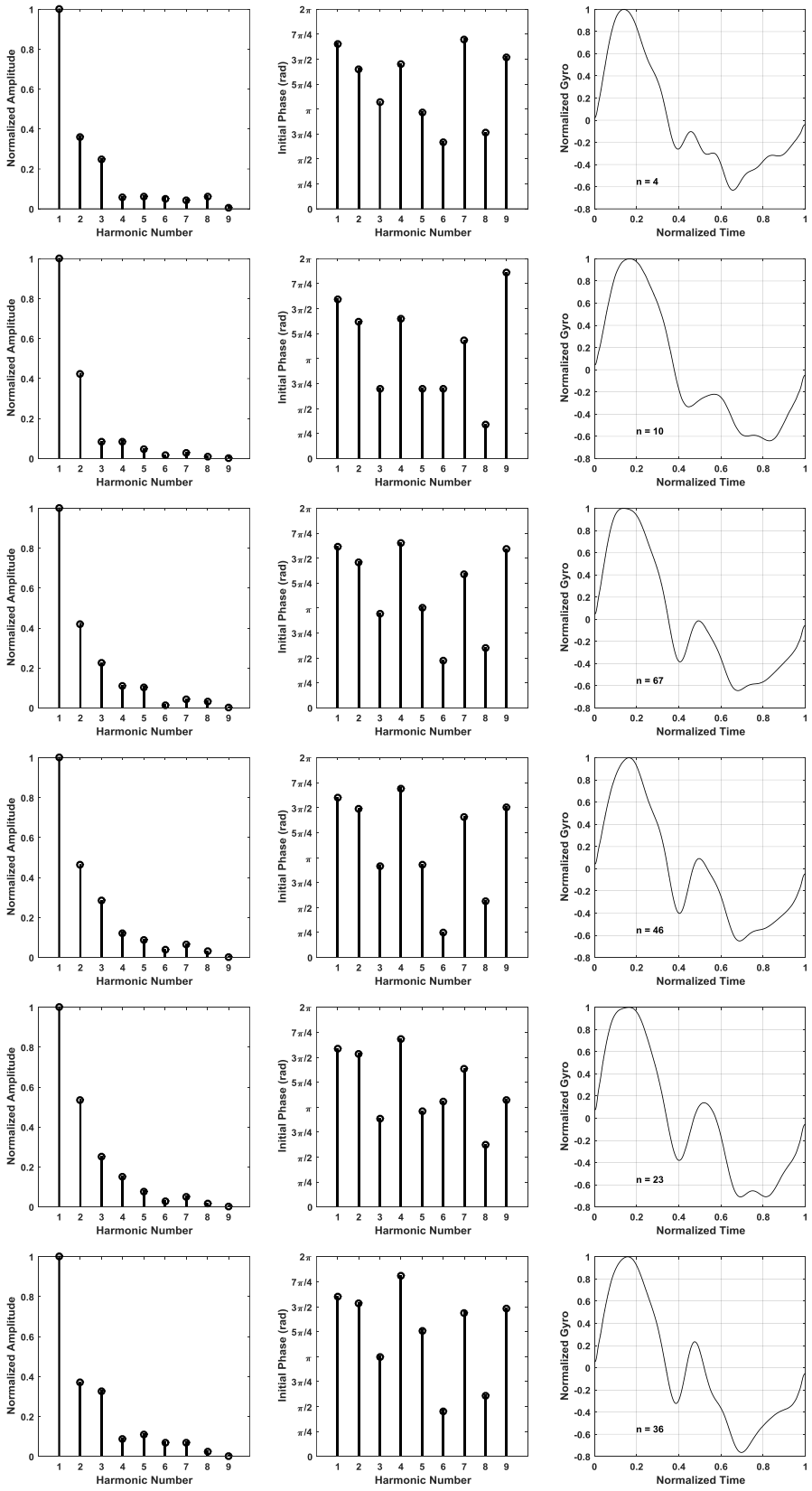

Figure 5.25 – Harmonic models of gyro signal for six commonly observed thigh angle patterns

TABLE X – COEFFICIENTS OF HARMONIC MODELS OF GYRO SIGNALS OF THE SIX COMMON THIGH ANGLE PATTERNS

Model	1st Harmonic		2nd Harmonic		3rd Harmonic		4th Harmonic		5th Harmonic	
	a_n	ϕ_n (rad)	a_n	ϕ_n (rad)	a_n	ϕ_n (rad)	a_n	ϕ_n (rad)	a_n	ϕ_n (rad)
1	1	5.19	0.36027	4.402	0.2489	3.3649	0.059486	4.5546	0.063368	3.0386
2	1	4.996	0.42343	4.3092	0.084499	2.1904	0.085638	4.3984	0.047704	2.1871
3	1	5.0759	0.42098	4.58	0.22486	2.9632	0.11145	5.1886	0.10383	3.1609
4	1	5.0243	0.46313	4.666	0.28408	2.8688	0.12266	5.3146	0.087658	2.9082
5	1	4.9736	0.53663	4.8087	0.25256	2.7775	0.15274	5.2844	0.077172	3.0107
6	1	5.0247	0.36973	4.8195	0.32584	3.1308	0.086019	5.6766	0.10968	3.9544

Model	6th Harmonic		7th Harmonic		8th Harmonic		9th Harmonic	
	a_n	ϕ_n (rad)	a_n	ϕ_n (rad)	a_n	ϕ_n (rad)	a_n	ϕ_n (rad)
1	0.051567	2.0871	0.043595	5.3394	0.06063	2.397	0.006469	4.7733
2	0.01632	2.187	0.028081	3.7139	0.008522	1.0669	0.00339	5.8446
3	0.014819	1.4992	0.042851	4.2084	0.031311	1.8894	0.002707	4.9969
4	0.039558	0.79304	0.064016	4.4247	0.030717	1.7806	0.002826	4.7229
5	0.029039	3.3201	0.049497	4.3447	0.015691	1.9591	0.000666	3.3624
6	0.069381	1.4251	0.067827	4.5243	0.022453	1.9092	0.000749	4.6469

5.5.4 Classification of Strides Using Harmonic Models

Identifying and classifying different stride patterns is important in rehabilitation and navigation applications because the prediction accuracies may be increased by using different models for different stride patterns. Therefore, the possibility of classifying strides using the harmonic models derived using IMU data, was also investigated in this research. The following sections discuss how the harmonic models derived earlier can be used to predict the thigh angle waveform and classify strides of a long walking trial.

5.5.4.1 Predicting Thigh Angle Using Harmonic Model

Thigh angle of a long walk (approximately 20 strides) of a single subject was first reconstructed using harmonic model extracted from the first stride. Normalised harmonic amplitudes and initial phases of harmonics were extracted from the first stride of the trial and were used to regenerate the thigh angle waveform for the full trial. The thigh angle was reconstructed using the timing of the stride and then rescaled in the amplitude axis to match the peak–to–peak variation of the measured thigh angle of the stride. The total stride was reconstructed with an RMSE of 1.33º

and a correlation of 0.997. The original thigh angle waveform and the thigh angle reconstructed using the harmonic model in (5.4) with 5 significant harmonics is shown in Figure 5.26. It can be seen in the figure that the reconstructed waveform is deviated from the original in some strides. That is because a person may have different stride patterns as discussed in Section 5.5.3. This observation was the basis for the work discussed in Section 5.5.4.2.

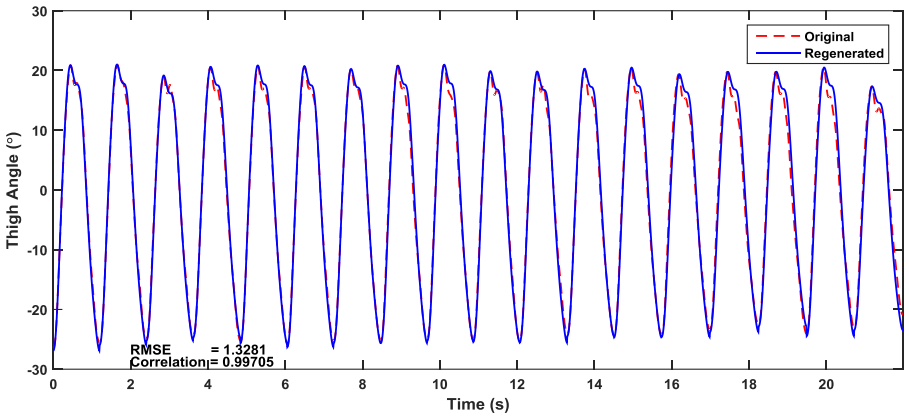

Figure 5.26 – Thigh angle waveform reconstructed using harmonic model with 5 harmonics and the original thigh angle waveform for a long walk

5.5.4.2 Classifying Strides

Based on the observation that a person may have different stride patterns even within the same trial, the possibility of classifying strides using the harmonic model was investigated. The correlation and RMSE of thigh angle of each stride with the thigh angle generated by the six models were computed for four different cases. The reconstructed thigh angle was scaled to match the measured thigh angle using the same method discussed before. The cases considered were walking with 3 self–selected stride rates (slow, medium and fast) on a hard floor and walking on sand (to test if this method can be used to distinguish different floor hardness). The variation of the stride pattern through the walk and for different cases can be seen by analysing the correlation and RMSE matrices. Figure 5.27 depicts the correlation matrices as colour maps. Each matrix shows the correlation of each stride of a given trial to the pattern reconstructed using each model. Each column of a matrix represents a single stride and a raw represents a particular model.

It can be seen in the figure that all the strides are having better correlation to Model 1 for slow walking whereas for medium walking, most of the strides have

closer correlation to Model 3 while some strides are of the patterns of Models 1, 4 or 6. For fast walking, the stride pattern has become that of Model 6 while on sand it becomes Model 1 except for few strides where the stride pattern is Model 3. According to the observations made during the trial on sand, the stride pattern becomes that of Model 3 when the sand is hard, and to Model 1 when sand in loose. These observations indicate that the harmonic models of thigh angle can be used to identify the variation of strides during a single walking trial.

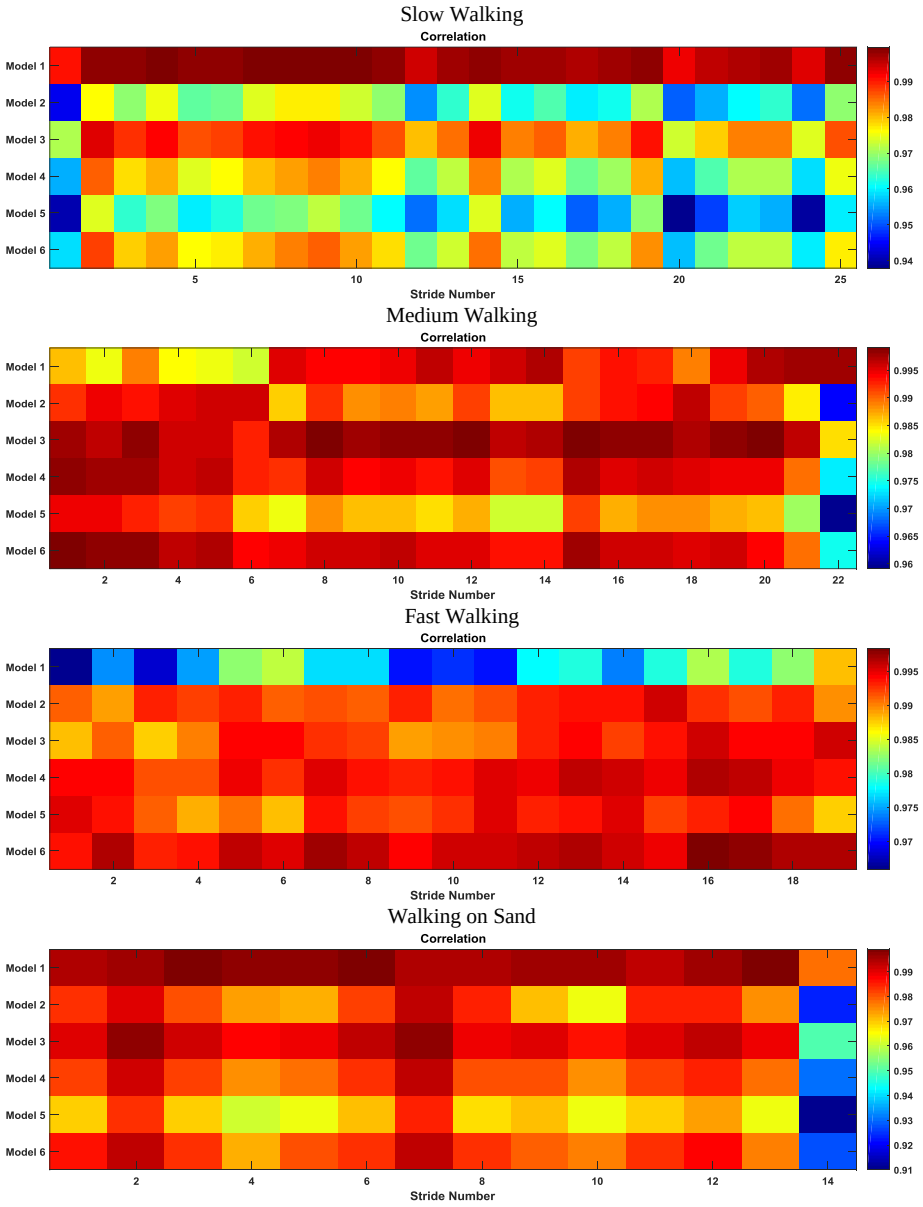

Figure 5.27 – Correlation of each stride with model generated waveform for different cases

The classification of strides using the correlation of the original stride waveform to the reconstructed waveform may be verified using RMSE between the stride waveform and the model. Figure 5.28 shows the RMSE matrices as a colour

map for afore said scenarios. It is clear that the RMSE matrices also followed the same pattern to the correlation matrices. The closer the correlation of the thigh angle waveform of a particular stride and the waveform generated by a particular model to 1, the higher the shape of the stride is of the shape of the model. In the case of RMSE, the smallest value represents the best model. Hence, the best model that represents the shape of a particular stride is the one that gives the highest correlation and the smallest RMSE.

The same classification can be performed using the gyro signal of each stride. As seen in Figure 5.25, the toe–off point is the positive zero crossing of the gyro signal. The classification performed with gyro signal also gives similar results as shown in Figure 5.29. This indicates that the classification and reconstruction can be performed using gyro signal.

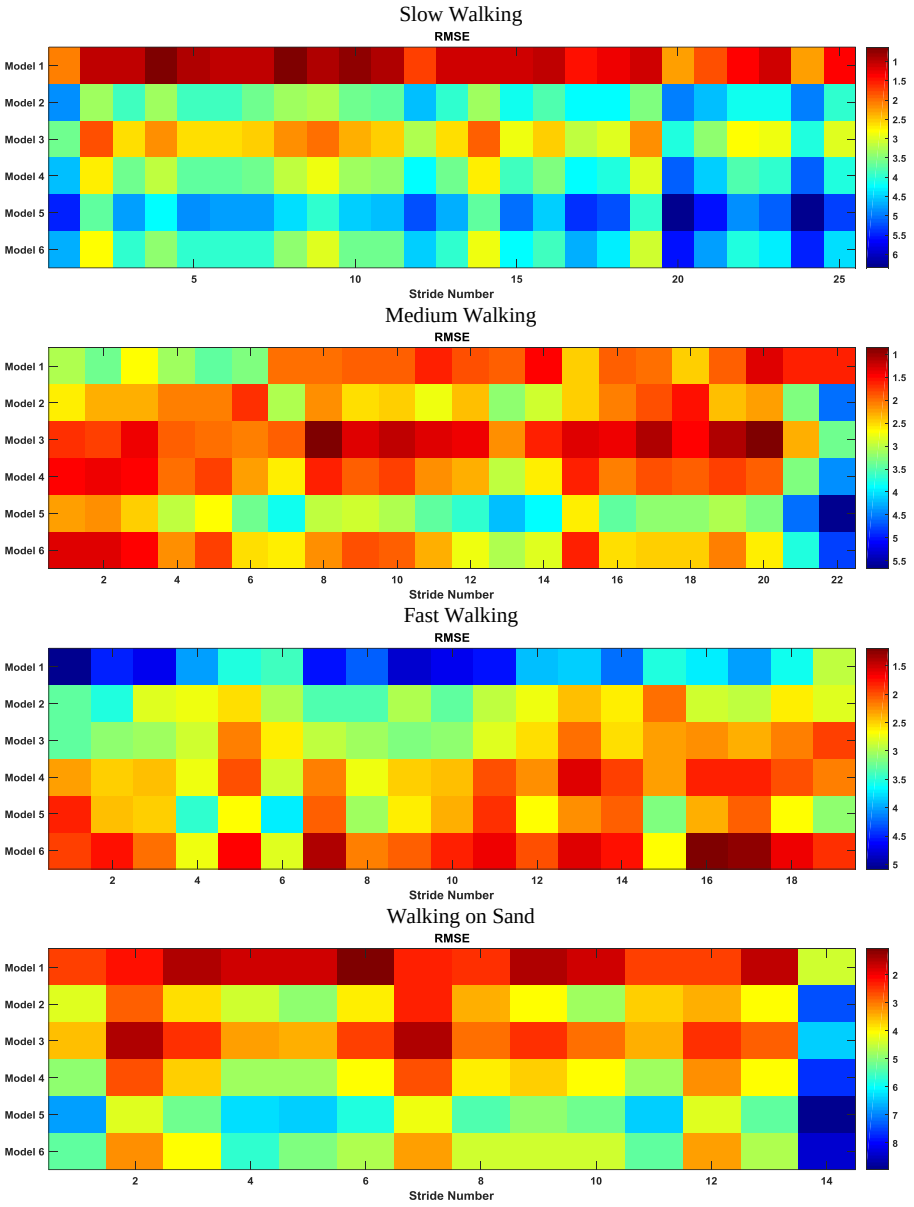

Figure 5.28 – RMSE of each stride with model generated waveform for different cases

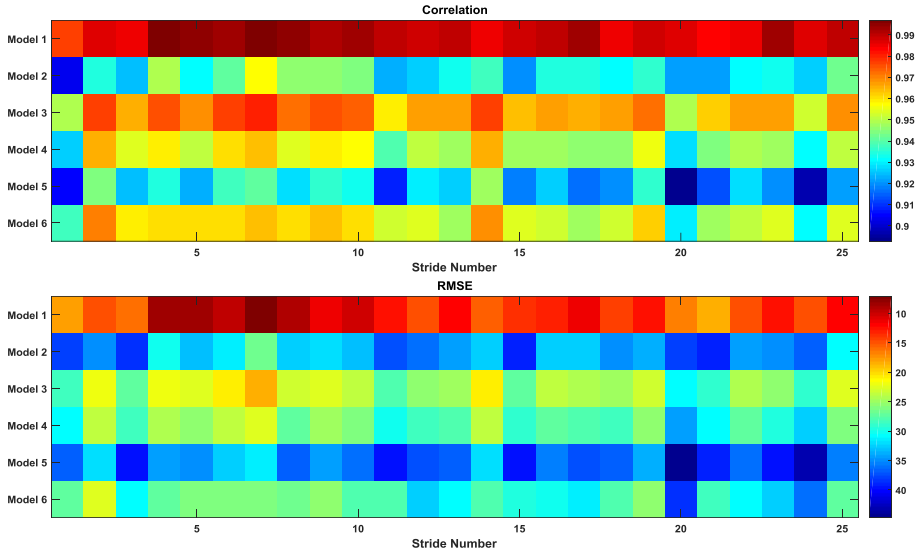

Figure 5.29 – Correlation and RMSE of gyro signal of each stride to the model generated waveform for slow walking

5.5.5 Summary and Discussion

Harmonic models for the thigh angle and the gyroscopic signal were presented in this section. By analysing spectrums of thigh angle of 372 level walking trials of 19 subjects, both male and female, it was observed that the first 5 harmonics are significant. The condition for significance was selected as 1% of the fundamental amplitude (*i.e.* the maximum amplitude). The harmonics were derived for the full trial of all samples using FFT and the waveforms were reconstructed using the harmonic model of (5.4). The correlation greater than 99.5% and RMSE less than 2° between the original and reconstructed indicated that the thigh angle waveform can be well reconstructed with a harmonic model with first 5 harmonics. For the gyro signal, the number of significant harmonic components is 9. The thigh angle and the gyro signal for each stride were reconstructed with the harmonic models with correlations greater than 99.9% and 99.99% and RMSE less than 1° and 5% respectively, which is a better fit than to the full stride.

Harmonic models for thigh angle and gyro signal for 6 commonly observed stride patterns were also presented in this section. The models were then used to classify strides of a trial of long flat walk (about 20 strides). It was shown that the correlation and the RMSE between the original and the model generated signals may be used together to identify the stride patterns. Correlations above 99% and RMSE less than 2º were observed with the best matching model. Best correlation and the

RMSE indicate the model that matches the particular stride most in the classification process. The thigh angle waveform of a long level walk was reconstructed using the harmonic model extracted from the first stride with 5 harmonics with a correlation of 99.7% and RMSE of 1.3°. All these correlation and RMSE figures are far better than the correlation and error figures achieved in [64] and [65]. Further, it can be seen that these harmonic models can be used for different applications as discussed in the following paragraphs.

Harmonic models for common stride patterns may be derived from a set of samples for the purpose of classification for a selected group of subjects. These groups may be people with no impairment or disability, patients having a certain lower limb disability or patients who underwent a lower limb surgery. These models may then be used to classify or identify one's stride patterns in order to identify certain lower limb disability or for pre and post movement analysis of a surgery, however, may need higher sampling rates and sensors with higher accuracy to identify fine details of the gait pattern.

Further, the harmonic models may be used to identify a person's stride patterns for the purpose of navigation application. Harmonic models may be extracted for a given subject to identify different stride patterns that a particular person has, with different terrains, activities or footwear. Figure 5.30 shows some sample strides for up and down walking on stairs and ramp. It can be seen that the stride patterns are quite different from the patterns of level walking in these cases, which may be used in activity recognition.

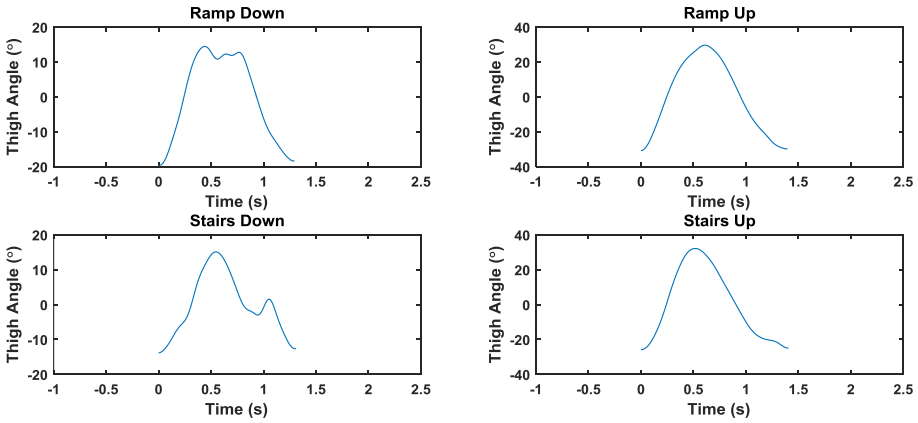

Figure 5.30 – Thigh angle patterns for different activities

It was also shown that the stride modelling and classification can be performed using the gyro signal and the harmonic models derived for the selected thigh angle patterns. However, in this case the first 9 harmonics became significant.

Thigh angle waveform patterns, similar to the patterns observed with non–vision–impaired subjects, were observed with vision impaired subject. Therefore, same techniques may be applicable to vision impaired subjects too.

In conclusion, the thigh angle can be reconstructed with a harmonic model with 5 harmonics and the gyro signal with 9 harmonics with great accuracy. These harmonic models may be used for many different navigation and rehabilitation applications.

5.6 Step Length Estimation

5.6.1 Introduction

Two different step length models that use the maximum and minimum thigh angle are presented in this section and the estimation performances are compared. A technique to estimate the peak thigh angles using the gyro peaks is also presented in this section. With this technique, one of the step length models was rewritten to derive an additional model for step length as a function of gyro peaks and time between peak and zero crossing. The performance of this model is also evaluated for the estimation accuracy taking gyro peaks as inputs.

5.6.2 Step Length Model

Figure 5.31 was used to derive a model to estimate step length as a function of the thigh angle. The figure represents the swing of the reference leg, which is shown in blue and the other leg that goes in stance phase is shown in red. In practical scenarios, the effective leg lengths and maximum flexion and extension angles are not identical stride to stride, hence different labels are used for each posture. Referring to the diagram, the step length, l_s, can be written as:

$$l_s = l_1 \sin\theta_1 + l_2 \sin\theta_2 + l_3 \sin\theta_3 + l_4 \sin\theta_4 + \varepsilon_1 + \varepsilon_2 \tag{5.5}$$

where l_1, l_2, l_3 and l_4 are the effective leg lengths and θ_1, θ_2, θ_3 and θ_4 are the angles of the thigh to vertical of the two legs at each posture as shown in Figure 5.31. ε_1 and ε_2 are the lengths that are not covered under the open angle of the leg. Analysing gait using a single thigh mounted IMU was considered in this study, as such, the angles of the non–reference leg is not measured. Therefore, to make the model simple and usable with a single thigh mounted IMU, it is assumed that $l_1 \approx l_3$, $l_2 \approx l_4$, $\theta_1 \approx \theta_3$, $\theta_2 \approx \theta_4$ and $\varepsilon_1 \approx \varepsilon_2$, which is depicted in Figure 5.32. With these assumptions, (5.5) can be deduced as

$$l_s = 2 \cdot \left(l_1 \sin\theta_1 + l_2 \sin\theta_2 + \varepsilon \right). \tag{5.6}$$

where all values are as in Figure 5.32.

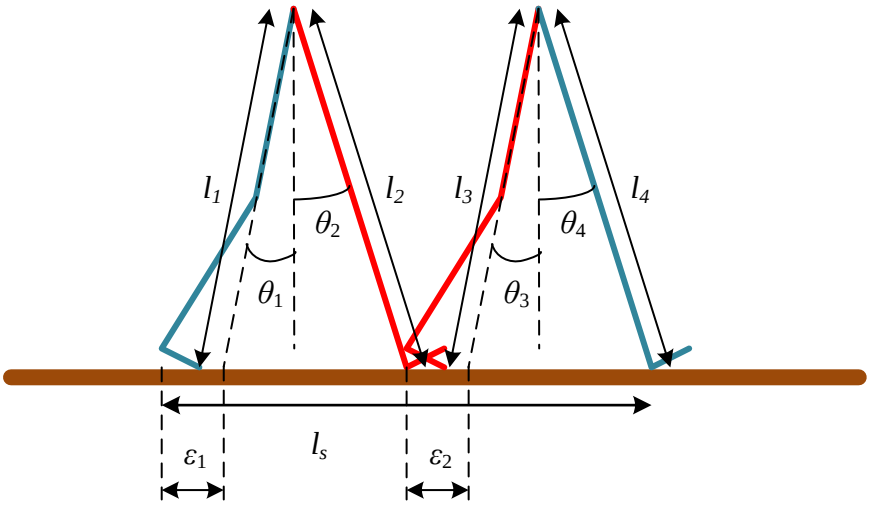

Figure 5.31 – Representation of leg positions during a step

Blue leg represents the reference leg.

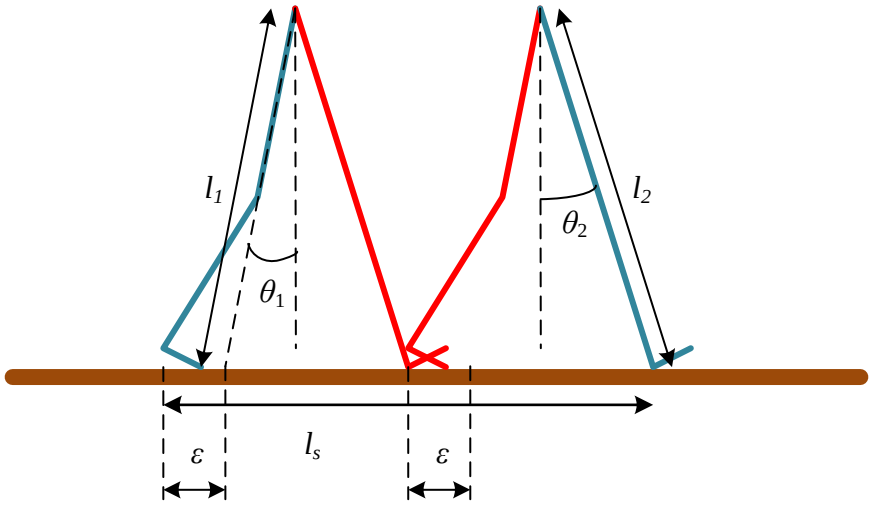

Figure 5.32 – Simplified representation of leg positions during a step

Blue leg represents the reference leg.

The model in (5.6) can be written in a generalized form as

$$l_s = a \cdot \sin\theta_1 + b \cdot \sin\theta_2 + c \tag{5.7}$$

where *a*, *b* and *c* are model parameters that need to be learnt per each subject, θ_1 and θ_2 are the thigh angles at toe off and Initial Contact of the particular step. It was shown in Section 5.4.2 (in Figure 5.6) that the minima of the thigh angle next to the positive peak synchronizes with the heel contact. It was also shown in Section 5.5 that this minima is invisible in some stride patterns. Therefore, the positive thigh angle peak has to be taken as θ_2 in practical scenarios. For small thigh angles, because $\sin\theta \approx \theta$, (5.7) may be further deduce as

$$l_s = a \cdot \theta_1 + b \cdot \theta_2 + c\,. \tag{5.8}$$

The models in (5.7) and (5.8) were considered in the experiment to test the accuracies of step length estimation. The experiment and the results are discussed in Section 5.6.5.

5.6.3 Estimating Maximum Thigh Flexion and Extension without Integration

The gyroscope signal is integrated to estimate the thigh angle in the orientation estimation algorithm discussed in Section 5.4. As discussed there, one

main issue faced in integrating gyro signal is the drift caused in the integration. When there is an error in the estimated thigh angle, that error will be translated into an error in the estimated step length. This subsection discusses the possibility of estimating the maximum flexion and extension angles of the thigh during walking without integrating the gyro signal.

It was observed that the peak of the gyro signal that comes before the zero crossing corresponds to a zero crossing of the thigh angle and the zero crossing of the gyro signal corresponds to the peak of the thigh angle as shown in Figure 5.33. Therefore, the gyro signal that contributes to the peak thigh angle is the part between the maxima of the gyro signal to the zero crossing. Hence, if the curve is approximated to a mathematically defined shape such as a straight line, cosine or a polynomial, the maximum thigh angle may be estimated using the peak gyro value and the time between the peak and the zero crossing. Three approximations for each part of the curve, *i.e.* the part from positive peak of the gyro signal to zero crossing and the part from negative peak of the gyro signal to zero crossing, were considered in this study. These sections were considered separately because of their different shapes. The three approximations considered are straight line, cosine and a polynomial fit for the gyro signal representing the shape of the sections.

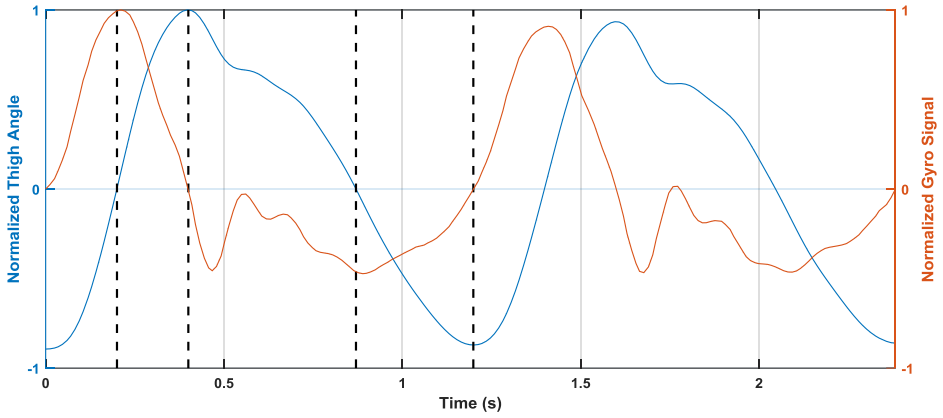

Figure 5.33 – Synchronization of gyro and thigh angle waveforms

Vertical dash lines indicate the key points

Figure 5.34 shows straight line approximation for the 2 sections of the gyro signal that contribute to positive (shown in blue) and negative (shown in red) peaks. Now, the integration of gyro of each potion can be approximated to the area of the

triangle between the line and the time axis as shown in Figure 5.34. In the case of the cosine and fitted curve approximations, the peak thigh angle may be approximated to the area under the curve. To fit a curve for each section of gyro signal, the mean curve of 948 samples was considered as the curve representing the set of curves. The fit was derived for both parts of the gyro signal separately and the best fit for both sections were 7th order polynomials. The coefficients of the polynomial for each section was estimated separately using Matlab Curve Fitting Tool. If θ is the corresponding peak thigh angle, G_P is the corresponding peak gyro value and t is the time between the gyro peak and zero crossing, then θ can be approximated by the three methods as given in (5.9).

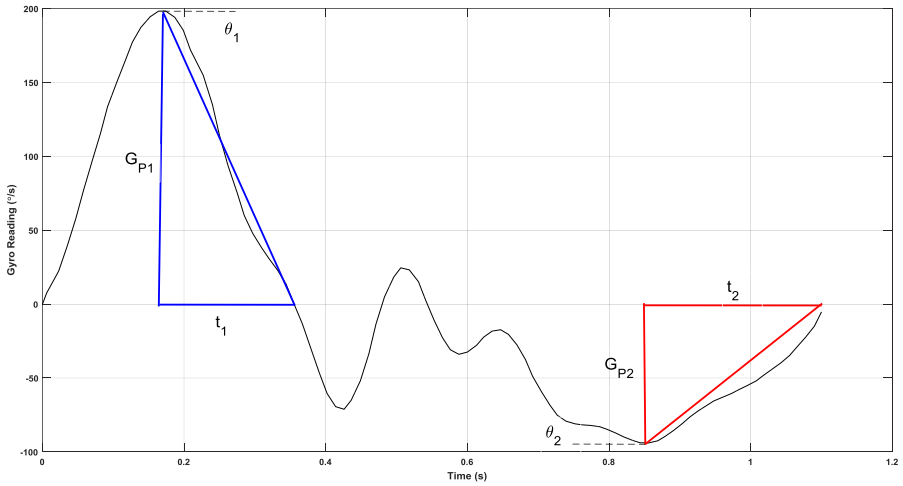

Figure 5.34 – Straight line approximations for the sections of the gyro curves that contribute to the thigh angle peaks

$$
\begin{aligned}
&Line: \quad \theta \approx 0.5 \cdot G_P \cdot t \\
&Cos: \quad \theta \approx \frac{2}{\pi} \cdot G_P \cdot t \\
&Poly: \quad \theta \approx \alpha \cdot G_P \cdot t; \\
&\alpha = 0.6279 \text{ for positive } \theta \text{ and } \alpha = 0.6308 \text{ for negative } \theta
\end{aligned}
\tag{5.9}
$$

It can be seen that all these approximations have a constant in front of the product of gyro peak and the time, which means that the plot of the estimated peak angle and the peak angle computed by integration should look similar except a gradient difference. The goodness of the three approximations given in (5.9) were tested using data collected. 948 strides were used for this assessment. The results indicated that the R–square and Adjusted R–square values of the line fitted in all

three cases take the same value. However, the RMSE was lowest for the straight line approximation while cosine approximation had the gradient closest to 1, which indicate that the cosine approximation is the closest approximation. Figure 5.35 shows the estimated peak thigh angle *vs*. integrated peak thigh angle with straight line approximation for positive and negative peak angles with the goodness figures.

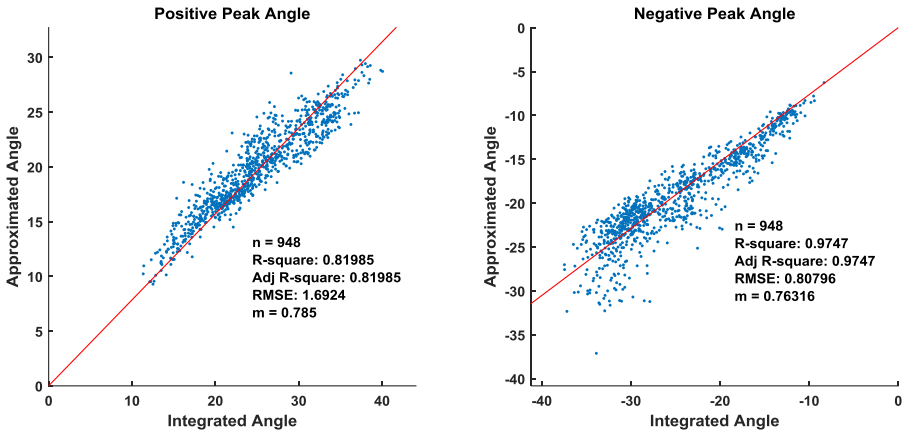

Figure 5.35 – Estimated peak thigh angle *vs*. integrated peak thigh angle with straight line approximation for positive and negative peak angles

5.6.4 Step Length as a Function of Gyro Peaks

With the approximations discussed in Section 5.6.3, the step length models can now be represented as functions of gyroscopic peaks. To generalize the approximations, the peak thigh angle, θ, can be replaced with a function of gyro peak and the time between the peak and zero crossing of gyro signal as

$$\theta = \alpha \cdot G_P \cdot t \tag{5.10}$$

where G_P and t are the gyro peak and the time between gyro peak and zero crossing that contributes to the particular peak thigh angle and α is a constant that includes the correction factors. Now (5.8) can be rewritten as in (5.11) by substituting (5.10).

$$l_s = a \cdot \alpha_1 \cdot G_{P1} \cdot t_1 + b \cdot \alpha_2 \cdot G_{P2} \cdot t_2 + c \tag{5.11}$$

Here, the numeric subscript 1 refers to the minimum thigh angle and 2 refers to the maximum thigh angle. (5.11) can be minimized as shown in (5.12) by considering all constants in each term into one lumped constant.

$$l_s = a_1 \cdot G_{P1} \cdot t_1 + a_2 \cdot G_{P2} \cdot t_2 + a_0 \tag{5.12}$$

5.6.5 Experiment and Results

Data required for these analysis was also collected in the same experiment conducted in MAL as described in Section 5.4. Marker clusters were attached to both thighs to caption the flexion and extension. One marker was attached to the heel of each shoe to capture the step length. An IMU was attached to the right thigh to measure the movement of the thigh. Data captured in such a way was cropped to extract the mid walk as described in Section 5.4. Gyro data were also cropped at the same points as thigh angle of each sample. Data cropped in this manner were used for the rest of the analysis as explained in the following discussion.

Minimum and maximum thigh angles for each stride were extracted using custom written Matlab functions listed in Appendix B. As seen in Figure 5.6, the heel contact occurs just after the positive peak of the thigh angle waveform. This feature was used in the custom written function to pick the two heel contact points that correspond to a particular step. Using this method, the minimum thigh angle (θ_1), the maximum thigh angle (θ_2) and the step length (l_s) were extracted for each step of each subject for both legs using MAL data. Then the straight line was fitted to data of each leg of a particular subject and this model was used to remove the outliers. If the error between the estimated and measured step lengths is greater than 1.5 times the standard deviation of measured step length, then that sample was considered as an outlier. The outlier removed step data were considered as the data set for the analysis. This data set was then divided into two parts: 25% for deriving model and the balance 75% for evaluating the model. This division was done per subject per each leg. Model parameters were derived for equations in (5.7) and (5.8) separately from the data set for the model and the remaining data set was used to evaluate the fits.

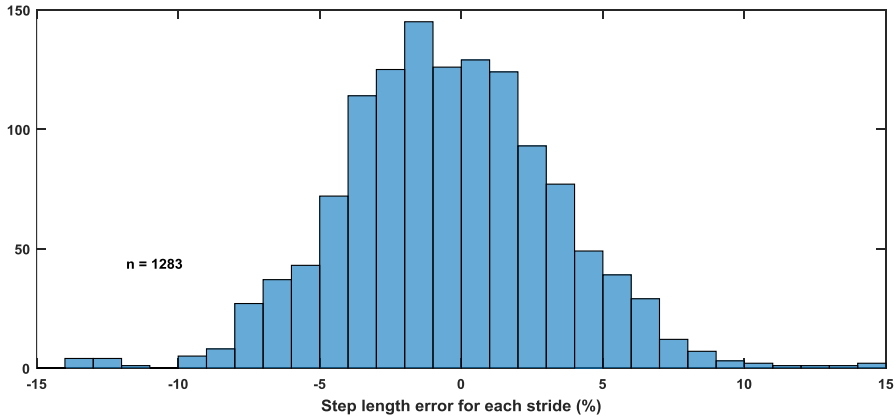

Figure 5.36 – Error percentage of step length estimated as a function of thigh angle peaks

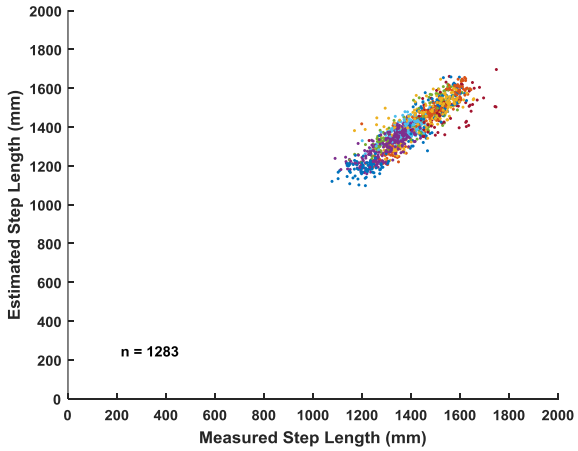

Figure 5.37 – Estimated step length *vs.* measured step length for step length as a function of thigh angle peaks

A total of 1283 step samples were included in the evaluating data set for 18 subjects: 9 males and 9 females. The RMSE of the step length for both legs was 54.60 mm when using (5.7) and 54.50 mm when using (5.8). This implies that using the approximation in (5.8) does not compromise the accuracy. The error percentage distribution of estimated step length for the model in (5.8) is shown in Figure 5.36 while Figure 5.37 shows the estimated step length *vs.* measured step length for all samples of all subjects used for evaluation. Figure 5.36 shows that the majority of error percentage per each step is in the range of ±7%.

Then the same analysis was performed using the gyro peaks as inputs, with the model in (5.12). Outliers were removed from the full sample using the same procedure as before, then each data set was divided into two part in a similar way. The total number of samples for all subjects after outliers being removed was 1018.

The RMSE of estimated step length was 55.92 mm, which is comparable with the RMSE reported for the model of step length as a function of peak thigh angles. Further, it was seen that the majority of the error lies between ±6% in this case which is slightly better than the previous case. The error distribution of the step length estimated with gyro peaks and the estimated step length *vs.* measured step length are shown in Figure 5.38 and Figure 5.39.

The model used in [71] that is shown in (2.12) was also tested on these data in a similar procedure to compare the performance of the proposed models with the model in (2.12). The RMSE was 56.97 mm when thigh angle peaks were taken as inputs to (2.12) and 56.28 when gyro peaks were taken as inputs. This indicates that the proposed step length estimation models perform better than the one in (2.12).

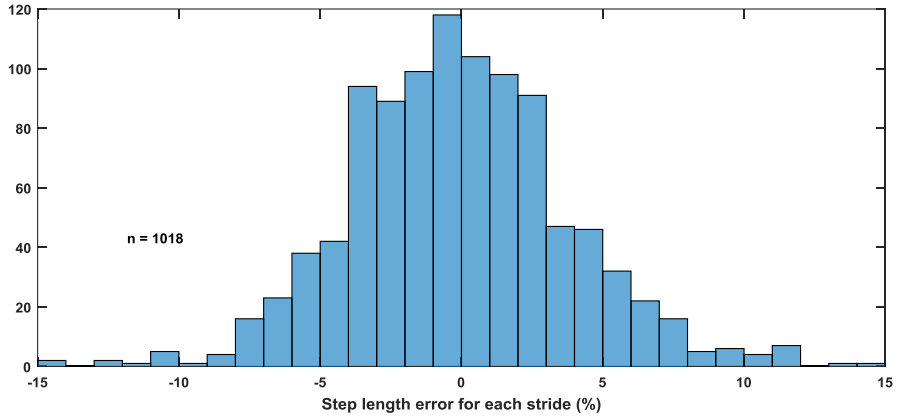

Figure 5.38 – Error percentage of step length estimated as a function of gyro peaks

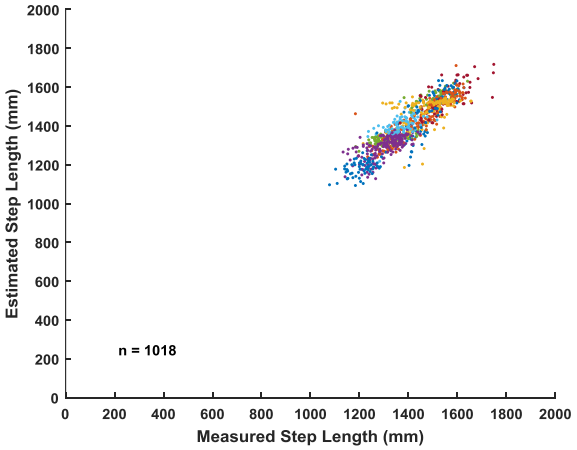

Figure 5.39 – Estimated step length *vs.* measured step length for step length as a function of gyro peaks

Similar experiment was conducted with the involvement of vision impaired subjects. The results of 4 female and 5 male vision impaired subjects indicated that the performance of the models are comparable to those of non–vision–impaired subjects, but with slightly higher error percentages. The error percentage distribution of estimated step length for the model in (5.8) for vision impaired subjects is shown in Figure 5.40 while Figure 5.41 shows the estimated step length *vs.* measured step length for all samples of all vision impaired subjects used for evaluation. Figure 5.40 shows that now the majority of error percentage per each step is in the range of -12% to +6%, which is a wider spread compared to non–vision–impaired case. When the model in (5.12) was used on data collected with vision impaired subjects, the results were comparable to the results when (5.8) is used on vision impaired data, as shown in Figure 5.42 and Figure 5.43. The RMSE values for the models in (5.7), (5.8) and (5.12) are 73.77 mm, 73.65 mm and 85.10 mm respectively.

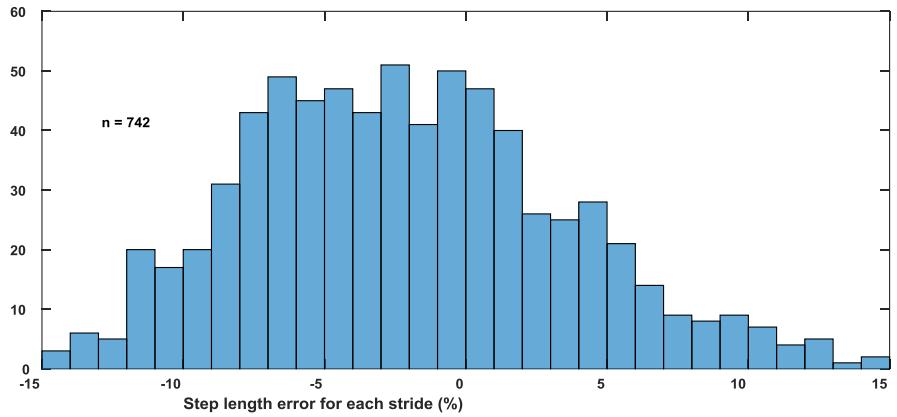

Figure 5.40 – Error percentage of step length estimated as a function of thigh angle peaks of vision impaired subjects

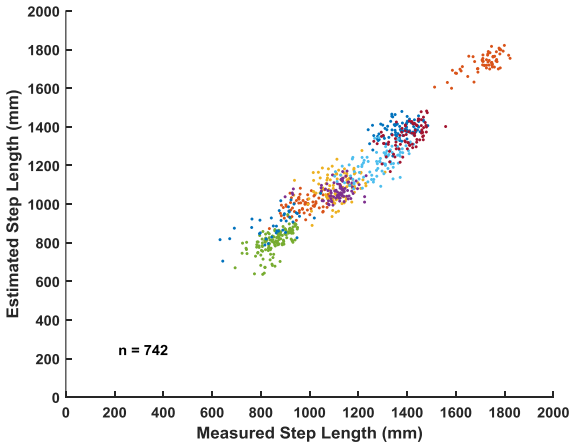

Figure 5.41 – Estimated step length *vs.* measured step length for step length as a function of thigh angle peaks of vision impaired subjects

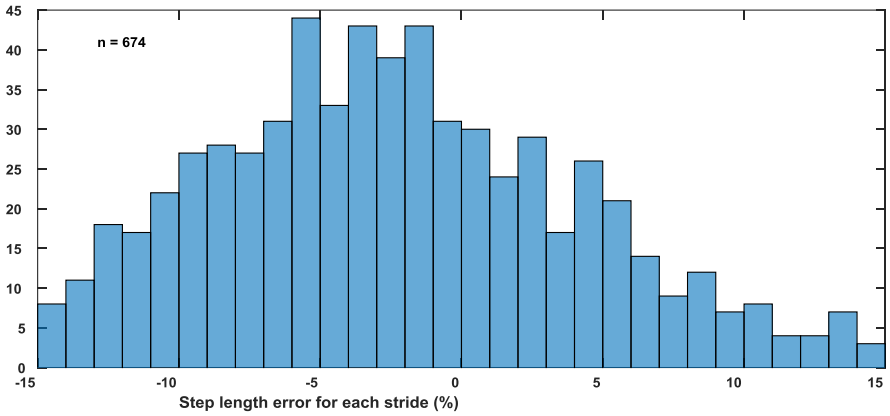

Figure 5.42 – Error percentage of step length estimated as a function of gyro peaks of vision impaired subjects

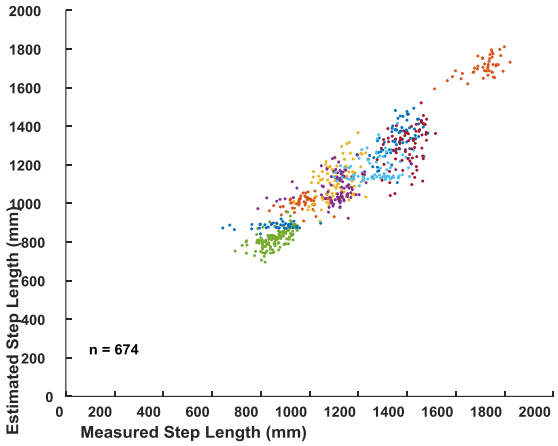

Figure 5.43 – Estimated step length *vs.* measured step length for step length as a function of gyro peaks of vision impaired subjects

5.6.6 Summary and Discussion

Two models for estimating step length using the peak thigh angles and gyroscopic peak values were presented in this section. In the first model, the step length is modelled as a function of the negative thigh angle peak (peak hip flexion angle) and positive thigh angle peak (peak hip extension angle). It was shown that the thigh angle peaks can be estimated by the product of the corresponding gyro peak and the time between the peak and the zero crossing of gyro signal. The second model uses this result and present step length as a function of negative gyro peak, time between negative peak and zero crossing of gyro signal, positive gyro peak and time between positive peak and zero crossing of gyro signal. It was shown that the step length can be predicted with similar accuracies with both these models.

The advantage of using the gyro peaks and time for zero crossing after peak, is that it avoids the integration of the gyro to derive thigh angle. Avoiding gyro integration is beneficial in two ways. Firstly, integrating uses significant amount of processor time and resources when deriving thigh angle, which is avoided when gyro peaks are used to estimate thigh angle peaks. Secondly, as discussed in Section 5.4, any static error present in gyro signal causes a drift in the angle that will cause errors in the step length estimated. Instead, when the gyro signal itself is used, this effect may be minimised.

The error reported when step length is estimated as a function of thigh angles is approximately 54 mm RMSE for the data set (1283 steps) used for the validation with an error percentage of ±7% to the measured step length for majority of samples. The RMSE reported was approximately 56 mm (for 1018 steps used for validation) when gyro peaks were used to estimate the step length with a percentage error of ±6% of the measured step length. Although these error figures appear to be larger when compared with the error figures presented in literature [71], the model in [71] reported greater errors when applied on the data set used in this study. This is an indication that the proposed models may perform better in practical applications.

These models perform in a similar way for vision impaired subjects, but with slightly higher errors. The RMSE reported when thigh angle peaks are used to estimate the step length was approximately 74 mm when compared with 54 mm for non–vision–impaired subjects. When gyro peaks are used to estimate the step length

the RMSE becomes 85 mm. This indicates that these models may be used with vision impaired subjects. However, the accuracies may improve if more subjects were considered and more samples were taken into consideration.

5.7 Gait Phase Identification

5.7.1 Introduction

Proper recognition of gait phases is important for accurate outcomes in gait modelling in pedestrian navigation and locomotion analysis applications. This section discusses the possibility of recognizing gait phases from the thigh angle and the gyro signal of single thigh mounted IMU. The signal features that may be used to identify key gait phases are also discussed in this section. The details of the two main phases and the eight sub phases of gait cycle are as discussed in Section 2.2.

5.7.2 Identify Gait Phases from the Thigh Angle and Gyro Waveforms

Figure 5.44 shows the thigh angle, gyro signal and time derivative of gyro signal, all normalised to their peak value and drawn on the same time axis. The letters *a* – *g* represent the key points of the stride cycle identifiable in the thigh angle waveform. Although it is the positive peak of the thigh angle waveform, point ***a*** is not the initial contact as shown in Figure 5.6. Point ***a*** is the end of the swing of the leg. The Initial Contact point is point ***b*** of the diagram. Description of all phases identifiable in the thigh angle waveform is given in Table XI. It can be seen that except point ***c***, all other points can be detected by detecting zero crossings of the gyro signal or its time derivative. Table XII shows which signal can be used to detect each point of the stride cycle. It should be noted that point ***g*** is as same as point ***b***. Further, the end of Loading Response (point ***c***) may be approximately detected by the relative maxima of the time derivative of gyro signal.

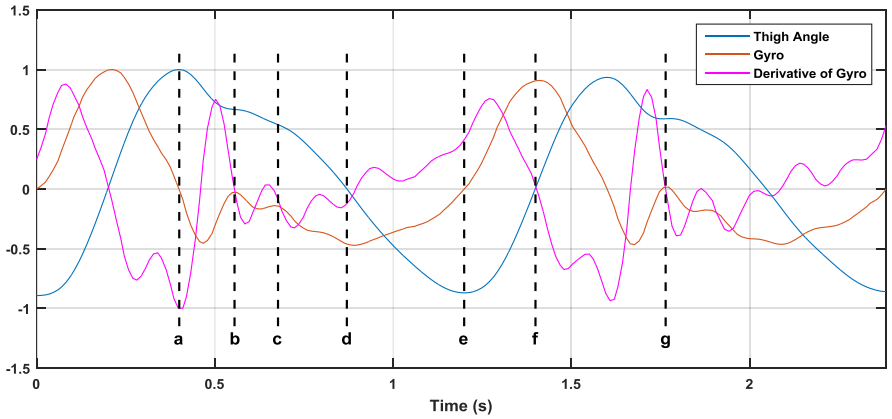

Figure 5.44 – Normalised thigh angle, gyro signal and time derivative of gyro signal

TABLE XI – PHASES OF GAIT CYCLE AS IDENTIFIED IN THE THIGH ANGLE WAVEFORM

Point/Points	Phase/Point of Gait Cycle
a	End of swing
b	Initial Contact
b–c	Loading Response
c–d	Mid Stance
d–e	Terminal Stance
e–f	Pre-Swing
f–g	Swing

It was observed that the three sub phases of Swing phase (Initial Swing, Mid Swing and Terminal Swing) cannot be distinguished in the thigh angle waveform. However, all five sub phases of Stance phase can be identified in the thigh angle waveform and four of these can be detected using zero crossing detectors on gyro signal and derivative of gyro signal. Implementing zero crossing detectors in real–time systems is not a difficult task as shown in Section 5.3.

TABLE XII – SIGNAL FEATURE THAT CAN BE USED TO DETECT EACH POINT OF THE STRIDE CYCLE

Point	Signal to Detect Zero Crossing to Detect Each Point
a	Gyro
b	Derivative of gyro
c	–
d	Derivative of gyro
e	Gyro
f	Derivative of gyro

5.7.3 Summary

A simple technique to identify phases of gait cycle using gyro signal and the first time derivative of gyro signal of a single thigh mounted IMU was presented in this section. Six key points of the gait cycle that are needed to detect gait sub phases were identified. Out of these six, five points can be detected using zero crossing detectors on gyro signal and derivative of gyro signal. Four sub phases of Stance phase as well as the Swing phase can be detected by this method in real time applications.

5.8 Activity Recognition

5.8.1 Introduction

Accurate human activity recognition plays a significant role in making pedestrian tracking accurate. Although many different activities are performed by people during navigation, the three main activities found in indoor navigation are standing, sitting and walking. Additional activities may include walking on stairs, going on an escalator or a travelator ramp and going in an elevator.

Researchers have used many approaches to detect different human activities. In most of these techniques, a 3–axis accelerometer is used to measure the acceleration of the trunk [72] or a section of a leg [73]. This section proposes a new approach for human activity detection using the thigh angle derived from a single thigh mounted IMU. Further, the outcomes of preliminary activity detection

algorithm are presented in this section. The activities considered in the data collection are standing, sitting and walking. No data filtering was included in the algorithm because minimal computational demand was the main aim when developing the algorithm. Some of work presented in this paper are published in [97].

The primary concerns of developing a navigation aid for vision impaired people were low cost devices which leads to the requirement of less computationally intense algorithms. Further, the scope of this research was to perform human gait analysis based on the thigh movement during walking. Hence, the activity recognition was also based on the thigh angle.

5.8.2 Indoor Activity Detection Algorithm

The observations used as the basis for developing the activity detection algorithm, details on the activity recognition algorithm and data processing technique used in it, and the empirical results are presented in this sub section.

5.8.2.1 Observations

The indoor activities considered in this study are walking, standing and sitting as they are the most common indoor activities performed by vision impaired people. Movement of the thigh was captured using the IMU discussed in Section 4.4. The IMU was strapped to the subject's thigh while performing a “sit, stand and walk” activity chain. Measurements were taken for standing posture with the test subject in slight motion, i.e., whist changing the supporting leg. Figure 5.45 shows the thigh angle computed for a trial of stand–sit–stand–walk–stand–sit–stand activity chain. Thigh angle was computed using the GIOF discussed in Section 5.4.

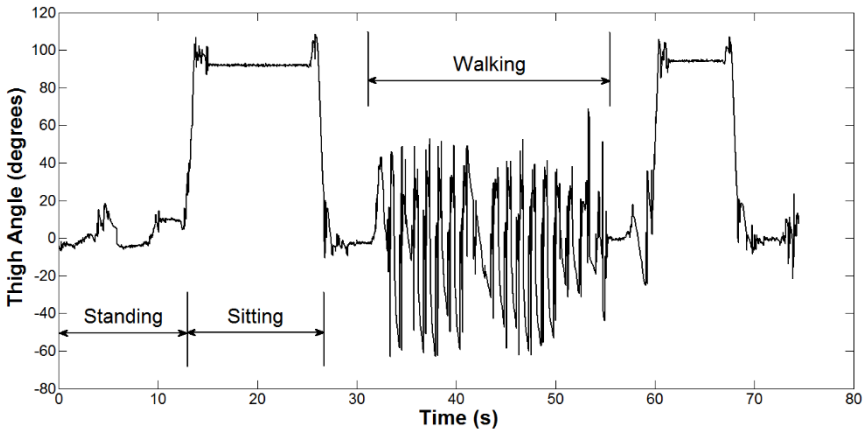

Figure 5.45 – Thigh angle while standing, sitting and walking

5.8.2.2 Data Processing and the Algorithm

The indoor activity detection algorithm is based on the envelope of the thigh angle and steps detected. As shown in Figure 5.45, the thigh angle is less than 20º when standing, close to 90º when sitting and the peak of thigh angle lies in between 20º and 70º when walking. Detection of steps is used to confirm if the subject is walking. Steps are detected by checking the delay between zero crossings of the thigh angle. If the delay is between 0.2 s and 1 s, then it is considered as a stride is detected. These times were selected to accommodate slow gait of 1.5 steps per second as presented in [88].

The envelope of the thigh angle is computed using a peak–hold mechanism. The positive peak of the thigh angle is taken as the envelope till the next positive peak is detected. Zero crossings of the thigh angle are detected simultaneously. Sitting is distinguished from standing and walking if the envelope of the thigh angle is larger than 70º. If the activity is not sitting, then if the envelope is less than 20º and walking is not detected, then the activity is taken as standing. Else the activity is considered as walking. Finally, this activity state is sent through a timing mechanism to avoid the activity state being switched to a different state for a very short period. Slow walking speed is in the range of 1.5 steps per second [88] and slow gait is observed in most of indoor navigation situations particularly for people with vision impairment in unfamiliar surroundings. Therefore the duration of the timer is set as 2 s, hence the activity is detected with a delay no more than one stride. The indoor activity detection algorithm is shown in Figure 5.46.

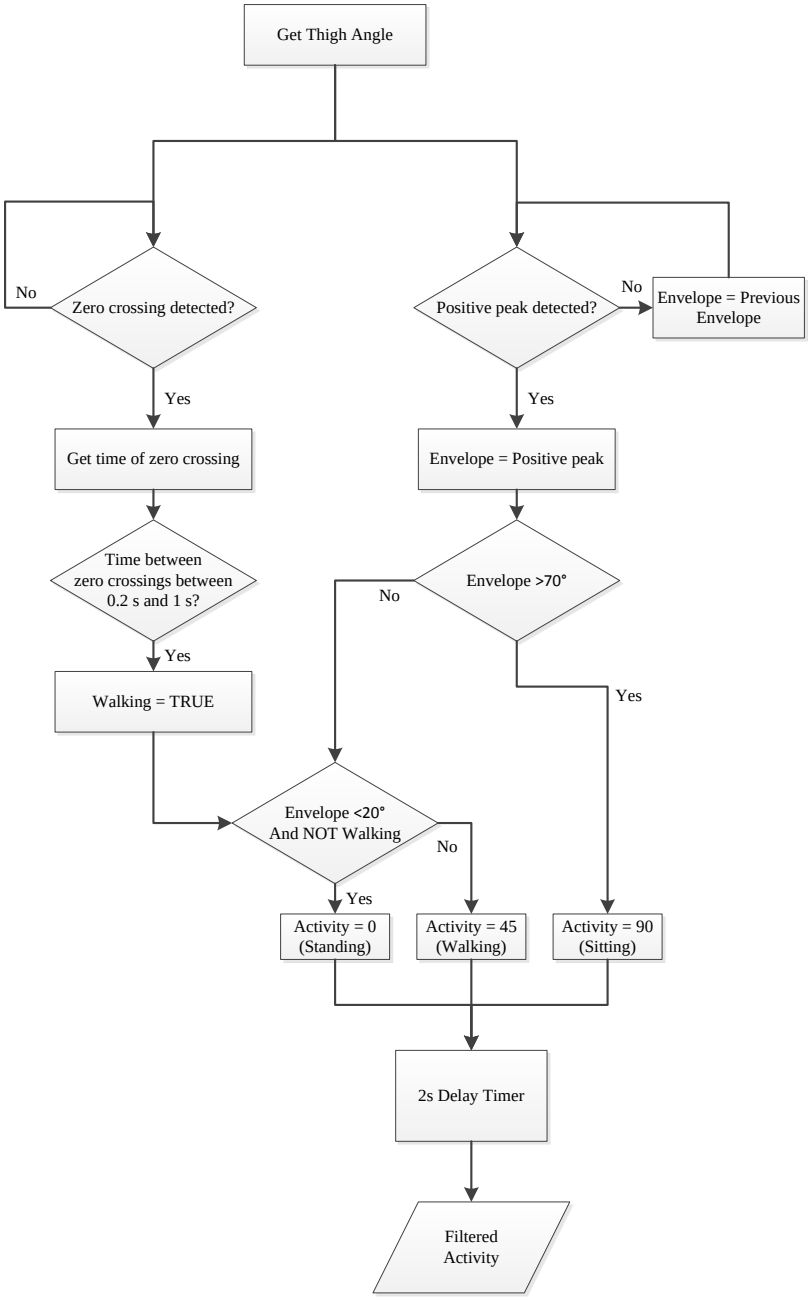

Figure 5.46 – Indoor activity detection algorithm

Figure 5.47 depicts the envelope detected by the algorithm and Figure 5.48 shows walking detected by the algorithm. For illustrative purposes, zero indicates that walking is not detected and 90 indicates areas where walking is detected. Figure 5.49 shows the final activity output (after the delay mechanism) of the algorithm. Each activity was represented by a value as shown in Table XIII for demonstrative purposes. The delay seen in the activity plot of Figure 5.49 is due to the delay timer in the algorithm.

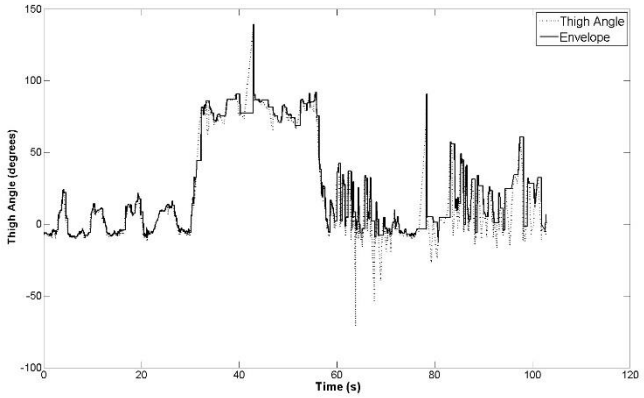

Figure 5.47 – Envelope detected by the algorithm

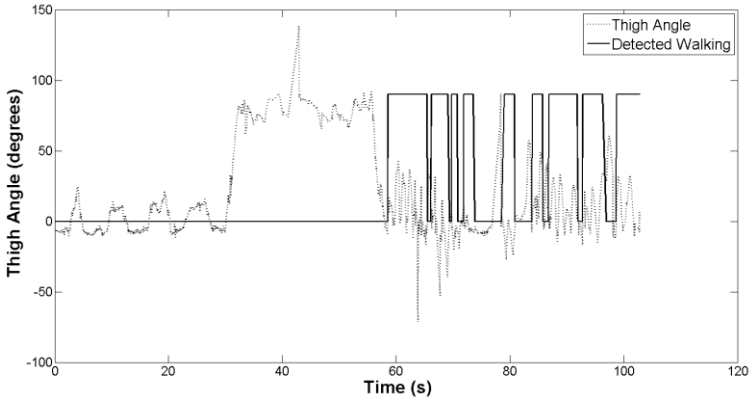

Figure 5.48 – Walking detected by the algorithm

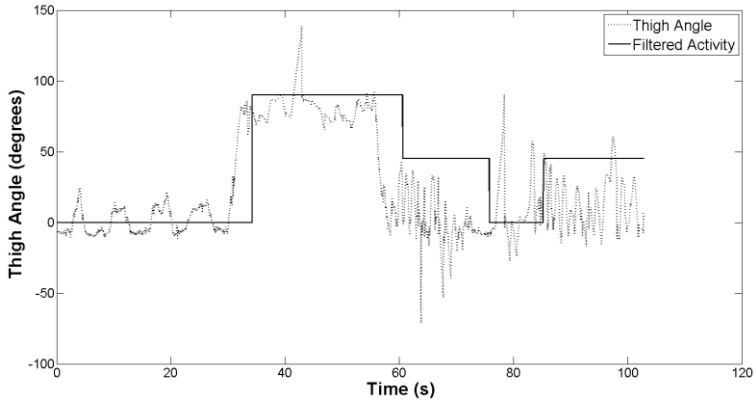

Figure 5.49 – Activities detected by the algorithm

TABLE XIII – VALUES ASSIGNED FOR ACTIVITIES

Activity	**Value**
Standing	0
Walking	45
Sitting	90

5.8.2.3 Experimental Setup

The experiment was conducted with the participation of two healthy females and two healthy males, all known to have no disability or impairment. Observations were recorded with the IMU (discussed in Section 4.4) attached to either thigh with two trials per each thigh. Subjects were asked to perform standing, sitting and walking activities. While standing, they were asked to behave naturally without conscious attempts to remain stationary and changing the support limb as they wish. In sitting posture, subjects were requested to move normally. Walking was done with medium and slow gait.

5.8.2.4 Empirical Results

The activities performed and activities detected by the algorithm were recorded by observing the thigh angle and the output of the algorithm. 78.26% of standing activities were detected as standing when the IMU is mounted to the left thigh and the rest were detected as walking. Walking and sitting activities were detected with no errors for the trials performed with IMU mounted to the left thigh.

When the IMU is mounted to the right thigh, standing was detected by the algorithm with an accuracy of 90% and walking with an accuracy of 92.86%. Some standing activities were detected wrongly as walking and some walking activities as standing. However, for this case too, sitting activities were detected without errors for the trials recorded. The difference of accuracies of the algorithm for two legs will have to be further studied. The overall performance of the activity detection algorithm is given in Table XIV. This indicate that the detection accuracy is above 80% for all three activities.

TABLE XIV – OVERALL ACTIVITY DETECTION PERFORMANCE OF THE ALGORITHM

Activity Performed	**Activity Detected**			**Activity Count (n)**
	Standing	**Sitting**	**Walking**	
Standing	83.72	0.00	16.28	43
Sitting	0.00	100.00	0.00	16
Walking	4.00	0.00	96.00	25

5.8.3 Using Pressure Variation for Activity Detection

The activities found in indoor navigation in addition to the activities considered in this algorithm are walking on a travelator ramp or a stair case, going on an escalator and going in an elevator. Preliminary observations of an experiment performed using a Google Nexus 5 smartphone indicated that the pressure sensor reading in combination with the activity detection algorithm discussed in Section 5.8.2 may be used to identify these activities. Figure 5.50 shows the pressure variation when walking on stairs while keeping the phone in the trouser pocket. The algorithm detects the activity as walking when walking on stairs too, but abrupt pressure changes were not observed when walking on level surfaces. Therefore, combining pressure data and the aforementioned algorithm may be used to identify walking on stairs and distinguish it with walking on level surfaces. The pressure readings when going on an escalator and a travelator ramp are shown in Figure 5.51. In both these cases, the algorithm detects them as standing as there is no leg movement. Therefore, the algorithm in combination with the pressure reading may be used to detect going on an escalator or a travelator ramp. Escalator and ramp may be distinguished from the gradient of the pressure variation.

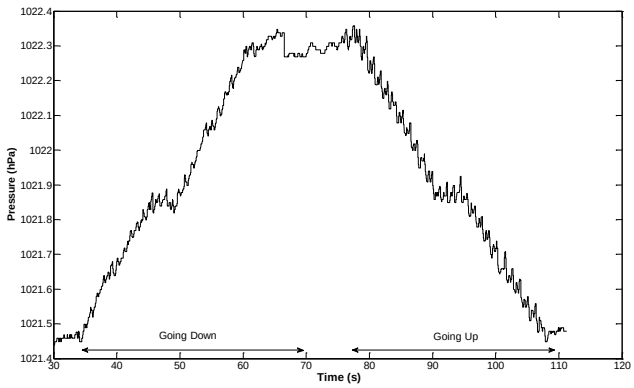

Figure 5.50 – Pressure reading when walking on stairs

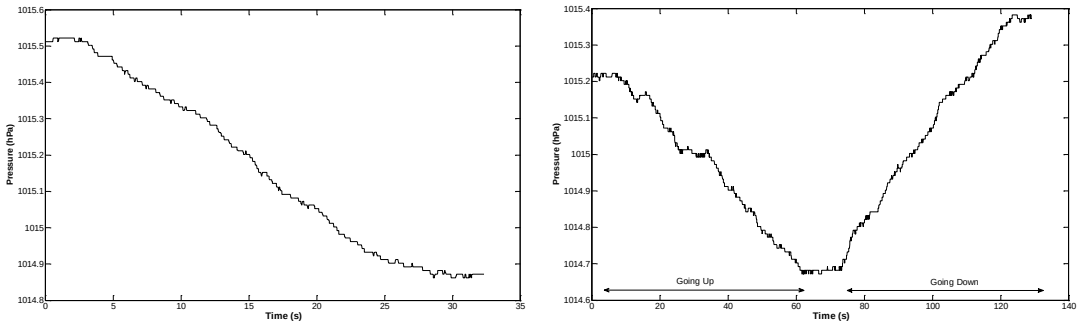

Figure 5.51 – Pressure reading on escalator going upwards (left) and on travellator ramp going up and down (right)

Pressure reading when going in an elevator is shown in Figure 5.52. Although a gradual pressure change was observed when going down, a sudden pressure drop was observed when going up. This was observed in all the trials conducted. This may be because of the characteristics of the air flow in to and out of the elevator. However, a significant pressure change is read when going in the elevator and the algorithm will detect this as standing. Hence, the algorithm in combination with the pressure reading may also be used to identify traveling in an elevator.

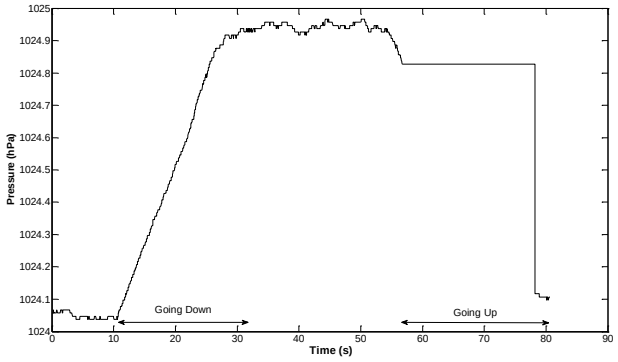

Figure 5.52 – Pressure reading when going down and up in an elevator

Further testing on the pressure data will have to be conducted to check if the pressure readings are consistent in repetitive measurements and over time. Once this is established, pressure input can also be taken into the algorithm and the algorithm can be improved to detect all possible indoor activities.

In addition, Section 5.5 illustrates that the thigh angle waveform has different shapes when walking on stairs and ramps than to level walking. This feature may also be used to identify walking up and down on stairs and ramps in conjunction with the algorithm discussed in this section.

5.8.4 Discussion

The simulation results of the algorithm indicates that it gives promising results. However, the activities identified in this algorithm are limited to sitting, standing and walking. Some of the errors in detecting the activities are due to non–smooth thigh angle waveform due to packet losses between the IMU and the computer that has caused as a result of signal drops of the radio. There were some occasions where the delay between two samples received were 1 s. Accuracies of the algorithm may improve when the algorithm is implemented in an embedded device that includes the sensor so that transmitting of samples is not required.

The capabilities of the algorithm may be expanded by using a pressure sensor in addition to the thigh mounted IMU. By fusing these two, sitting, standing, level walking, walking in an elevator, walking on stairs and waking on an escalators and travellator ramps can be detected. This set of activities covers most of the activities found in vision impaired indoor navigation.

5.8.5 Summary

This section proposed a human indoor activity detection algorithm with minimal computational demands. It was observed that the algorithm detects activities with mean accuracies above 83% with lower processing and storage requirements than existing algorithms. However, the activities detectable by the algorithm are limited to walking, sitting and standing.

Preliminary observations of the possibility of using pressure data to detect walking on travelator ramps, escalators, stairs and in elevators were also presented. Results indicated that pressure input may be effectively used to improve the algorithm to detect all possible indoor activities. Harmonic models of thigh angle waveform may be used in combination with the pressure to identify walking on ramps and stairs.

Chapter 6

CONCLUSION AND FUTURE DIRECTIONS

6.1 Conclusions

During the initial experiments, it was observed that the flexion–extension reading taken from a single thigh mounted gyroscope provides sufficient information for step detection and gait analysis for pedestrian walking. Inter–step correlation of the gyroscope signal was better than that of the accelerometer signal of a thigh mounted IMU. Further, the gyroscopic signal has a clearly visible periodic nature which was less visible in the reading of a hip mounted and hand held accelerometer. This indicated that a single thigh mounted IMU provides sufficient information for gait analysis for pedestrian navigation.

From this observation, a pedometer algorithm based on a single axis gyro reading (axis that reads the flexion–extension movement of the thigh) was developed and tested for accuracy. The step counting in the algorithm is based on zero crossing detection of the low pass filtered gyro signal. The algorithm was implemented on an Apple iPhone 4S and tested with the involvement of multiple male and female volunteers and demonstrated step counting accuracies above 97% for level walking at different walking speeds, including slow walking (50 steps/min). This pedometer algorithm had been used by Kwon *et al.* in their cross–platform and cross–device pedometer system that has reported accuracies above 99% over more than 6000 steps. This has confirmed the higher accuracy of the gyro based pedometer algorithm (compared to acceleration based algorithms) despite its lower processing demands.

A single axis orientation estimation algorithm, Gyro Integration Based Orientation Filter (GIOF) was developed and validated for accuracy against an optical motion capture system. The estimation of inclination is based on integration of gyro signal. The drift caused by the integration is corrected using the inclination estimated by accelerometer data and the correction is performed only when the accelerometer reads gravity only. The minimum correlation reported between the angle estimated by GIOF and the angle computed from the optical motion capture system was greater than 97% with an average correlation of 99.5%. It was also

shown that the GIOF consumes one half of the computation time consumed by the complementary filter (known to have lower computational demands) on low end embedded systems. The main reason for this is that GIOF performs the angle estimation using the accelerometer signal using $arctan$, only when the accelerometer reads gravity only, whereas the complementary filter performs $arctan$ in its each iteration. Performing $arctan$ requires longer computational times and resources in low end embedded systems such as 8–bit microcontrollers. The RMSE reported was less than 2.5º with mean RMSE of 1.85º, which is better than errors reported in techniques that use high end Kalman filters. Although GIOF was implemented and tested for one dimension, it may be extended to 3–D.

The thigh angle estimated using GIOF was used to model the thigh movement during level walking. Thigh movement was also modelled using the flexion–extension gyro axis data. Analysing 372 level walking trials of 19 subjects, both male and female, it was shown that only first 5 harmonics have normalised amplitudes greater than 1% in the spectrum of thing angle. The thigh angle regenerated for the full trial using a harmonic model with 5 significant harmonics had correlations greater than 99.5% with the original waveform and RMSE less than 2º. Therefore, it can be concluded that the thigh angle during level walking can be modelled with sufficient accuracy for pedestrian navigation with a harmonic model with 5 harmonic components. There are 9 significant harmonic components for the gyro signal spectrum. The thigh angle and the gyro signal for each stride were regenerated with 5–harmonic model for thigh angle and 9–harmonic model for gyro signal with correlations greater than 99.9% and 99.99% respectively and RMSE less than 1º and less than 5% of the peak respectively, which indicates that each stride can be modelled using a harmonic model with better accuracies compared to the full trial. Therefore, it can be concluded that the thigh angle waveform for level walking can be modelled with accuracies better than the accuracies of acceleration based modelling reported in literature, using a harmonic model with 5 significant harmonics and the gyro signal of level walking using a harmonic model with 9 significant harmonics.

Harmonic models for thigh angle and gyro signal for 6 commonly observed stride patterns were presented and they were used to classify the strides of a long level walk. The best correlation and the best RMSE indicates the best matching

model to the particular stride. Correlations greater than 99% and RMSE less than 2º were observed for the best matching thing angle model. It was observed that the stride pattern may vary during a single continuous walking trial of a given subject. Further, the stride pattern changes with different terrains (such as hard floor and sand) and walking task (such as stairs and ramps). Harmonic models may be used to identify the different walking tasks and terrains if a complete sample database is available.

A model to estimate step length based on the peak flexion and peak extension angles of the thigh was also presented in this thesis. The step length estimation error reported is approximately 54 mm RMSE for a data set of 1283 steps with an error percentage of ±7% to the measured step length for majority of samples. Although these error figures appear to be larger than the error figures reported in literature, the errors reported when these models were tested with the collected data set was higher than the error reported with the proposed model. A method to derive thigh angle peaks using gyro peaks and time between peak and zero crossing of gyro signal was proposed to avoid integration of gyro signal to derive thigh angle peaks. The relationship between the thigh angle peaks estimated with this method and the peak derived by integration gyro signal was linear with RMSE of approximately 1º for a sample base of 948 strides. The step length estimation model was re–written to derive a new model for step length as a function of gyro peaks and time between peak and zero crossing of gyro signal. The RMSE of step length reported with this model was approximately 56 mm for 1018 steps, with an error percentage of ±6% of the measured step length for majority of samples. These two step length models performed similarly for vision impaired subjects, but with slightly higher errors: 74 mm for step length as a function of thigh angle peaks and 85 mm for step length as a function of gyro peaks and time between peak and zero crossing of gyro signal. It should be noted that the number of vision impaired subjects was less than the number of non–vision impaired subjects, which may have affected poor accuracies for vision impaired subjects.

A simple technique to identify gait phases based on zero crossing detection of gyro signal and the first time derivative of gyro signal of a single thigh mounted IMU was presented in this thesis. Six key points of the stride cycle that are needed to detect sub phases can be detected using this technique. Four sub phases of the Stance

phase can be distinguished with this method. However, although the Swing phase can be identified, sub phases of Swing phase cannot be distinguished with this method. The advantages of this technique compared to the techniques available in literature are the lower computational cost and use of a single point sensor.

An indoor activity detection algorithm based on the flexion–extension angle of the thigh was also proposed in this thesis. The flexion–extension angle estimation was performed using GIOF with data from a single thigh mounted IMU as input. The algorithm could recognize sitting, standing and walking activities with accuracies greater than 83% in an experiment conducted with the participation of multiple healthy male and female subjects performing sit–stand–walk activity chain. The errors were only reported during activity transitions. The feasibility of using the pressure sensor to enable recognising activities such as going in an elevator, on an escalator and on stairs, was also tested and was successful. When the single thigh mounted IMU and a thigh mounted pressure sensor is combined, it may be possible to detect most of the activities one would perform during indoor navigation.

With these observations and results, it can be concluded that single axis (flexion–extension measuring axis) gyroscopic data of the single thing mounted IMU and the flexion and extension derived from a single thigh mounted IMU can be effectively used for step detection, indoor activity recognition and gait modelling for pedestrian navigation with higher accuracies compared to hip and foot mounted techniques and other acceleration based gait modelling techniques. The key advantages of the thigh mounted gyroscope based step detection and gait modelling techniques presented in this thesis are the simplicity and lower computational demands that enable them to be used in low cost, low end embedded devices, but experimentally proven to have comparable or better accuracies compared to the existing techniques that incorporate intense computations.

6.2 Future Directions

Directions for future research based on the observations and results presented in this thesis are as follows.

The pedometer algorithm presented in this thesis was implemented and tested by the author as well as by Kwon *et al.* on smartphones, where there are limitations in using the full control and capabilities of hardware. The performance of the algorithm may be further improved if it is implemented on an embedded device. The embedded device may be improved as a miniature wearable device so that the usability of the device increases and it becomes convenient to use. Further, the presented algorithm assumes that the device is kept in a fixed placement on the thigh which limits the flexibility of the algorithm. The usability and the flexibility of the algorithm can be improved by introducing tilt detection to detect if the device is tilted with respect to the thigh and selecting a different measurement axis and/or change the thresholds of the algorithm according to the tilt of the device.

The GIOF was implemented and tested during this research only for a single axis. However, it can be extended to 2–D easily by considering both pitch and roll axes and into 3–D by adding the magnetometer reading to get a correction for yaw.

It was shown that harmonic models can be used to extract different stride patterns a particular person or a group of people has and also to identify the variation of the stride pattern with varying circumstances, such as hard floor, sand, ramps and stairs. Further, harmonic models of thigh mounted gyro and/or the flexion–extension angle of the thigh may be used to study the following:

- Compare normal stride patterns with stride patterns observed when a certain lower limb injury is present.
- Compare pre and post operation stride patterns of a lower limb operation.
- To recognize foot drop of patients who are having L6 problem.

This thesis presented 6 commonly observed stride patterns of healthy subjects. However, to study the variation of stride pattern with different conditions and disabilities, a sufficient database for each stride pattern or subject group has to be collected. Models derived in such a way can then be used to identify the variation of stride pattern of a particular person with different activities and conditions. Further, these models can be used to identify a particular disability or to identify whether a recovering patient has achieved normal walking. In addition, the harmonic models of gyro signal and thigh angle obtained from a single thigh mounted IMU can be used

for activity detection. Further collection of data and analysis are needed for these applications.

REFERENCES

[1] World Health Organization, “Visual impairment and blindness,” August 2014. [Online]. Available: http://www.who.int/mediacentre/factsheets/fs282/en/. [Accessed 21 May 2015].

[2] Australian Network on Disability, “Stats and Facts,” 2015. [Online]. Available: http://www.and.org.au/pages/disability-statistics.html#_ftnref3. [Accessed 21 May 2015].

[3] Cure Blindness, “World Blindness Overview,” [Online]. Available: http://www.cureblindness.org/world-blindness/. [Accessed 21 May 2015].

[4] GPS.GOV, “GPS Accuracy,” [Online]. Available: http://www.gps.gov/systems/gps/performance/accuracy/. [Accessed 21 May 2015].

[5] C. Benavente-Peces, V. M. Moracho-Oliva, A. Domínguez-García and M. Lugilde-Rodríguez, “Global System for Location and Guidance of Disabled People: Indoor and Outdoor Technologies Integration,” in *Fifth International Conference on Networking and Services, 2009. ICNS '09.*, Valencia, 2009.

[6] A. R. Golding and N. Lesh, “Indoor navigation using a diverse set of cheap, wearable sensors,” in *The Third International Symposium on Wearable Computers, 1999. Digest of Papers.*, San Francisco, 1999.

[7] S. Feiner, B. MacIntyre, T. Hollerer and A. Webster, “A Touring Machine: Prototyping 3D Mobile Augmented Reality Systems for Exploring the Urban Environment,” in *First International Symposium on Wearable Computers, 1997. Digest of Papers.*, Cambridge, 1997.

[8] I. Murray and N. Abhayasinghe, “Arata News: Beyond the White Cane,” December 2013. [Online]. Available: http://www.arata.org.au/uploads/newsletter/2013No3ARATANews.pdf. [Accessed 21 May 2015].

[9] N. Rajakaruna, C. Rathnayake, N. Abhayasinghe and I. Murray, "Inertial Data Based Deblurring for Vision Impaired Navigation," Presented at Fifth International Conference on Indoor Positioning and Indoor Navigation (IPIN2014), 2014. [Online]. Available: http://www.ipin2014.org/wp/pdf/5C-2.pdf.

[10] J. Jayakody, N. Abhayasinghe and I. Murray, "AccessBIM Model for Environmental Characteristics for Vision Impaired Indoor Navigation and Way Finding," Presented at Third International Conference on Indoor Positioning and Indoor Navigation (IPIN2012), 2012. [Online]. Available: http://www.surveying.unsw.edu.au/ipin2012/proceedings/submissions/98_Paper.pdf.

[11] P. Rupasinghe, N. Abhayasinghe and I. Murray, "Efficient, Authentication and Access control Implementation in Mobile Ad hoc Networks (MANET) as applied to Indoor Navigation Guidance System for Vision Impaired People," Presented at Third International Conference on Indoor Positioning and Indoor Navigation (IPIN2012), 2012. [Online]. Available: http://www.surveying.unsw.edu.au/ipin2012/proceedings/submissions/67_Paper.pdf.

[12] J. Perry and J. M. Burnfield, Gait Analysis: Normal and Pathological Function 2nd Edition, Thorofare, New Jersey: SLACK Incorporated, 2010.

[13] M. A. Watkins, D. L. Riddle, R. L. Lamb and W. J. Personius, "Reliability of goniometric measurements and visual estimates of knee range of motion obtained in a clinical setting," *Physical Therapy*, vol. 71, no. 2, pp. 90-96, 1991.

[14] J. Z. Edwards, G. A. Kenneth, . R. S. Davis, . M. W. Kovacik, . D. A. Noe and M. J. Askew, "Measuring flexion in knee arthroplasty patients," *The Journal of Arthroplasty*, vol. 19, no. 3, pp. 369-372, 2004.

[15] R. Williamson and B. J. Andrews, "Detecting absolute human knee angle and angular velocity using accelerometers and rate gyroscopes," *Medical and Biological Engineering and Computing*, vol. 39, no. 3, pp. 294-302, 2001.

[16] S. J. M. Bamberg, A. Y. Benbasat, D. M. Scarborough, D. E. Krebs and J. A. Paradiso, "Gait Analysis Using a Shoe-Integrated Wireless Sensor System," *IEEE Transactions on Information Technology in Biomedicine,* vol. 12, no. 4, pp. 413-423, 2008.

[17] A. Mansfield and G. M. Lyons, "The use of accelerometry to detect heel contact events for use as a sensor in FES assisted walking," *Medical Engineering & Physics,* vol. 25, no. 10, pp. 879-885, 2003.

[18] M. P. Murray, "Gait as a total pattern of movement," *American Journal of Physical Medicine,* vol. 46, p. 290–332, 1967.

[19] J. L. Geisheimer, E. F. Greneker III and W. S. Marshall, "A high-resolution Doppler model of human gait," in *Proceedings of SPIE on Radar Technology*, 2002.

[20] B. Mariani, C. Hoskovec, S. Rochat, C. Büla, J. Penders and K. Aminian, "3D gait assessment in young and elderly subjects using foot-worn inertial sensors," *Journal of Biomechanics,* vol. 43, no. 15, pp. 2999-3006, 2010.

[21] K. Kurihara, S. Hoshino, K. Yamane and Y. Nakamura, "Optical motion capture system with pan-tilt camera tracking and real time data processing," in *Proceedings. ICRA '02. IEEE International Conference on Robotics and Automation, 2002.*, 2002.

[22] Vicon, [Online]. Available: http://www.vicon.com/. [Accessed 1 July 2015].

[23] Tracklab, [Online]. Available: http://www.tracklab.com.au. [Accessed 1 Jul 2015].

[24] Qualisys, [Online]. Available: http://www.qualisys.com. [Accessed 1 Jul 2015].

[25] M. Windolf, . N. Götzen and M. Morlock, "Systematic accuracy and precision analysis of video motion capturing systems—exemplified on the Vicon-460 system," *Journal of Biomechanics,* vol. 41, no. 12, p. 2776–2780, 2008.

[26] S.-h. P. Won, W. W. Melek and F. Golnaraghi, “A Kalman/Particle Filter-Based Position and Orientation Estimation Method Using a Position Sensor/Inertial Measurement Unit Hybrid System,” *IEEE Transactions on Industrial Electronics,* vol. 57, no. 5, pp. 1787-1798, 2010.

[27] Y. Tao, H. Hu and H. Zhou, “Integration of vision and inertial sensors for 3D arm motion tracking in home-based rehabilitation,” *The International Journal of Robotics Research,* vol. 26, no. 6, p. 607–624 , 2007.

[28] N. Miller, O. C. Jenkins, M. Kallmann and M. J. Mataric, “Motion capture from inertial sensing for untethered humanoid teleoperation,” in *IEEE-RAS International Conference on Humanoid Robotics*, Santa Monica, CA, 2004.

[29] G. Pons-Moll, A. Baak, T. Helten, M. Müller, H.-P. Seidel and B. Rosenhahn, “Multisensor-fusion for 3D full-body human motion capture,” in *2010 IEEE Conference on Computer Vision and Pattern Recognition (CVPR)*, San Francisco, CA, 2010.

[30] A. Noureldin, T. B. Karamat and J. Georgy, Fundamentals of inertial navigation, satellite-based positioning and their integration, Berlin: Springer, 2013.

[31] M. Park and Y. Gao, “Error and Performance Analysis of MEMS-based Inertial Sensors with a Low-cost GPS Receiver,” *Sensors,* vol. 8, no. 4, pp. 2240-2261, 2008.

[32] R. Nave, “Rotation Vectors,” [Online]. Available: http://hyperphysics.phy-astr.gsu.edu/hbase/rotv.html. [Accessed 1 Jul 2015].

[33] S. Chumkamon, P. Tuvaphanthaphiphat and P. Keeratiwintakorn, “A blind navigation system using RFID for indoor environments,” in *5th International Conference on Electrical Engineering/Electronics, Computer, Telecommunications and Information Technology, 2008. ECTI-CON 2008.*, Krabi, 2008.

[34] T. Riehle, P. Lichter and N. Giudice, “An indoor navigation system to support the visually impaired,” in *30th Annual International Conference of the IEEE*

Engineering in Medicine and Biology Society, 2008. EMBS 2008., Vancouver, BC, 2008.

[35] S. S. Chawathe, "Marker-Based Localizing for Indoor Navigation," in *IEEE Intelligent Transportation Systems Conference, 2007. ITSC 2007.*, Seattle, WA, 2007.

[36] M. Kourogi and T. Kurata, "A method of personal positioning based on sensor data fusion of wearable camera and self-contained sensors," in *Proceedings of IEEE International Conference on Multisensor Fusion and Integration for Intelligent Systems, MFI2003.*, 2003.

[37] L. Koski, T. Perälä and R. Piche, "Indoor positioning using WLAN coverage area estimates," in *2010 International Conference on Indoor Positioning and Indoor Navigation (IPIN).*, Zurich, 2010.

[38] M. Kourogi and T. Kurata, "Personal positioning based on walking locomotion analysis with self-contained sensors and a wearable camera," in *Proceedings. The Second IEEE and ACM International Symposium on Mixed and Augmented Reality, 2003.*, 2003.

[39] M. Hynes, H. Wang and L. Kilmartin, "Off-the-shelf mobile handset environments for deploying accelerometer based gait and activity analysis algorithms," in *Annual International Conference of the IEEE Engineering in Medicine and Biology Society, 2009. EMBC 2009.*, Minneapolis, MN, 2009.

[40] R. LeMoyne, T. Mastroianni, M. Cozza, C. Coroian and W. Grundfest, "Implementation of an iPhone as a wireless accelerometer for quantifying gait characteristics," in *2010 Annual International Conference of the IEEE Engineering in Medicine and Biology Society (EMBC)*, Buenos Aires, 2010.

[41] T. Iso and K. Yamazaki, "Gait analyzer based on a cell phone with a single three-axis accelerometer," in *Proceedings of the 8th conference on Human-computer interaction with mobile devices and services (MobileHCI '06). ACM*, New York, 2006.

[42] H. Hile and G. Borriello, “Positioning and Orientation in Indoor Environments Using Camera Phones,” *IEEE Computer Graphics and Applications,* vol. 28, no. 4, pp. 32-39, 2008.

[43] A. Mulloni, D. Wagner, D. Schmalstieg and I. Barakonyi, “Indoor Positioning and Navigation with Camera Phones,” *IEEE Pervasive Computing,* vol. 8, no. 2, pp. 22-31, 2009.

[44] G. J. Jerome and C. Albright. (2011, June), “Accuracy of Five Talking Pedometers under Controlled Conditions,” The Journal of Blindness Innovation and Research, 1(2), [Online]. Available: https://nfb.org/images/nfb/publications/jbir/jbir11/jbir010203.html. [Accessed 27 Oct. 2011].

[45] S. E. Crouter, P. L. Schneider, M. Karabulut and D. R. Bassett, “Validity of 10 Electronic Pedometers for Measuring Steps, Distance, and Energy Cost,” *Medicine & Science in Sports & Exercise*, vol. 35, no. 8, pp. 1455-1460, 2003.

[46] E. Garcia, H. Ding, A. Sarela and M. Karunanithi, “Can a mobile phone be used as a pedometer in an outpatient cardiac rehabilitation program?,” in *The 2010 IEEE/ICME International Conference on Complex Medical Engineering*, Gold Coast, Australia, 2010.

[47] W. Waqar, A. Vardy and Y. Chen, “Motion modelling using smartphones for indoor mobilephone positioning,” in 20th Newfoundland Electrical and Computer Engineering Conference, Newfoundland, Canada, 2011. [Online]. Available: http://necec.engr.mun.ca/ocs2011/viewpaper.php?id=55&print=1. [Accessed 1 July 2015].

[48] M. Oner, J. A. Pulcifer-Stump, P. Seeling and T. Kaya, “Towards the run and walk activity classification through Step detection - An Android application,” in *34th Annual International Conference of the IEEE Engineering in Medicine and Biology*, San Diego, CA, 2012.

[49] Y. P. Lim, I. T. Brown and J. C. T. Khoo, “An accurate and robust gyroscope-based pedometer,” in *30th Annual International Conference of the IEEE Engineering in Medicine and Biology Society (EMBS 2008)*, Vancouver, BC,

2008.

[50] M. Ayabe, . J. Aoki, K. Ishii, K. Takayama and H. Tanaka, “Pedometer accuracy during stair climbing and bench stepping exercises,” *Journal of Sports Science and Medicine,* vol. 7, no. 2, pp. 249-254, 2008.

[51] D. Sachs, “Sensor Fusion on Android Devices: A Revolution in Motion Processing,” Google Tech Talk, 2 Aug. 2010. [Online]. Available: http://www.youtube.com/watch?v=C7JQ7Rpwn2k. [Accessed 27 Oct. 2011].

[52] CHRobotics LLC, “Understanding Euler Angles,” [Online]. Available: http://www.chrobotics.com/library/understanding-euler-angles. [Accessed 1 Jul. 2015].

[53] CHRobotics LLC, “Fundamentals of Attitude Estimation,” [Online]. Available: http://www.chrobotics.com/library/attitude-estimation. [Accessed 1 Jul. 2015].

[54] Olliw, “IMU Data Fusing: Complementary, Kalman, and Mahony filter,” [Online]. Available: http://www.olliw.eu/2013/imu-data-fusing/. [Accessed 1 Jul. 2015].

[55] S. O. H. Madgwick, A. J. L. Harrison and R. Vaidyanathan, “Estimation of IMU and MARG orientation using a gradient descent algorithm,” in *IEEE International Conference on Rehabilitation Robotics (ICORR),* Zurich, Switzerland, 2011.

[56] F. Alam, Z. ZhaiH and H. JiaJia, “A Comparative Analysis of Orientation Estimation Filters using MEMS based IMU,” Presented at 2nd International Conference on Research in Science, Engineering and Technology (ICRSET’2014), [Online]. Available: http://iieng.org/siteadmin/upload/7697E0314552.pdf.

[57] H. J. Luinge and P. H. Veltink, “Measuring orientation of human body segments using miniature gyroscopes and accelerometers,” *Medical and Biological Engineering and Computing,* vol. 43, no. 2, pp. 273-282, 2005.

[58] YEI Technology, “YEI 3-Space Sensor,” [Online]. Available: http://www.yeitechnology.com/yei-3-space-sensor. [Accessed 17 July 2014].

[59] x-io Technologies, “x-IMU,” [Online]. Available: http://www.xio.co.uk/products/x-imu/. [Accessed 14 July 2014].

[60] S. Onyshko and D. A. Winter, “A mathematical model for the dynamics of human locomotion,” *Journal of Biomechanics,* vol. 13, no. 4, pp. 361-368, 1980.

[61] S. Siegler, R. Seliktar and W. Hyman, “Simulation of human gait with the aid of a simple mechanical model,” *Journal of Biomechanics,* vol. 15, no. 6, pp. 415-425, 1982.

[62] K. Tong and M. H. Granat, “A practical gait analysis system using gyroscopes,” *Medical Engineering and Physics,* vol. 21, no. 2, pp. 87-94, 1999.

[63] W. Zijlstra and A. L. Hof, “Assessment of spatiotemporal gait parameters from trunk acceleration during human walking,” *Gait and Posture,* vol. 10, pp. 1-10, 2003.

[64] R. K. Ibrahim, “Novel Gait Models and Features for Gait Patterns Classification,” Ph.D. Thesis, School of Electrical Engineering and Telecommunication, The University of New South Wales, Australia, 2011.

[65] H. Qiuyang and Y. Zaiyue, “Frequency-Estimation-Based Thigh Angle Prediction in Level-Ground Walking Using IMUs,” in *2013 International Conference on Cyber-Enabled Distributed Computing and Knowledge Discovery (CyberC),* Beijing , 2013.

[66] S. H. Shin, C. G. Park, J. W. Kim, H. S. Hong and J. M. Lee, “Adaptive Step Length Estimation Algorithm Using Low-Cost MEMS Inertial Sensors,” in *Sensors Applications Symposium, 2007. SAS '07. IEEE,* San Diego, CA, 2007.

[67] D. Gusenbauer, C. Isert and J. Krösche, “Self-contained indoor positioning on off-the-shelf mobile devices,” in *2010 International Conference on Indoor Positioning and Indoor Navigation (IPIN),* Zürich, Switzerland, 2010.

[68] V. Renaudin, M. Susi and G. Lachapelle, “Step Length Estimation Using Handheld Inertial Sensors,” *Sensors,* vol. 12, no. 7, pp. 8507-8525, 2012.

[69] J. H. Lee, B. Shin, C. Kim, J. Kim, S. Lee and T. Lee, “Real time adaptive step length estimation for smartphone user,” in *2013 13th International Conference on Control, Automation and Systems (ICCAS),* Gwangju, 2013.

[70] K. Zhao, B.-H. Li and A. G. Dempster, “A New Approach of Real Time Step Length Estimation for Waist Mounted PDR System,” in *2014 International Conference on Wireless Communication and Sensor Network (WCSN),* Wuhan, 2014.

[71] E. M. Diaz and A. L. M. Gonzalez, “Step Detector and Step Length Estimator for an Inertial Pocket Navigation System,” Presented at Fifth International Conference on Indoor Positioning and Indoor Navigation (IPIN2014), Oct. 2014. [Online]. Available: http://www.ipin2014.org/wp/pdf/2A-1.pdf.

[72] M. Bocksch, J. Seitz and J. Jahn, “Pedestrian Activity Classification to Improve Human Tracking and Localization,” Presented at Forth International Conference on Indoor Positioning and Indoor Navigation (IPIN2013), Oct. 2013. [Online]. Available: http://ipin2013.sciencesconf.org/conference/ipin2013/eda_en.pdf.

[73] J. R. Kwapisz, G. M. Weiss and S. A. Moore, “Activity recognition using cell phone accelerometers,” *ACM SIGKDD Explorations Newsletter,* vol. 12, no. 2, pp. 74-82, 2010.

[74] S. Zhong, L. Wang, A. M. Bernardos and M. Song, “An accurate and adaptive pedometer integrated in mobile health application,” in *IET International Conference on Wireless Sensor Network, 2010. IET-WSN.,* Beijing, 2010.

[75] R. E. Mayagoitia, A. V. Nene and P. H. Veltink, “Accelerometer and rate gyroscope measurement of kinematics: An inexpensive alternative to optical motion analysis systems,” *Journal of Biomechanics,* vol. 35, no. 4, p. 537–542, 2002.

[76] K. Abhayasinghe and I. Murray, “A novel approach for indoor localization using

human gait analysis with gyroscopic data," Presented at Third International Conference on Indoor Positioning and Indoor Navigation (IPIN2012), 2012. [Online]. Available: http://www.surveying.unsw.edu.au/ipin2012/proceedings/submissions/22_Paper.pdf.

[77] M. Marder, "Notes for Research Methods," 15 Jan. 2007. [Online]. Available: http://iwany.staff.uns.ac.id/files/2011/08/research_methods.pdf. [Accessed 27 Oct. 2011].

[78] R. Meier, Professional Android 2 Application Development, 2nd ed., Chichester: Wiley Publishing, Inc., 2010.

[79] N. Abhayasinghe and I. Murray, "The Application of "off-the-shelf" Components for Building IMUs for Navigation Research," Presented at Fifth International Conference on Indoor Positioning and Indoor Navigation (IPIN2014), Oct. 2014. [Online]. Available: http://www.ipin2014.org/wp/pdf/2A-3.pdf. [Accessed 1 Jul. 2015].

[80] Invensense, [Online]. Available: http://www.invensense.com. [Accessed 17 July 2014].

[81] STMicroelectronics, "LSM9DS0 iNEMO inertial module:3D accelerometer, 3D gyroscope, 3D magnetometer," [Online]. Available: http://www.st.com/web/catalog/sense_power/FM89/SC1448/PF258556. [Accessed 17 July 2014].

[82] Bosch Sensortec, "BMX055," [Online]. Available: http://www.boschsensortec.com/en/homepage/products_3/9_axis_sensors_5/ecompass_2/bmx055_1/bmx055. [Accessed 17 July 2014].

[83] Arduino, [Online]. Available: http://arduino.cc/. [Accessed 17 July 2014].

[84] Nordic Semiconductor, "nRF24L01 Single Chip 2.4GHz Transceiver Product Specification," [Online]. Available: http://www.nordicsemi.com/eng/nordic/download_resource/8041/1/62622944. [Accessed 25 July 2014].

[85] S. Jayalath and N. Abhayasinghe, "A Gyroscopic Data Based Pedometer Algorithm," in *8th International Conference on Computer Science & Education*,

Colombo, Sri Lanka, 2013.

[86] S. Jayalath, N. Abhayasinghe and I. Murray. (2013), "Accurate Pedometer for Smartphones," International Journal of Systems and Control, 2013 vol. 1. [Online]. Available: http://www.insightplanet.org/IJSC.html. [Accessed 3 Apr. 2014].

[87] S. Jayalath, N. Abhayasinghe and I. Murray, "A Gyroscope Based Accurate Pedometer Algorithm," in Forth International Conference on Indoor Positioning and Indoor Navigation (IPIN2013), Montbéliard, France, 2013, pp. 510–513., [Online]. Available: http://ipin2013.sciencesconf.org/conference/ipin2013/eda_en.pdf. [Accessed 19 Nov. 2013].

[88] T. Oberg, A. Karsznia and K. Oberg, "Basic gait parameters: Reference data for normal subjects, 10–79 years of age," *J. Rehabil. Res. Dev.*, vol. 30, no. 2, pp. 210-223, 1993.

[89] Apple Inc. (2010, Aug. 10), "Ambient Light Sensor," Apple Developer Forums, [Online]. Available: https://devforums.apple.com/message/274229. [Accessed 8 July 2013].

[90] Y. Kwon, K. Kang, C. Bae and R. J. Cha, "Cross-platform and cross-device pedometer system designed for healthcare services," in *8th International Conference on Systems Biology (ISB)*, Qingdao, China, 2014.

[91] F. Olsson, J. Rantakokko and J. Nygards, "Cooperative Localization by Foot-Mounted Inertial Navigation Systems and Ultrawideband Ranging," Presented at Fifth International Conference on Indoor Positioning and Indoor Navigation (IPIN2014), Oct. 2014. [Online]. Available: http://www.ipin2014.org/wp/pdf/2A-4.pdf.

[92] J.-O. Nilsson, A. K. Gupta and P. Handel, "Foot-mounted Inertial Navigation Made Easy," Presented at Fifth International Conference on Indoor Positioning and Indoor Navigation (IPIN2014), Oct. 2014. [Online]. Available: http://www.ipin2014.org/wp/pdf/1A-4.pdf.

[93] E. M. Diaz, A. L. M. Gonzalez and F. de Ponte Müller, "Standalone Inertial Pocket Navigation System," in *Position, Location and Navigation Symposium - PLANS 2014*, Monterey, CA, 2014.

[94] A. B. Albu, R. Bergevin and S. Quirion, "Generic Temporal Segmentation of Cyclic Human Motion," *Pattern Recognition,* vol. 41, pp. 6-21, 2008.

[95] C. Chang, R. Ansari and A. Khokha, "Efficient tracking of cyclic human motion by component motion," *IEEE Signal Processing Letters,* vol. 11, no. 12, pp. 941-944, 2004.

[96] B. G. Quinn and E. J. Hannan, The Estimation and Tracking of Frequency, Cambridge, U.K.: Cambridge Univ. Press, 2001.

[97] N. Abhayasinghe and I. Murray, "Human Activity Recognition Using Thigh Angle Derived from Single Thigh Mounted IMU Data," Presented at Fifth International Conference on Indoor Positioning and Indoor Navigation (IPIN2014), Oct. 2014. [Online]. Available: http://www.ipin2014.org/wp/pdf/2A-2.pdf.

[98] Android Developers, "Sensor Event," 26 July 2012. [Online]. Available: http://developer.android.com/reference/android/hardware/SensorEvent.html#values. [Accessed 1 Aug. 2012].

APPENDIX A

Comparison of Key Specifications of the Inertial Sensors [80] – [82]

Specification	Accelerometer			Gyroscope			Magnetometer		
	MPU-9150	**LSM9DS0**	**BMX055**	**MPU-9150**	**LSM9DS0**	**BMX055**	**MPU-9150**	**LSM9DS0**	**BMX055**
Resolution	N/A	N/A	0.98 mg	N/A	N/A	0.004 °/s	N/A	N/A	0.3 µT
Measurement Ranges	±2 g, ±4 g, ±8 g, ±16 g	±2 g, ±4 g, ±6 g, ±8 g, ±16 g	±2 g, ±4 g, ±8 g, ±16 g	±250 °/s, ±500 °/s, ±1000 °/s, ±2000 °/s	±245 °/s, ±500 °/s, ±2000 °/s	±125 °/s, ±250 °/s, ±500 °/s, ±1000 °/s, ±2000 °/s	±1200 µT	±200 µT, ±400 µT, ±800 µT, ±1200 µT	±1300 µT (x,y), ±2500 µT (z)
Sensitivity	16384 LSB/g , 8192 LSB/g, 4096 LSB/g, 2048 LSB/g	16384 LSB/g , 8197 LSB/g, 5464 LSB/g, 4098 LSB/g, 1366 LSB/g	1024 LSB/g , 512 LSB/g, 256 LSB/g, 128 LSB/g	131 LSB/°/s, 65.5 LSB/°/s, 32.8 LSB/°/s, 16.4 LSB/°/s	8.75 m°/digit, 17.5 m°/digit, 70 m°/digit	262.4 LSB/°/s, 131.2 LSB/°/s, 65.6 LSB/°/s, 32.8 LSB/°/s, 16.4 LSB/°/s	0.3 µT/LSB	0.008 µT/LSB, 0.016 µT/LSB, 0.032 µT/LSB, 0.048 µT/LSB	1 µT/µT
Zero-point Offset	± 80 mg (x, y), ± 150 mg (z)	± 60 mg	± 70 mg	± 20 °/s	± 10 °/s, ±15 °/s, ± 25 °/s	± 1 °/s	±1000 LSB	N/A	± 40 µT
Noise Density	400 µg/$\sqrt{Hz}$	N/A	150 µg/$\sqrt{Hz}$	0.005 °/s /$\sqrt{Hz}$	N/A	0.014 °/s /$\sqrt{Hz}$	N/A	N/A	0.6 µT

This page is intentionally left blank.

APPENDIX B

Custom Written Matlab Functions

Harmonic Extraction Function

```
function [h_f,h_amp,h_phs]=harmonics(f,r,alpha,n_ham)

% ========================================================================
% This function pics harmonics and the DC component of a frequency spectrum
% where the fundamental has the highest amplitude. Below are the definitions
% of variables.
%
% Inputs:
% f - frequencies of the spectrum
% r - amplitudes of the spectrum
% alpha - phases of the spectrum
%
% Outputs:
% h_f - Harmonic frequencies where h_f(1) is 0 that represent DC component
% h_amp - Harmonic amplitudes where h_amp(1) is the DC component
% h_phs - Phases of harmonic where h_phs(1) is 0 to represent DC component
% ========================================================================

[pks,index]=findpeaks(r);
peak=max(pks);



for i=1:1:length(index)
    pksf(i)=f(index(i));
    if pks(i)==peak
        if r(index(i)+1)>=0.99*r(index(i))
            fundamental=(f(index(i)+1)+f(index(i)))/2;
            h_f(1)=fundamental;
            h_amp(1)=peak;
            h_phs(1)=(alpha(index(i)+1)+alpha(index(i)))/2;
        else
            fundamental=pksf(i);
            h_f(1)=fundamental;
            h_amp(1)=r(index(i));
            h_phs(1)=alpha(index(i));
        end

    end
end


n=2;
for i=1:1:length(f)
    if roundn(f(i),-1)==roundn(fundamental*n,-1)
        if n<5
            if r(i-1)>r(i)
                h_amp(n)=r(i-1);
                h_f(n)=f(i-1);
                h_phs(n)=alpha(i-1);
            elseif r(i+1)>r(i)
                h_amp(n)=r(i+1);
                h_f(n)=f(i+1);
                h_phs(n)=alpha(i+1);
            else
                h_amp(n)=r(i);
                h_f(n)=f(i);
                h_phs(n)=alpha(i);
            end
        else
            h_amp(n)=r(i);
            h_f(n)=f(i);
            h_phs(n)=alpha(i);
        end
```

```
        n=n+1;
    end
    if n==n_ham+1
        break;
    end
end
h_amp=[r(1) h_amp];
h_f=[0 h_f];
h_phs=[0 h_phs];
```

Function that Extracts Thigh Angle Peaks

```
function [tMax,ThetaMax,tMin,ThetaMin]=thetaextrema(t,Theta)
% Identify Maximas and minimas of thigh angle
dataLength=length(t);
j=0;
l=0;
threshold1=2; % Threshold for peak detection
threshold2=-2; % Threshold for peak detection
t1=0;
t2=0;
max_pre=0;
min_pre=0;
k=0;
m=0;
a=0;
b=0;

for i=2:1:dataLength-1
    % Pick Maximas
    if (Theta(i)>Theta(i-1))&&(Theta(i)>Theta(i+1))
        if Theta(i)>=threshold1
            if t1==0
                j=j+1;
                tMax(j)=t(i);
                ThetaMax(j)=Theta(i);
                t1=t(i);
                if max_pre~=0
                    k=k+1;
                    max_gap(k)=t(i)-max_pre;
                end
                max_pre=t(i);
            elseif (t(i)-t1)>0.3
                j=j+1;
                tMax(j)=t(i);
                ThetaMax(j)=Theta(i);
                t1=t(i);
                if max_pre~=0
                    k=k+1;
                    max_gap(k)=t(i)-max_pre;
                end
                max_pre=t(i);
            end
        end
    end

    % Pick Minimas
    if (Theta(i)<Theta(i-1))&&(Theta(i)<Theta(i+1))
        if Theta(i)<=threshold2
            if t2==0
                l=l+1;
                tMin(l)=t(i);
                ThetaMin(l)=Theta(i);
                t2=t(i);
                if min_pre~=0
                    m=m+1;
                    min_gap(m)=t(i)-min_pre;
                end
                min_pre=t(i);
            elseif (t(i)-t2)>0.3
                l=l+1;
```

```
                tMin(l)=t(i);
                ThetaMin(l)=Theta(i);
                t2=t(i);
                if min_pre~=0
                    m=m+1;
                    min_gap(m)=t(i)-min_pre;
                end
                min_pre=t(i);
            end
        end
    end
end
```

Zero-crossing Detector

```
function [tz,yzeros] = zerocrosss(t,y)

% This function detects zero crossings of the time series y.
% It interpolates y data to find the exact zero crossing point.

    tz=[];

    for i=1:1:length(t)-1

        if y(i)==0
            tz=[tz,t(i)];


        elseif (y(i)*y(i+1))<0
            m=(y(i+1)-y(i))/(t(i+1)-t(i));
            newtz=(-y(i)/m)+t(i);
            tz=[tz,newtz];


        end

    end
    yzeros=zeros(size(tz));

end
```

Matlab Code that was used to Extract Thigh Angle Peaks and Heal Contact Points

```
clear;
close all;

mf='F';

fs=100;

radindeg=180/pi();
deginrad=pi()/180;

for subjectn=4:1:11
    for trial=3:1:20
        %% MAL Data Read
        if trial<10
            fileName1=['Data/' mf int2str(subjectn) '/Trial 0' ...
                int2str(trial) '.csv'];

        else
            fileName1=['Data/' mf int2str(subjectn) '/Trial ' ...
                int2str(trial) '.csv'];
        end

        if exist(fileName1, 'file')
```

```
outputfolder=['Output/' mf int2str(subjectn) '/'];
A=exist(outputfolder, 'dir');
if ~exist(outputfolder, 'dir')
    mkdir(outputfolder)
end
rightoutfile=['Output/' mf int2str(subjectn) '/'  mf ...
    int2str(subjectn) 'T' int2str(trial) '_right.csv'];
leftoutfile=['Output/' mf int2str(subjectn) '/' mf ...
    int2str(subjectn) 'T' int2str(trial) '_left.csv'];
figfile=['Output/' mf int2str(subjectn) '/' mf ...
    int2str(subjectn) 'T' int2str(trial) '.jpg'];

inputM=csvread(fileName1,5,0);

if size(inputM,2)==20
    t=inputM(:,1)/fs;
    rightleg=inputM(:,3:11);
    leftleg=inputM(:,12:20);

    rt=[];
    rth1x=[];
    rth1y=[];
    rth1z=[];
    rth2x=[];
    rth2y=[];
    rth2z=[];
    rhx=[];
    rhy=[];
    rhz=[];


    for i=1:1:length(t)
        if rightleg(i,1)&&rightleg(i,2)&&rightleg(i,3)&&...
                rightleg(i,4)&&rightleg(i,5)&&rightleg(i,6)...
                &&rightleg(i,7)&&rightleg(i,8)&&rightleg(i,9)
            rt=[rt;t(i)];
            rth1x=[rth1x;rightleg(i,1)];
            rth1y=[rth1y;rightleg(i,2)];
            rth1z=[rth1z;rightleg(i,3)];
            rth2x=[rth2x;rightleg(i,4)];
            rth2y=[rth2y;rightleg(i,5)];
            rth2z=[rth2z;rightleg(i,6)];
            rhx=[rhx;rightleg(i,7)];
            rhy=[rhy;rightleg(i,8)];
            rhz=[rhz;rightleg(i,9)];
        end
    end

    % rt=rt-rt(1);

    lt=[];
    lth1x=[];
    lth1y=[];
    lth1z=[];
    lth2x=[];
    lth2y=[];
    lth2z=[];
    lhx=[];
    lhy=[];
    lhz=[];


    for i=1:1:length(t)
        if leftleg(i,1)&&leftleg(i,2)&&leftleg(i,3)&&...
                leftleg(i,4)&&leftleg(i,5)&&leftleg(i,6)&&...
                leftleg(i,7)&&leftleg(i,8)&&leftleg(i,9)
            lt=[lt;t(i)];
            lth1x=[lth1x;leftleg(i,1)];
            lth1y=[lth1y;leftleg(i,2)];
            lth1z=[lth1z;leftleg(i,3)];
            lth2x=[lth2x;leftleg(i,4)];
            lth2y=[lth2y;leftleg(i,5)];
            lth2z=[lth2z;leftleg(i,6)];
            lhx=[lhx;leftleg(i,7)];
            lhy=[lhy;leftleg(i,8)];
            lhz=[lhz;leftleg(i,9)];
        end
```

```
end

% lt=lt-lt(1);

%% ======= Right Leg Analysis =======

if rhx(1)>rhx(end)
    rthx=rth1x-rth2x;
else
    rthx=rth2x-rth1x;
end
rthy=rth1y-rth2y;
rthz=rth1z-rth2z;

rtheta=atan2(rthx,rthz)*radindeg;

%Filter Theta at 15 Hz
fc=15;
F_order=4;
Wn=fc/fs;
[b1,a1]=butter(F_order,Wn);

rtheta=filtfilt(b1,a1,rtheta);

if isempty(lt)
    limits=[min(rt) max(rt)];
elseif isempty(rt)
    limits=[min(lt) max(lt)];
else
    limits=[min(min(lt),min(rt)) max(max(lt),max(rt))];
end



% Extremas of Right Leg
[rthetamax,irthetamax,rthetamin,irthetamin] = extrema(rtheta);
[rhzmax,irhzmax,rhzmin,irhzmin] = extrema(rhz);

irhzmin=sort(irhzmin);
rhzmin=rhz(irhzmin);

% Filter extremas
newirhzmin=[];
newrhzmin=[];
newirhzmin(1)=irhzmin(1);
newrhzmin(1)=rhzmin(1);
n=1;
for i=2:1:length(irhzmin)
    if (rhzmin(i)>newrhzmin(n)+2) || (rhzmin(i)<newrhzmin(n)-2)
        n=n+1;
        newirhzmin(n)=irhzmin(i);
        newrhzmin(n)=rhzmin(i);
    end
end

irhzmin=newirhzmin';
rhzmin=newrhzmin';

newirthetamax=[];
newrthetamax=[];
for i=1:1:length(irthetamax)
    if rthetamax(i)>=10
        newirthetamax=[newirthetamax;irthetamax(i)];
        newrthetamax=[newrthetamax;rthetamax(i)];
    end
end

irthetamax=sort(newirthetamax);
rthetamax=rtheta(irthetamax);

newirthetamin=[];
newrthetamin=[];
for i=1:1:length(irthetamin)
    if rthetamin(i)<=0
        newirthetamin=[newirthetamin;irthetamin(i)];
        newrthetamin=[newrthetamin;rthetamin(i)];
    end
```

```
end

irthetamin=sort(newirthetamin);
rthetamin=rtheta(irthetamin);

fig1=figure;
subplot(411); plot(rt,rtheta,rt(irthetamax),rthetamax,...
    'r.',rt(irthetamin),rthetamin,'r.');
xlim(limits); grid on;
for i=1:1:length(irthetamax)
    text(rt(irthetamax(i)),rthetamax(i),...
        num2str(irthetamax(i)),'horiz','left','vert',...
        'bottom','fontsize',6);
end
for i=1:1:length(irthetamin)
    text(rt(irthetamin(i)),rthetamin(i),...
        num2str(irthetamin(i)),'horiz','left','vert',...
        'bottom','fontsize',6);
end

subplot(412); plot(rt,rhz,rt(irhzmin),rhzmin,'r.');
xlim(limits); grid on;

for i=1:1:length(irhzmin)
    text(rt(irhzmin(i)),rhzmin(i),num2str(irhzmin(i)),...
        'horiz','left','vert','bottom','fontsize',6);
end


%% ======= Left Leg Analysis =======

if ~isempty(lt)
    if lhx(1)>lhx(end)
        lthx=lth1x-lth2x;
    else
        lthx=lth2x-lth1x;
    end
    lthy=lth1y-lth2y;
    lthz=lth1z-lth2z;

    ltheta=atan2(lthx,lthz)*radindeg;

    ltheta=filtfilt(b1,a1,ltheta);

    % Extremas of Left Leg
    [lthetamax,ilthetamax,lthetamin,ilthetamin] = extrema(ltheta);
    [lhzmax,ilhzmax,lhzmin,ilhzmin] = extrema(lhz);

    ilhzmin=sort(ilhzmin);
    lhzmin=lhz(ilhzmin);

    % Filter extremas

    newilhzmin=[];
    newlhzmin=[];
    newilhzmin(1)=ilhzmin(1);
    newlhzmin(1)=lhzmin(1);
    n=1;
    for i=2:1:length(ilhzmin)
        if (lhzmin(i)>newlhzmin(n)+2) || (lhzmin(i)<newlhzmin(n)-2)
            n=n+1;
            newilhzmin(n)=ilhzmin(i);
            newlhzmin(n)=lhzmin(i);
        end
    end

    ilhzmin=newilhzmin';
    lhzmin=newlhzmin';

    newilthetamax=[];
    newlthetamax=[];
    for i=1:1:length(ilthetamax)
        if lthetamax(i)>=10
            newilthetamax=[newilthetamax;ilthetamax(i)];
            newlthetamax=[newlthetamax;lthetamax(i)];
        end
    end
```

```
                    ilthetamax=sort(newilthetamax);
                    lthetamax=ltheta(ilthetamax);

                    newilthetamin=[];
                    newlthetamin=[];
                    for i=1:1:length(ilthetamin)
                        if lthetamin(i)<=0
                            newilthetamin=[newilthetamin;ilthetamin(i)];
                            newlthetamin=[newlthetamin;lthetamin(i)];
                        end
                    end

                    ilthetamin=sort(newilthetamin);
                    lthetamin=ltheta(ilthetamin);


                    subplot(413); plot(lt,ltheta,lt(ilthetamax),lthetamax,...
                        'r.',lt(ilthetamin),lthetamin,'r.');
                    xlim(limits); grid on;
                    for i=1:1:length(ilthetamax)
                        text(lt(ilthetamax(i)),lthetamax(i),...
                            num2str(ilthetamax(i)),'horiz','left','vert',...
                            'bottom','fontsize',6);
                    end
                    for i=1:1:length(ilthetamin)
                        text(lt(ilthetamin(i)),lthetamin(i),...
                            num2str(ilthetamin(i)),'horiz','left','vert',...
                            'bottom','fontsize',6);
                    end

                    subplot(414); plot(lt,lhz,lt(ilhzmin),lhzmin,'r.');
                    xlim(limits); grid on;

                    for i=1:1:length(ilhzmin)
                        text(lt(ilhzmin(i)),lhzmin(i),num2str(ilhzmin(i)),...
                            'horiz','left','vert','bottom','fontsize',6);
                    end

                end

                %% ===== Output Data =====

                rightoutputM=[];
                leftoutputM=[];

                rightoutputM=[irthetamin,rthetamin;...
                              0,0;...
                              irthetamax,rthetamax;...
                              0,0;...
                              irhzmin,rhx(irhzmin)];

                if ~isempty(lt)
                    leftoutputM=[ilthetamin,lthetamin;...
                              0,0;...
                              ilthetamax,lthetamax;...
                              0,0;...
                              ilhzmin,lhx(ilhzmin)];
                end

                %% ===== Save =====

                csvwrite(rightoutfile,rightoutputM);
                if ~isempty(lt)
                    csvwrite(leftoutfile,leftoutputM);
                end
                saveas(fig1,figfile);

                close(fig1);
            end
        end
    end
end
```